N° d'ordre 2015ISAL0067
Année 2015

Thèse

Amélioration du contrôle vibratoire autonome de smart structures par échange modal d'énergie

-

Enhanced Self-powered Vibration Damping of Smart Structures by Modal Energy Transfer

Présentée devant
L'institut national des sciences appliquées de Lyon

Pour obtenir
Le grade de docteur

Formation doctorale
Génie Mécanique

École doctorale
Mécanique, Energétique, Génie Civil, Acoustique

Par
Zhen WANG

Soutenue le 20 juillet 2015 devant la Commission d'examen

Jury MM.

Philippe LECLAIRE	Professeur (ISAT-Drive)	Rapporteur
Jean-Louis ROBERT	Professeur (UBP-Institut Pascal)	Rapporteur
Claire JEAN-MISTRAL	Maitre de Conférences (INSA-Lyon-LaMCoS)	Co-Directeur de Thèse
Luc GAUDILLER	Professeur (INSA-Lyon-LaMCoS)	Directeur de Thèse

Laboratoire de recherche :
Laboratoire de Mécanique des Contacts et des Structures (LaMCoS)
CNRS UMR5259 - INSA de Lyon

Enhanced Self-powered Vibration Damping of Smart Structures by Modal Energy Transfer

---

Abstract

In a context of embedded structures, the next challenge is to develop an efficient, energetically autonomous vibration control technique. Synchronized Switch Damping techniques (SSD) have demonstrated interesting properties in vibration control with a low power consumption. For compliant or soft smart structures, modal control is a promising way as specific modes can be the target. This Ph-D work examines a novel energy transfer concept and design of simultaneous energy harvesting and vibration control on the same host structure. The basic idea is that the structure is able to extract modal energy from the chosen modes, and utilize this harvested energy to suppress the target modes via modal control method. We propose here a new technique to enhance the classic SSD circuit due to energy harvesting and energy transfer.

Our architecture called Modal Synchronized Switching Damping and Harvesting (Modal SSDH) is composed of a harvesting circuit (Synchronized Switch Harvesting on Inductor SSHI), a Buck-Boost converter and a vibration modal control circuit (SSD). Various alternatives of our SSDH techniques were proposed and simulated.

A real smart structure is modeled and used as specific case to test the efficiency of our concept. Piezoelectric sensors and actuators are taken as active transducers, as they develop the direct and inverse effects useful for the energy harvesting and the vibration damping.

Optimization are running out and the basic design factors are discussed in terms of energy transfer. Simulations, carried out under bi-harmonic and noise excitation, underline that our new SSDH concept is efficient and robust. Our technique improves the damping effect of semi-active method compared to classic SSD method thanks to the use of harvested modal energy.

Key words: vibration control - energy harvesting - piezoelectric materials - energy transfer - modal control

Amélioration du contrôle vibratoire autonome de smart structures par échange modal d'énergie

Résumé

Le travail de cette thèse propose une nouvelle méthode de contrôle appelée SSDH (Synchronized Switch Damping and Harvesting) basée sur l'idée de redistribution de l'énergie récupérée pour réduire l'énergie vibratoire d'une structure. De nombreuses recherches ont concerné le contrôle de vibration des structures souples. L'utilisation de l'approche modale pour ce genre de structure présente de nombreux intérêts. Dans le cadre de cette thèse l'idée est de récupérer l'énergie des modes qui ne sont pas contrôlés de façon à améliorer l'effet d'amortissement des modes ciblés par le contrôle sur une même structure. Pour cela, sur la base de la technique semi-active de contrôle, un circuit de contrôle modal a été conçu pour être compatible, via un convertisseur, avec des techniques semi-active de récupération d'énergie qui ont-elles-mêmes été adaptées en modal. Plusieurs variantes de la méthode SSDH ont été testées en simulation.

De façon à estimer l'efficacité du concept, une application sur un modèle expérimental d'une smart structure simple est proposée. Actionneurs et capteurs utilisent des matériaux piézoélectriques qui présentent les effets directs et inverses utiles pour la récupération d'énergie et le contrôle vibratoire.

Après optimisation des différents paramètres électromécaniques et électriques, les résultats des simulations menées sous excitations bisinusoidale ou en bruit blanc, montrent que la nouvelle méthode de contrôle autoalimentée SSDH est efficace et robuste. Elle améliore sensiblement l'amortissement produit par les techniques semi-actives modales de base (SSDI) grâce à l'utilisation de l'énergie modale récupérée.

Mots-Clés : contrôle des vibrations - récupération d'énergie - matériaux piézoélectriques - transfert d'énergie – modale contrôlé

Acknowledgement

Foremost, thanks all my friends who helped me in the past several years.

I would like to thanks Prof. Luc Gaudiller, Dr. Claire Jean-Mistral and Dr. Simon Chesne, the supervisors of my thesis.
Their meticulous work attitude and unique analytical approach have shaped my research style. Their passion and patient give me enough faith to fix the tricky problem one by one.

I also would like to express my gratitude to the committee members, for their corrections and suggestions.

I also would like express my gratitude to Prof. Georges Jacquet-Richardet for his guidance and kindly help.

I would like thank all the colleagues in LAMCOS.

Besides, I would like to thank my supervisor in my master stage, Prof. Zhichun YANG, for always sharing his experience with me.

Finally, I would like to acknowledge the China Scholarship Council (CSC) for the financial support.

My parents receive my deepest gratitude and love for their endless support and encouragement.

Table of contents

NOTATIONS

Piezoelectric related parameters

T	mechanical stress
D	electrical displacement
S	mechanical strain
E	electrical field
d	piezoelectric charge constant
g	piezoelectric voltage constant
e	piezoelectric constant
h	piezoelectric stiffness constant
s	piezoelectric elastic compliance
β	piezoelectric dielectric constants
c	piezoelectric elastic stiffness constant
k or k_2	piezoelectric coupling factor, i.e. k33
f	frequency
ω	angular frequency
ω_D (corresponding to foc)	open circuit angular frequency
ω_E (corresponding to fcc)	short circuit angular frequency
ε_0	absolute permittivity
ε	relative permittivity
C_0	blocked capacitance of piezoelectric element

Electrical parameters

C	capacitor
L	inductor
R	resistor
Z	impedance
X	reactance
Y	admittance
G	conductance
B	susceptance
P	harvested power
N	turn ratio
E	energy
I or i	current
V	voltage

Other modelling parameters

ρ	density
K	lumped stiffness
C	lumped viscous loss
Q_E	electrical quality factor
Q_M	mechanical quality factor
$tan\delta$	the (mechanical) loss
ζ	system damping ratio

κ	curvature
G	shear modulus
Y	Young's modulus
t	thickness
m or M	the lumped mass
U	displacement
t_1 or Δt	switching time

Superscripts

T	mechanical stress is constant
D	electrical displacement is constant
S	mechanical strain is constant
E	electrical field is constant

Subscripts

S	source
p , P or P_Z	piezoelectric element

ABBREVIATIONS

SSDI	Synchronized Switch Damping on Inductor
SSDS	Synchronized Switch Damping on Short
SSDV	Synchronized Switch Damping on Voltage sources
parallel-SSHI	Synchronized Switch Harvesting on Inductor (placed in parallel)
series-SSHI	Synchronized Switch Harvesting on Inductor (placed in series)
SECE	Synchronous Electric Charge Extraction
Series-DSSH	Double Synchronized Switch Harvesting (placed in series)
Parallel-DSSH	Double Synchronized Switch Harvesting (placed in parallel)
SSDVC (I)	SSDV on Capacitor (I): Constant intermediate voltage
SSDVC (II)	SSDV on Capacitor (II): Capacitor discharge
SSDH	Modal Synchronized Switching Damping and Harvesting

1 Background and Literature Review

1.1 Introduction

This chapter is the state of the art of the structural control using smart materials. Various smart materials, devices and control techniques involved in vibration control are outlined. Many vibration energy harvesting techniques have been developed and are applied into the commercial area. But, the main problem is the energy consumption of active vibration control. The first step to limit this consumption is to use semi-active control, but the energy consumption of control techniques can also be optimized by electromechanical energy harvesters. The combination of these ideas is the main subject of this work.

1.2 Vibration control

The material fatigue, shortening the operation life and also increasing the maintenance cost, is a result of the mechanical vibrations of structure. Consequently, vibration control is an important issue in the mechanical engineering. In various industrial domains such as manufacturing, infrastructure engineering, instrumentation, automotive, aerospace, electronic communications, computer, and other high-technical domains, significant advances have been made in structural control researches to avoid the undesirable vibration problems.

Various methods for vibration control including vibration elimination, vibration isolation and structural modification exist and can be classified such as passive control, active control, semi-active control, hybrid control, etc.

Compared with passive vibration control, active control has been known to provide greater vibration suppression. Nevertheless, due to the needs of the high power drive for the actuator and the complexity of the control system and algorithms, the active control techniques may be expensive. The large number of components leads to a difficult integration. In that context, semi-active vibration control techniques have been proposed to improve the damping performance without using external operative energy.

Regarding tools and materials used to perform the control, one can highlight their variety including viscoelastic materials, silicone rubber for passive control, or electro rheological fluid, shape memory alloys, piezoelectric materials for active and semi active control, and so on.

Nowadays, the piezoelectric materials which has good electromechanical coupling with flexible structures has been widely used for vibration control. Indeed, compared with other materials, piezoelectric material has many advantages for active or semi-active control: wide frequency response range, fast response, maturing and mature production technology to make it easier to achieve with precision high electomechanical coupling with the structure. When they are bonded to flexible structure, and thanks to the piezoelectric effect and inverse piezoelectric effect [1], they can be used as sensors to monitor structural vibration or actuators to act on the structure in order to add damping for example.

In the past decades, many approaches using piezoelectric materials have been developed for vibration suppression in smart structures. One can underline the approaches using piezoelectric shunt which consist in adding simple electronic circuits comprising inductors, capacitors, and resistors. They are simple to design and work without any additional power amplifiers.

1.3 Smart systems

Usually, a smart structure is a mechanical structure provided with a set of actuators and sensors using smart materials, coupled to a controller, as shown in Figure.1.1 [2]. Along with the development of smart structures, smart materials have attracted lots of attentions and have been developed very quickly. Generally, the Smart Materials mainly include shape memory alloys (SMA), magneto-strictive materials, electro-rheological (ER) fluids/magneto-rheological (MR) fluids and piezoelectric materials.

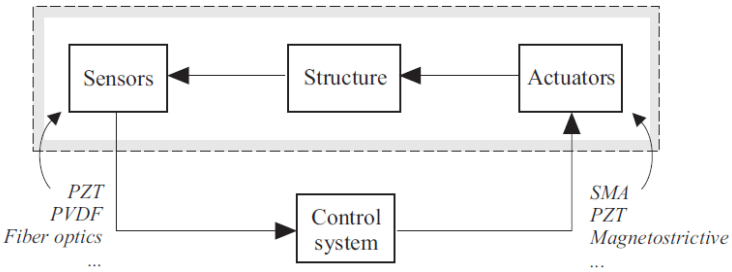

Figure 1.1 Smart structure [2]

1.3.1 Shape memory alloy (SMA)

Shape-memory alloy (SMA) is part of the class of shape memory materials (SMMs). SMA is an alloy that comes back to its original shape when subjected to certain stimulus such as thermo-mechanical. SMA have different shape-memory effects. Two common effects types are one-way and two-way shape memory [3]. Due to its features, this material is a lightweight-elastic-compact and can easily react directly to environmental stimuli. There are many applications in industries including automotive, aerospace, biomedical and robotics [4]. The best known SMA is Nitinol, an alloys of nickel and titanium (NiTi), which is used for most applications due to its stability, practicability and superior thermo-mechanic performance [5].

SMA may be exploited to achieve damping, for low frequency, and low cycle applications such as earthquake protection due to its super-elastic behavior, but they are sparsely used in active vibration control [6] [7].

1.3.2 Magnetostrictive materials

Magnetostrictive materials are ferromagnetic. They can change their shape or dimensions in response to the application of a magnetic field. James Joule [8] identified the effect in 1842, when he was observing a sample of iron. Magnetostrictive materials are used to build actuators and sensors [9] because of their property allowing to convert magnetic energy into kinetic energy, or to convert kinetic energy into magnetic one.

1.3.3 Electrorheological (ER) fluids / magnetorheological (MR) fluids

ER fluids and MR fluids are smart materials with controllable rheological properties, obtained by tuning the intensity of electric field or magnetic field [10][11][12][13]. When an electric field or a magnetic field is applied, the particles can instantly respond by transforming from liquid to chain-like structures which results in enhancement of apparent viscosity and allows increasing the strength of the material within a few milliseconds. When the electric or the magnetic field strength reaches a certain value, the suspension will be solidified and has high yield stress; conversely, the suspension can be liquefied once more by the removal of the applied field. These fea-

tures provide simple, quiet, rapid response interfaces between electronic controls and mechanical systems.

Although there are many advantages of these materials, they are limited in commercial feasibility due to the important volume of operating iron, the expensive cost of producing high-quality fluids, and the difficulty to settling ferro-particles.

1.3.4 Piezoelectric materials

Piezoelectricity was discovered in 1880 by French physicists Jacques and Pierre Curie [14].

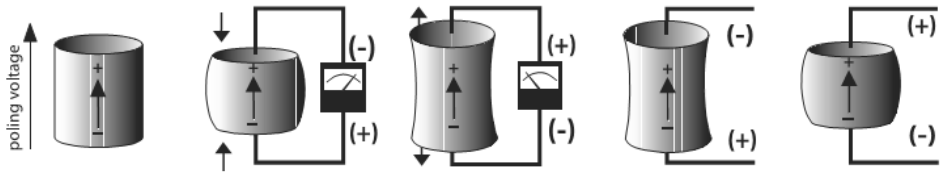

Figure 1.2 Reaction of a poled piezoelectric element to applied stimuli.[15]

The piezoelectric material has two reversible process effects (Fig 1.2): The direct piezoelectric effect which allows to generate an electrical charge resulting from an applied mechanical force. This property allows converting mechanical energy to electrical one. On the contrary, the inverse piezoelectric effect consists to generate a deformation of the piezoelectric element when an electrical field is applied. Piezoelectric materials can exhibit strong coupling between mechanical and electrical energies. Because of these properties, piezoelectric materials has been widely used in vibration control applications [16] [17] [18] [19].

In particular, piezoelectric materials can be used in thin sheet as embedded actuators as well as embedded sensors. For example, piezoelectric actuators are used to add damping to smart structures, while sensors are used to measure structure vibrations.

Among the different type of piezoelectric elements, piezo ceramics such as PZT (piezo zircon titanium) are increasingly used in vibration control as actuator thanks to their high electromechanical coupling coefficient. Piezoelectric polymer such as PVDF (polyvinylidene fluoride) are mainly used as sensors and may be attractive in applications because of its higher tensile strength and lower stiffness.

According to this quick overview of smart materials, we will focus our development on vibration control methods using piezoelectric materi-

als. The description of the piezoelectric effect and modeling of our smart structure are proposed and detailed in chapter 2.

1.4 Vibration control methods using piezoelectric materials

1.4.1 Electromechanical passive techniques

Passive shunt damping technique has several advantages: simple implementation, compact, stable, no external energy, no hardware, low cost... The idea is simple: the converted electrical energy coming from a piezoelectric element is dissipated into electric component (passive or active one). It requires no feedback sensors, any electronics or power supply. This technique offers stability, robustness and performances [15] [20] [21].

The various passive shunt damping techniques are depicted in Figure 1-3[15], and the corresponding techniques are discussed in detail in the following subsections.

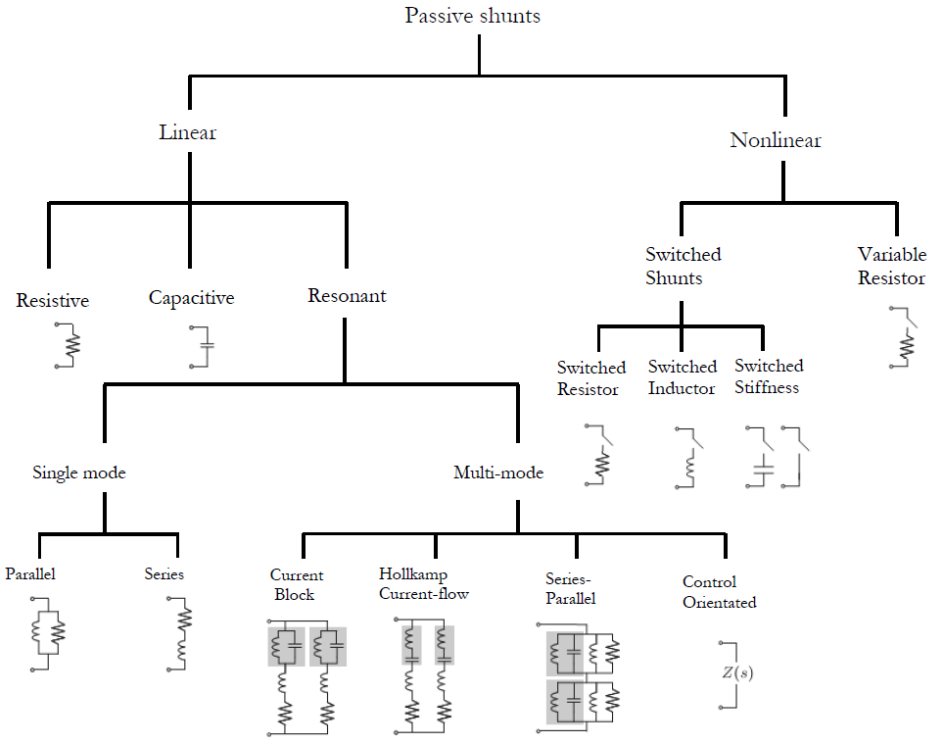

Figure 1.3 Passive piezoelectric shunt damping techniques [15]

The linear shunt damping technique can be defined as any added impedance with a linear current-to-voltage relationship over the bandwidth of interest. On the opposite, non-linear techniques gather adaptive shunts and switched shunts. The impedance can slowly vary such as in adaptive

shunts and shunts implemented by switched-mode amplifier [22]. One can note that the switch and its control law induce non linearity. These techniques are named semi-passive techniques and will be detailed in section 1.4.3.

Resistive piezoelectric shunt circuits

The main idea is to exploit the fact that a resistor R connected between the terminals of piezoelectric elements can dissipate electrical energy thanks to Joule effect. This concept was initially introduced by Forward in 1979.

In 1991, Hagood *et al.*[23] presented a detailed study on this technique of structure damping mechanism based on piezoelectric materials shunted by passive electrical circuits composed of a resistance (figure 1-4). They underline that the damping performances depend on the system electromechanical coupling coefficient. This kind of shunt circuit is simple, and has a low power cost. However, its damping performance is poor.

A multi-piezoelectric element and dispersed resistors to build a piezoelectric shunt circuit are proposed by Lesieutre and Davis [24] in 1998. This circuit can get a better vibration damping in multi-mode, but is limited to few dB.

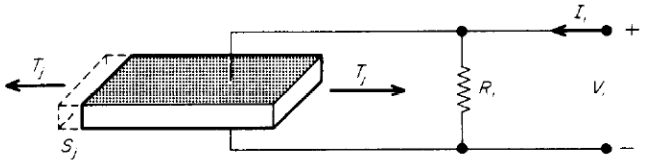

Figure 1.4 Passive piezoelectric shunt on a resistor [23]

Resonant (inductive) piezoelectric shunt circuits

The purpose is to create a resonant circuit using the capacitance of the piezoelectric element with an added inductor L and resistor R. This concept was firstly proposed by Hagood and Wu. This technique can be used into resonant single mode and resonant multi-mode shunts.

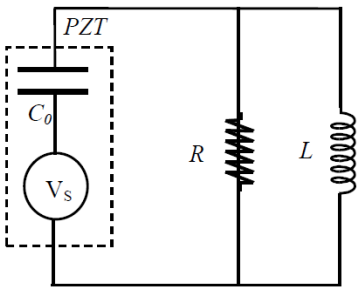

Figure 1.5 R-L resonant shunt in parallel [25]

In the case of resonant single-mode shunt circuit, the circuit is tuned so that the piezoelectric element acts as a damped vibration absorber for only a single mode [25]. The shunt can be a series configuration or a parallel one (as shown in figure 1.5). Similar damping performance are achieved by these two circuits, series and parallel, but the parallel structure is less sensitive to resistance values while series circuit needs optimal value.

For multi-modal vibrations, multi piezoelectric patch bonded on the same structure was proposed, each one used to control a specific mode. Nevertheless, this technique needs a large number of piezoelectric elements leading to an increase of the structure weight. Regarding research using a single piezoelectric transducer for multi-modal vibrations, Hollkamp [26] proposed a new resonant shunt circuit as shown in Figure 1.6 (a). Each branch (Ri, Li) is adjusted to tune one frequency. Nevertheless, tuning the inductor in one shunt branch would interfere with the detuning of the other branch or even the entire shunt circuit.

To solve this difficulty, Wu [27] designed a blocking circuit for multi-mode control, as shown in Figure 1.6 (b). The performance of blocking circuit is slightly better for damping 2 or 3 structural modes, but it becomes very complex for damping more than 3 structural modes.

Behrens [28] developed a circuit for simplifying the implementation of high-order multi-mode shunt circuit, as shown in Figure 1.6 (c). Compared to the circuits proposed by Hollkamp and Wu, this shunt circuit requires less components (resistors, capacitors and inductors) but performs well damping effect on multiple modes. Huge inductance value is the essential drawback of this shunt damping technique. To solve this problem, Fleming *et al.* [29] proposed to place an additional capacitance across the terminals of the piezoelectric element for reducing inductive component, as shown in Figure 1.7. Theoretical analysis and experiments have been presented to justify its effectiveness.

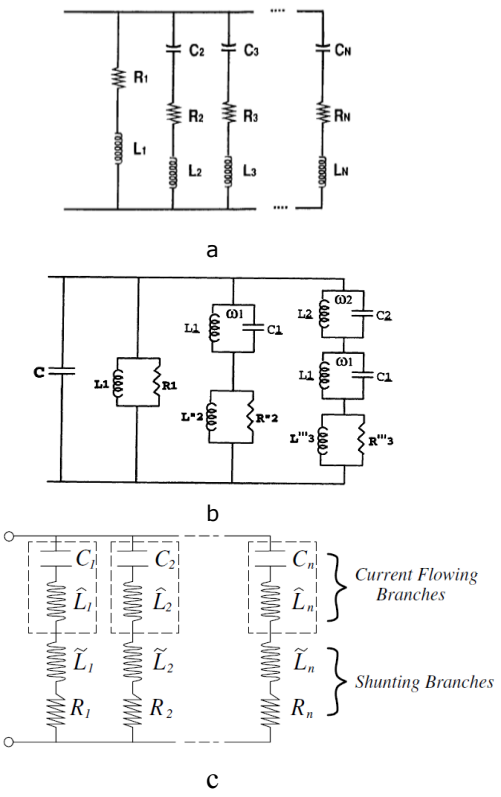

Figure 1. 6 Resonant shunt configurations

a. Generalized multiple-mode shunt circuit by Hollkamp . [26]; b. Modified shunt circuit targeting three modes at ω1, ω2 and ω3 by Wu. [27] ; c. 'Current flowing' multiple mode shunt circuit by Behrens. [28]

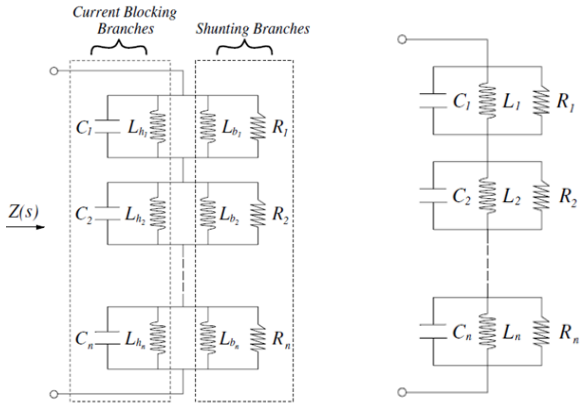

Figure 1. 7 a. Series–parallel impedance structure; b. Simplified circuit [29]

Generally, the damping performance of shunt technique is very sensitive to the variation of the system parameters. Thus, variable shunt ap-

proaches (Hagood), iterative method or optimal tuning (Park) were investigated. Another main disadvantage of passive shunt is that very huge inductor is required to tune low frequency modes. Let's consider the opposite vibration control method: active technique in the next section,

1.4.2 Electromechanical active techniques

Due to rather good adaptability and usually great vibration suppression, active vibration control systems are widely used and viable means for minimizing the vibration of flexible structures. An active structural control system has the basic configuration shown schematically in Figure 1.8 [30]. It consists of sensors to measure either external excitations or structural response variables, controller devices to translate information and compute necessary the needed control force, external sources to produce the required power to actuators.

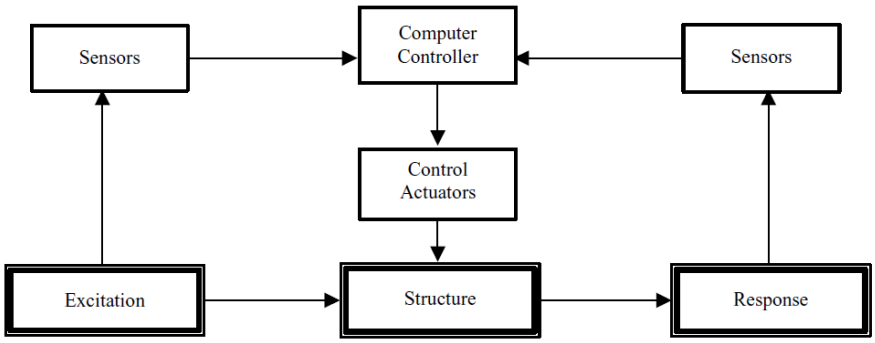

Figure 1. 8 Structure with Active Control [30]

In the past few decades, various methods of active vibration control have been developed. The algorithms utilized can be classified under two general categories: feedback and feedforward active vibration control. Variations of the two general methods exist, each with advantages and disadvantages, as shown in Table 1.1 [31]. In the case of vibration control, modal strategy can be used. This needs descriptions in terms of modal modes or in terms of wave propagation [18][31]. Modal control aims to control the global behavior (i.e. the modes of vibration) of the structure while wave control aims to control the flow of vibration energy through the structure.

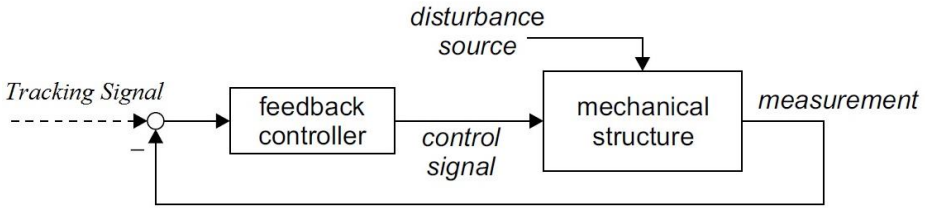

Figure 1. 9 Feedback control [32]

The scheme of feedback control is depicted in Figure 1.9 [32]. Feedback control consists of measuring the output or response of the structure and using these measurements to control the force to apply to the structure to obtain a desired response. An error signal is generated from the comparison of the measurement output of the system with the tracking signal. It is introduced into a feedback controller, and applied to the mechanical structure system thanks to an actuator. The appropriate feedback gains must be determined to induce the sought-after performance without affecting the closed-loop system stability.

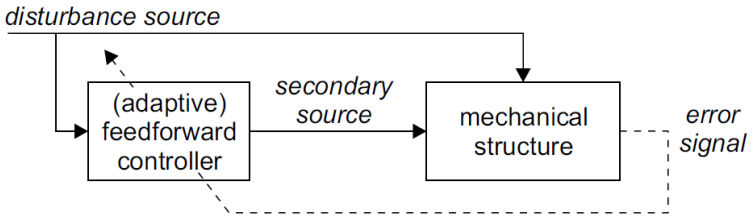

Figure 1. 10 Feedforward control[32]

Feedforward control is a local control based on the knowledge of the disturbances. It can significantly improve the performance by generating a secondary source that effectively cancel the disturbance applied to the system. As shown in Figure 1.10, an adaptive feedforward controller manipulates the signal that is correlated to the primary disturbance and the output is applied to the system by an actuator. The filter coefficients are adapted in such a way that an error signal at one or several critical points is minimized.

The table 1.1 depicts the main advantages and drawbacks of these various approaches.

Table 1.1 Comparison of control strategies [31]

Type of control	Advantages	Disadvantages
Feedback		
Active damping	• Simple to implement and requires fewer computation • Does not require accurate model of the system • Guarante stability when actuators and sensors are collocated	• Effective only near resonance
Model based	• Global method • Requires accurate model of the system • Attenuates all disturbance within the control bandwidth	• Limited bandwidth • Requires low delay for wide bandwidth • Spillover
Feedforward		
Adaptive filtering of reference	• No model is necessary • Robust to inaccuracies in system estimation and to change in system transfer functions • More effective for narrowband disturbance	• Reference / error signal is required • Local method that may amplify vibration somewhere else • Large amount of real-time computations

Active control systems require a large external power source to supply control forces to the system, as well as they need complex system to ensure effectiveness and robustness. So, it is not always possible to use them in many volume and weight limited applications (embedded applications)

1.4.3 Electromechanical semi-active techniques

Semi-active control strategies combine the best of both passive and active control systems while maintaining its simplicity. Semi-active control can modify the global characteristics of controlled system in a desired manner, such as control spring stiffness [33][34] or coefficient of viscous damping [35][36] of the structure, with the smaller external energy required. The other advantages of these techniques are: facility of implementation, compactness, control performance more superior than passive technics and robustness.

The vibration reduction techniques based on the variation of the stiffness of the structure is switched shunt technique: implementation of a switch and components (R, L, C), as depicted in figure 1.3. A simple switch can be realized with a low consumption MOSFET component. Shunt technique don't require power for operation and only small amount of energy for the control part. The control part is basically the switch sequence synchronized with the structure motion.

Davis *et al.* [37] have developed a capacitive shunting technique, which tuned the stiffness of the global system by changing the stiffness of the bonded piezoelectric elements, meanwhile keeping the system damping a constant value. Recently, many researchers worked on this topic because this technic is less sensitive to environmental variations. However, stability according to the change in piezoelectric properties must be increased.

William W. Clark [33][38] improved a state switch damping technique based on switching the shunt circuit of a piezoelectric actuator between open-circuit (high stiffness) and short / resistive-circuit (low stiffness) states. In this technique, initially proposed by Larson in 1994, energy is stored in the actuator from the structure while the actuator is in its high-stiffness state. This energy is dissipated by switching the actuator to its low-stiffness state. The damping effect can be ascribed to the stiffness change between the two switch states.

In addition, a variable-stiffness control was proposed by Onoda *et al.*[39]. In this technique, a second stiffness Δk can be added or canceled to the system thanks to a switch (figure 1.11). The switching timing can be determined by several control laws such as maximum strain law, maximum amplitude law [39] or maximum energy benefit [40].

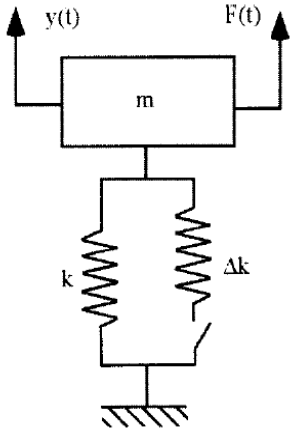

Figure 1.11 Type II mechanical spring

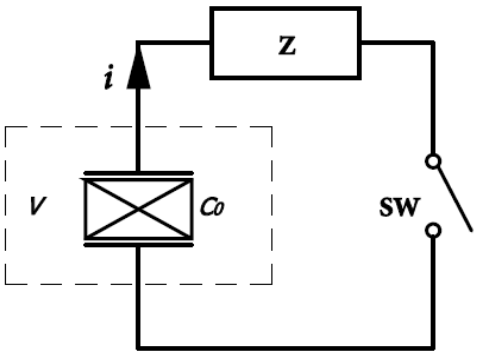

Figure 1.12 A classic circuit for SSD technique

Among all the semi-active vibration control techniques, a particular switching method (Figure 1.12) got great attention in the recent years due to its simplicity and good control ability: that is the Synchronized switch damping (SSD). This nonlinear technique consists of connecting the piezoelectric element to a passive shunt (R and/or L) each time the voltage (or strain) reaches an extremum. No external operative energy is needed. Due to the switching process, the voltage across the piezoelectric element is boosted up and a phase shift between voltage and strain appears, thus creating an energy dissipation and/or conversion.

SSDS

Based on the piezoelectric shunt control technique, Richard *et al.* [35] proposed a semi-active control approach named Synchronized Switch Damping on Short circuit (SSDS) at the end of the nineties. The circuit of SSDS consists of a piezoelectric element, a switch and a small resistor as shown in Figure 1.13.

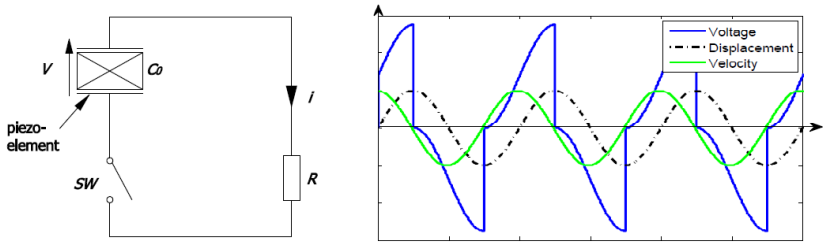

a b

Figure 1.13 The classic SSDS method
a. SSDS circuit; b. SSDS waveforms

Driven by a mechanical excitation, a piezoelectric transducer develops a voltage in phase with the mechanical strain or displacement. In the SSDS technique, a switch is closed a short time period when the displace-

ment reaches an extreme value. And during this switching time, the impedance of this shunt circuit is changing. After the switching time, the voltage follows the strain or displacement again. When the switch is open (OFF state) the electrical energy is extracted from the structure and is stored in the piezoelectric elements as electrical energy. When the switch is closed (ON state), this energy is dissipated in the electrical circuit as joule heat. The mechanical energy of the vibration is finally dissipated into the circuit.

SSDI

Synchronized Switch Damping on Inductor technique (SSDI) is fully described by Richard *et al.* [36]. Compared with SSDS circuit, an additional inductor is added into the circuit, basic implementation is schematically shown on Figure 1.14 SSDI technique (a).

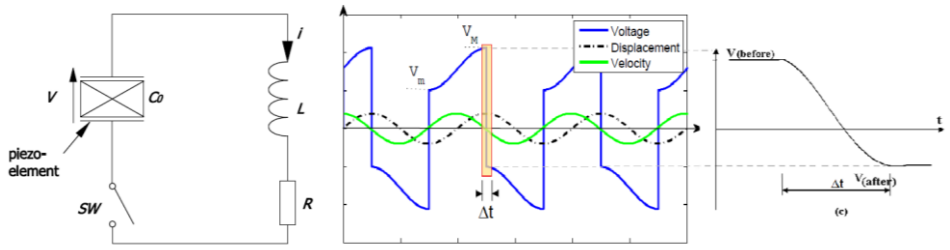

a b c

Figure 1.14 SSDI technique

a. The SSDI electrical circuit; b. Typical waveforms for a sinusoidal excitation; c. The zoom of the voltage oscillation for inversion

When a voltage or displacement extremum occurs, the switch is closed and a voltage inversion is obtained due to an oscillating circuit composed of the piezoelectric element capacitance C_0 and the inductor L. The switching timing (Δt) is equal to a semi-pseudo-period of the electric oscillator, as shown in the Figure 1.14 SSDI technique(c). Since the voltage inversion is not perfect due to the losses in the electrical network, the reversed voltage V_{after} is lower than the voltage prior the inversion V_{befor}.

SSDV

As shown in Figure 1.15, Lefeuvre *et al.* [41] presented a semi-active method named Synchronized Switch Damping on Voltage sources (SSDV) in order to improve the damping effect by artificially enhancing the inversion voltage, especially for systems with low electromechanical coupling. Indeed, the SSDI method which is a voltage inversion method is

more efficient than the SSDS technique which is a voltage cancelation. Thus, improving the inversion quality will improve the damping performances.

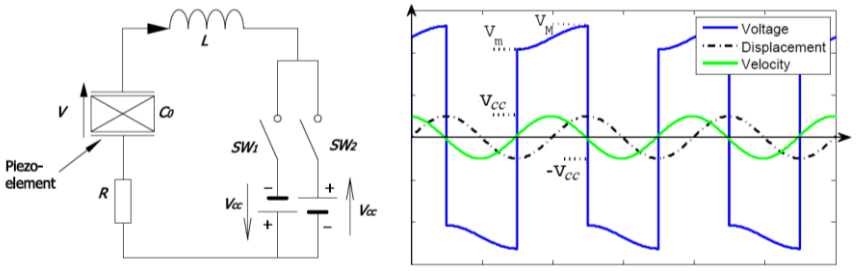

a b

Figure 1.15 The original SSDV method

a. Original SSDV circuit; b. SSDV waveforms

The control strategy of the electronic switches consists in alternatively closing SW_1 and SW_2 as follows: when the maximum displacement occurs corresponding to the maximum voltage, the SW_1 is closed and a pseudo periodic voltage oscillation starts around the voltage $-Vcc$, until opening the SW_1. And inversely when the minimum displacement is reached.

Badel *et al.* [42] developed an enhanced SSDV method, so called SSDV on adaptive voltage sources (SSDVa) in order to solve stability problems. The applied voltage is automatically adjusted and is proportional to the structure deflection, which is represented in Figure 1.16.

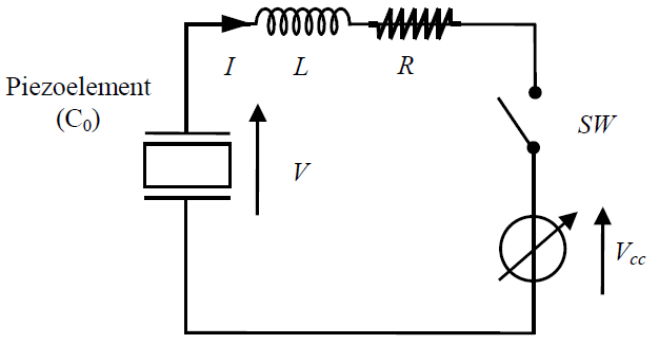

Figure 1.16 Electrical circuit of enhanced SSDV method

Synchronized Switch Damping (SSD) are well-known techniques and a promising compromise between simplicity, external power requirements, vibration control performances and embedded weight. Nevertheless, these solutions show drawbacks in the case of multimodal and complex vibrations, as they need a perfect synchronization of extremum values (voltage

of strain) to achieve a high damping. Local extreme, noise drastically reduces the performance of SSD techniques.

One can note that switches used in SSD techniques can be self-powered. These self-powered SSD controls are based on an envelope detector which is powered by the piezoelectric element. These techniques approaches improve the control performance without any external power supply requirements [43] [44][45].

1.4.4 Semi-active switched shunt control methods for multimodal damping

In the recent years, many researches are focused on the semi-active switched shunt control methods for multimodal damping. Petit *et al.* showed that the performance of SSD method is better than classic passive shunt (RL shunt) to suppress the vibration of a steel cantilever beam under broadband excitation. The main limitation is due to the difficulty to properly define the switching time. To overcome this issue, various specific switch control laws have been developed.

Guyomar *et al.* [46] presented a new probabilistic multimodal control law for the SSD techniques in the case of wide band multimodal excitation. It is based on the measurement of the probabilistic distribution of the piezoelectric voltage. The switch control law to operate the piezoelectric voltage inversion depends on a statistically threshold voltage value. The inversion can occur when the voltage across the piezoelectric element is greater than the threshold voltage value. This value is obtained in an observation time after each voltage inversion so that the probability of observing an inversion is equal to a pre-defined value (chosen by the user). Other laws based on statistics were proposed to define the threshold and to automatically adjust it to the vibration level.

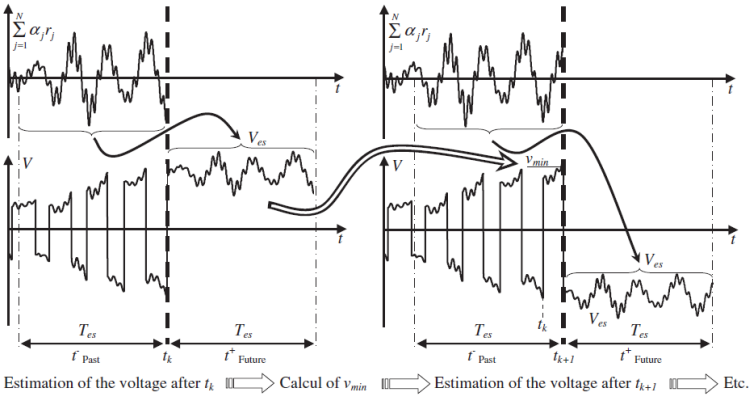

Figure 1.17 Estimation of the piezoelectric voltage after an inversion process [46].

These technics for multimodal damping are promising but require complex algorithm and a proper filtered signal [47]. Another way regarding the control of complex vibrations is based on modal technics. Performances of these technics are quite interesting.

1.4.5 Modal-SSD technique

Based on a modal model and SSD techniques of the controlled structure, the so called Modal-SSDI has been developed [48][49][50] at LaMCoS/LGEF laboratories. This technique consists of synchronizing the switch sequence on a given modal coordinate instead of the voltage. It therefore combines the simplicity, the robustness and low power operation of SSDI techniques, with the possibility of mode targeting and precision of active control strategies.

As shown in Figure 1.18, Harari developed this semi-active method in the case of wide bandwidth excitations. This very efficient technique uses the modal description of structures and concentrates the modal energy on one or several target modes. A modal observer and a controller are used in the proposed method.

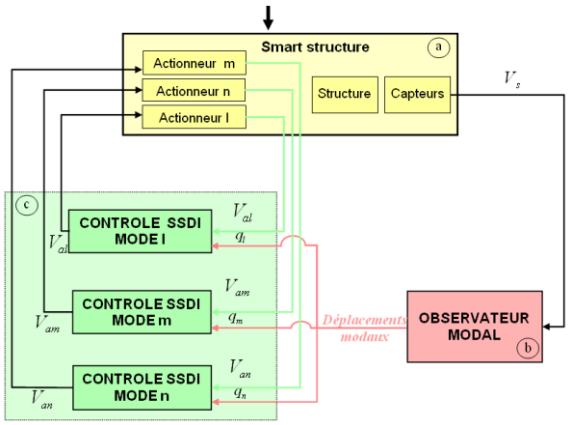

Figure 1.18 Schema of SSDI Modal [48][49][50]

Several variations of this technique have been developed by LaMCoS/LGEF teams:

Hybrid-Active-Modal-SSDI technique [51] consists in using together Modal-SSDI and active control. It leads to performances similar to modal active control while reducing significantly the overall operative energy, which results in lower power requirements and size reduction of the active control amplifiers.

The SSDI-Max method [52][53] derived from Modal-SSDI was developed to improve the damping performance by the maximization of the self-generated voltage amplitude using an enhanced switching sequence relying on both the desired modal coordinate and the voltage signals.

The work presented in this thesis will be mainly based on these modal approaches and a more detailed description will be presented in the next chapters.

1.5 Vibration energy harvesting technology based on the effect of electromechanical conversion

The use of conversion mechanism to harvest electrical energy from various ambient sources has been studied for many years [54]. The researches about energy recovery technology in mechanical vibration indicate that generated power reaches generally micro-watts or milli-watts level, it is usually enough for micro-power systems [55]. Existing studies about vibrational energy harvesting technology can be divided into three transduction types [56] [57]: (1) electro-magnetic: using electric and magnetic transducers; (2) electrostatic converter: the basis of electrostatic energy conversion is the variable capacitor. This generator consists of two conductors separated by a dielectric (i.e. a capacitor), which move relatively are to one another; (3) piezoelectric converter: using the piezoelectric effect of the piezoelectric material to convert mechanical energy to electrical energy.

In the case of vibrations of mechanical structures, the scavenged energy density is about 335 $mJ.cm^{-3}$ for piezoelectricity, around $44mJ.cm^{-3}$ using electrostatic principle and around 400 $mJ.cm^{-3}$ with electromagnetics transducers [58]. These values are maximal theoretical values. Classic current values are around 20% of these maximum.

Piezoelectricity offer a good energy density, an easy integration and a large range of available materials. Electrostatic transducers harvest less energy than the two other principles in a macroscopic level but they are the easiest to integrate and compatible with MEMS technologies. The main disadvantage is the necessity of high voltage (>100 V) to polarize the structure leading to hybrid structure combining electrostatic and electret for example. Electromagnetic transducers scavenge an interesting amount of energy on the macro-scale but their integration is not easy mainly due to the use of an inductor leading to size issue and loss issue (resistance) for ambient frequencies. One can also underline that resonant transducers are well adapted when the excitation frequency is well known. When it is not the

case, broadband or adaptive system can be designed. To scavenge 10 μW at ambient frequencies, the transducers can have mill metric size. Because piezoelectricity is a direct effect and exhibits interesting energy densities as well as an easy integration into a system [59] [60], we will focus on these transducers in the following part of this work.

1.5.1 Energy harvesting technology

To improve the efficiency of energy harvesting, not only the structure or materials of the piezoelectric vibration energy recovery system should be optimized, but the interface circuits also. Indeed, they allow the energy to be removed from the piezoelectric elements and transferred to the energy storage elements in a more efficient way and form.

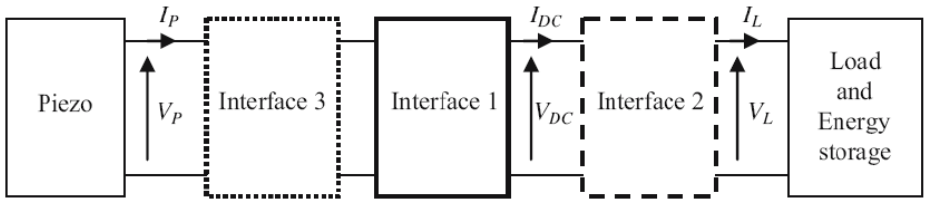

Figure 1.19 The general structure of the power conversion schematic diagram

Lefeuvre [61] proposed a power conversion chain with three different interfaces, as represented on Figure 1.19. This first "Interface 1" conversion is realized by an AC–DC converter, such as a diode bridge rectifier, which rectifies the alternate voltage generated by piezoelectric element to a direct current to be used or stored. The "Interface 2" ensures the maximal power point tracking of the device composed of the electromechanical structure and interface 1, which can be for example implemented using a DC-DC converter [62] [63]. An additional "Interface 3" can be used for increasing the power produced by the piezoelectric element, by performing a non-linear treatment on the piezoelectric element voltage [64] [65] [66][67] [68][69].

Regarding interface 1 and 2, various topologies have been proposed. Kim *et al.* [70] studied cymbal piezoelectric energy recovery system using a standard energy storage circuit and a standard interface (full bridge rectifier and charging capacitor). Han *et al.* [71] developed a highly efficient energy conversion interface circuit in two parts: a rectifier and a DC-DC converter which constitute the two interface circuits. Through theoretical analysis and experimental testing, energy recovery efficiency increase by 400% than standard interface circuit. Ottman and Lesieutre [64] [72]

studied a step-down voltage converter interface circuit. The buck converter efficiency was in the range of 70% with different amplitudes of the exciting force, shown in Figure 1-20. The experimental results show that the converter makes increase the harvested power by approximately 325% than standard interface circuit.

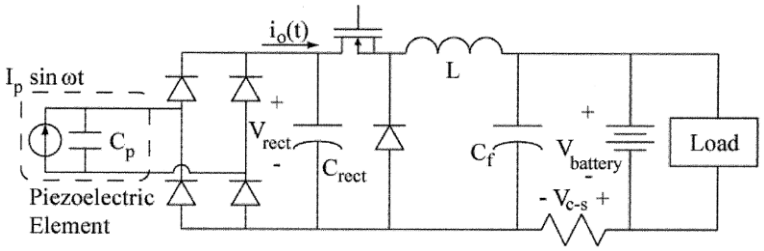

Figure 1.20 Energy harvesting circuit

Lefeuvre *et al.* [72] studied a low consumption Buck-Boost converter interface circuit. A 4.8V rechargeable battery can be efficiently charged between 1.6-5.5V and the efficiency was up to 84%. Shenck *et al.* [73] studied a DC-DC converter based on forward-switching in order to improve the amount of harvested energy. The experimental results underline an harvested power up to 1.3 mW with an efficiency up to 17.6%, as twice as originally designed (linear switching converters). One can note that Ottman *et al.* [64] [72] indicated that the optimal value of duty cycle of step-down converter is related to the exciting force amplitude. And Ammar *et al.* [74] use an adaptive algorithm to optimize the duty cycle of the converter, to improve the efficiency of energy harvesting circuit.

Regarding interface 3, Guyomar *et al.* [65] developed a new electronic interface circuit to enhance power extraction using non-linear treatment. It is called Synchronized Switch Harvesting on Inductor (SSHI). This approach was derived from the so-called Synchronized Switch Damping (SSD). It is shown that the electrical harvested power can be increased by as much as 400–900% over the standard technique.

Lefeuvre and Badel *et al.* [66] [67] [68] [69] proposed SSHI parallel/SSHI series technique. The block diagram is shown in Figure 1.21 (b),(c).

The basic principle is composed of a non-linear processing circuit (composed of an inductor *L* in series with an electronic switch *S* connected in parallel/series with the piezoelectric element, and a rectifier bridge. Most of the time, the piezoelectric element is in open circuit configuration. The electronic switch is briefly turned on when the mechanical displacement reaches maximum or minimum value. The energy stored in the piezoelec-

tric element is transferred to the storage capacitors through the rectifier bridge.

In subsequent studies, Lefeuvre and Guyomar *et al.* [75] [66] [68] compared SSHI parallel/series technique with SECE technique in two different cases of operation: the power generator is first driven with constant force amplitude, and then it is driven with constant displacement amplitude. Theoretical and experimental results show that the four techniques have the same maximum harvested power when there is constant force amplitude. Under the constant displacement amplitude, standard interface requires an impedance adaptation of the terminal electric load. Theoretical and experimental results presented show that with an optimized impedance adaptation of the terminal electric load R_L, Parallel-SSHI and the Series-SSHI reach a power gain of 15 by comparison with the standard technique and the factor gain is 4 for the Synchronous Charge Extraction technique (SECE), as shown in Figure 1.22.

One can note that Parallel-SSHI and Series-SSHI, dramatically increase the harvested power in the case of weakly coupled systems or in the case of non-resonant systems.

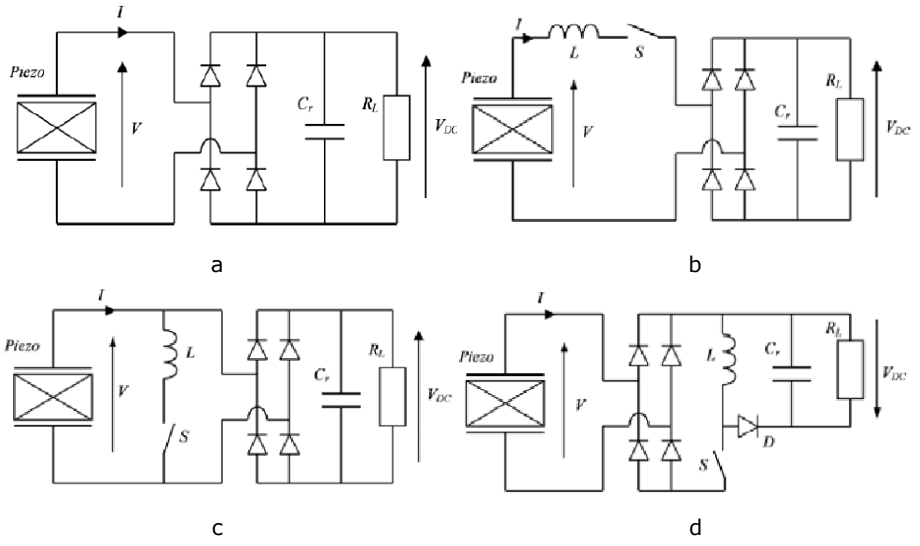

Figure 1.21 SSHI Energy harvesting interface circuit
a. Standard interface circuit; b. Series-SSHI interface circuit;
c. Parallel-SSHI interface circuit; d. Synchronous charge extraction interface circuit

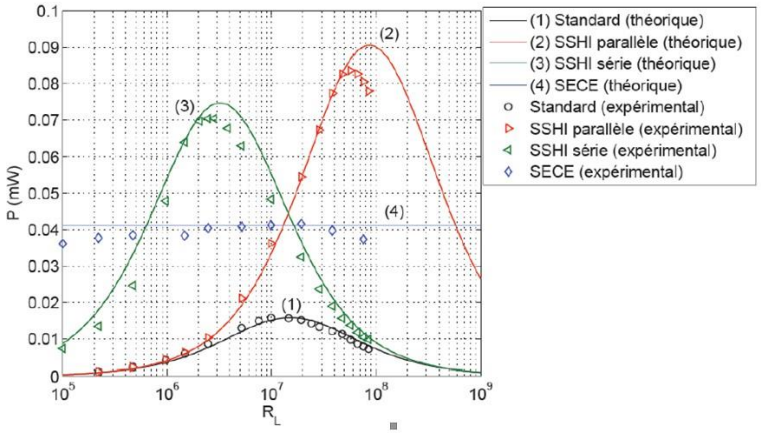

Figure 1.22 Harvested powers using different techniques

Lallart *et al.* [76] presented DSSH (Double Synchronized Switch Harvesting that two simultaneous switching energy recovery) technology interface circuit to optimize the energy harvesting efficiency, shown as in Figure 1.23. It has been theoretically and experimentally proved that in the DSSH technique, the load of subsequent circuit has no relationship with the harvested power. An intermediate switching stage ensures an optimal harvested power whatever the load connected to the microgenerator.

In addition, this technique reach power gain of more than 500% in terms of harvested energy compared with the standard energy harvesting technique. This technique is still developed and studied, we can cite for example, Lefeuvre *et al.* [61], who proposed the use of Ericsson thermodynamic cycle, which optimizes the electrical power flow from piezoelectric devices to energy storage elements.

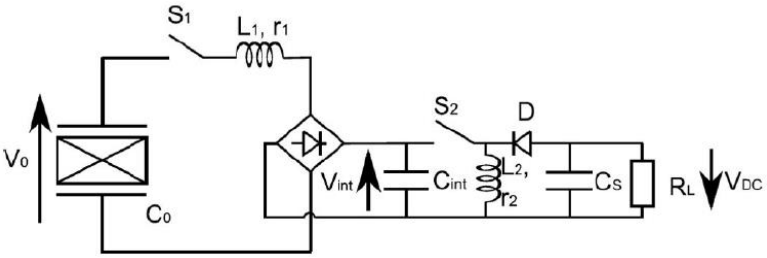

Figure 1.23 DSSH interface circuit

Shen *et al.*[77] developed a new self-powered technique to optimize energy harvesting by using piezoelectric microgenerators called Enhanced Synchronized Switch Harvesting (ESSH). This technique is based on the concept of DSSH, with the same energy extraction circuit but a different control switch strategy. Compared with the standard technique, a harvested power gain of more than 300% is achieved in the same vibration

condition. ESSH technique also ensures an optimal harvested power whatever the load connected to the micro-generator. Furthermore, this technique can be truly self-powered; thanks to a start-up system connected to a second piezoelectric element, a self-powered circuit which implements the technique is proposed.

1.5.2 Energy transferring technology

The energy harvesting techniques have experienced a great development over the last decades. As a result, a vibration damping system powered by harvested energy using piezoelectric elements have been studied in the past few years.

Li *et al.* [78] proposed a SSDET circuit to harvest energy on one structure and to transfer this energy to a second one (the targeted one) thanks to an intermediate simple electrical circuit, as shown in Figure 1.24.

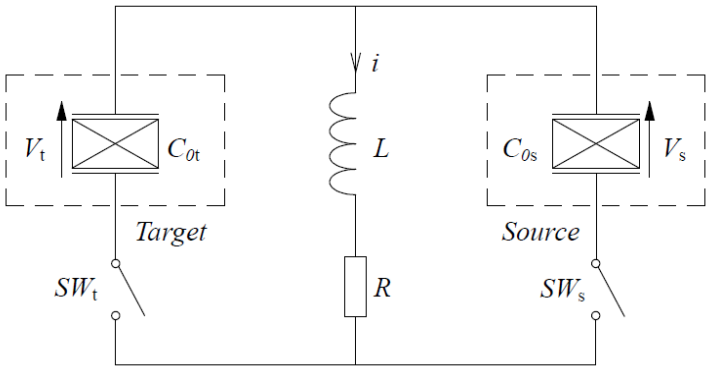

Figure 1.24 SSDET interface circuit

When an inversion is needed on the target structure, the switch S_{Ws} is firstly closed. The voltage across the second piezoelectric (called source in figure 1.24) drops until it reaches zero. The current in the inductor increases. Then after a quarter of oscillating period of the RLC_{0s}, the switch SW_s is opened and the switch SW_t is closed. The inversion across the piezoelectric element on the target structure is thus reinforced thanks to the initial current flowing through the inductor. After half a period of the oscillating circuit RLC_{0t}, the switch SW_t is opened. Figure 1.25 shows the variations of the voltage and current of SSDI and SSDET techniques during the closing of the switches.

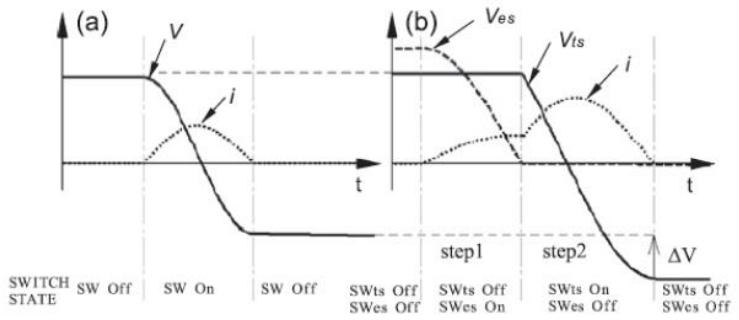

Figure 1.25 Comparison between SSDI and SSDET techniques
a. SSDI waveforms; b. SSDET waveforms

The main drawback of this concept is that two different structures are used and that it is impossible to synchronize both sides.

Wu *et al.*[79] developed a global approach based on global energy redistribution by means of a network of piezoelectric element, so called ¨SSDT, SSDD network ¨. Various topologies and chosen the scavenge energy on low frequency modes (mode 1 to 3) are studied to increase the damping effect of a high frequency mode (mode 4). All the piezoelectric elements are bonded on the same plate and the structure is excited by a multi-sinusoidal source or by a pulse. This technique is a modal technique that requires a modal observer and a modal model of the structure. The various switches are closed on extremum of modal quantities (q_1 to q_4) or on the sum of the modal quantities. Figure 1.26 presents one of the best promising circuit.

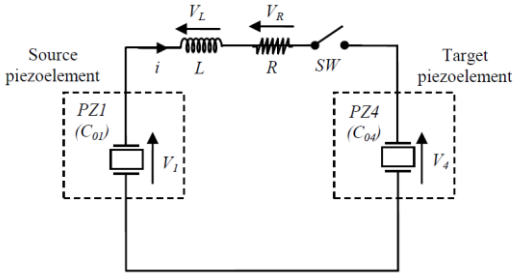

a

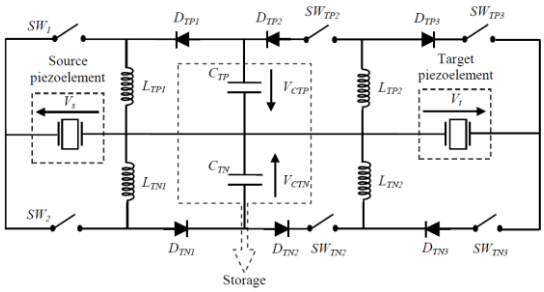

b

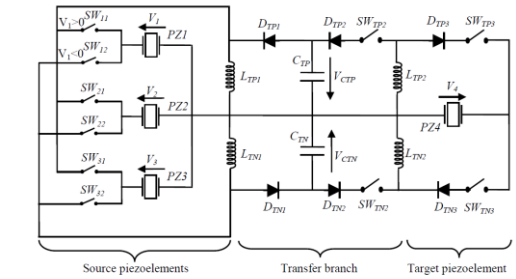

c

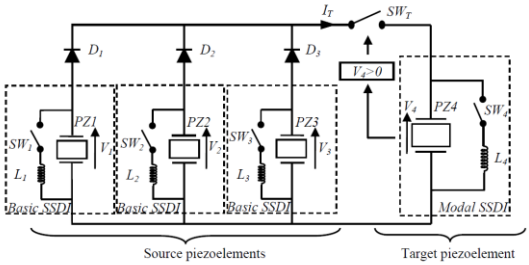

d

Figure 1.26 Schemes of different techniques [79]

a. Basic SSDT1; b. Scheme of the basic SSDT3; c. Extended SSDT3; d. Extended SSDD

For a multi-sinusoïdal excitation, the damping performances of the network strongly depend on the energy distribution between modes. The damping improvement can get up to 18 dB even with a piezoelectric element weakly coupled, but with an amount of energy on source modes (ES) at least six times greater than the one available on the target mode (ET). Figure 1.27 presents a comparison of the damping performance of various topologies.

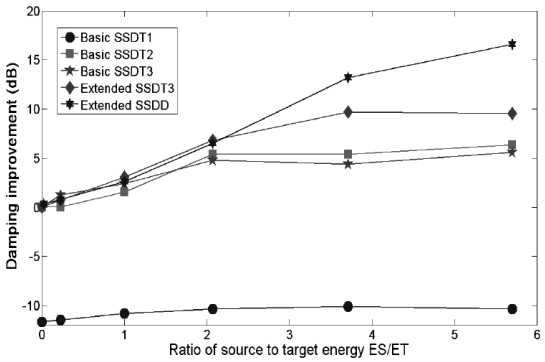

Figure 1.27 Damping performance of various SSDT and SSDD topologies

For pulse excitation, the damping performance drops: only 2.3 dB to 4.3 dB is added compared to a standard modal SSDI technique. With a

noise excitation, compared to Modal-SSDI method, a damping improvement of 2.4 dB is obtained for extended SSDT-case3.

The main drawbacks of this relevant study are (1) the fact that the target mode is a high frequency mode. In practical cases, most of the time, it is a low frequency mode that the control must focus and (2) the fact that the source modes must enclose a large amount of energy to target high damping value on the targeted mode.

1.6 Research questions and organization of this thesis

The object of the research work described here is to develop an approach that enhances the damping effect of a smart structure with the minimal output energy.

In the previous sections, we have introduced and summarized various structure control technique. For embedded structures using a piezoelectric element as actuator, the energy required is high making active control is delicate and semi-active techniques useful. Indeed, active control needs are external source while semi-active control can extract itself the required energy from the structure. Damping performance of semi-active technique based on Synchronized Switch Damping (SSD) is less than the one obtained thanks to active control. SSD technique remain promising compared to passive technique and can be used to aim specific modes thanks to a modal approach. Figure 1.28 classify all the techniques in according to their performance in terms of damping and their operative energy.

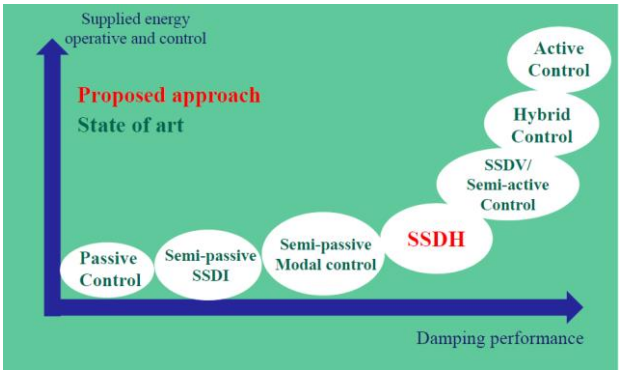

Figure 1.28 Performances of control strategies

There is clearly a need for innovative technique with enhanced performances compared to classic modal SSDI but with low operative ener-

gy. To do that, our research will focus on approaches that enhance the damping performances by energy transfers between modes in the same structure with piezoelectric transducers.

One can note that in real cases, structures and systems suffer multi-sinusoidal excitation, noise or pulse. As discussed previously, a promising way to ensure a robust and performing damping even with complex vibration is the modal approach. Thus, in this thesis, control strategy is based on modal control technique for applications in multimodal case with complex excitation.

As the damping attenuation can be improved thanks to energy transfer, the aim is to maximize the power transfer between modes on a same structure: energy is harvested on non-controlled mode to increase the damping of a target mode, as shown in Figure 1.29.

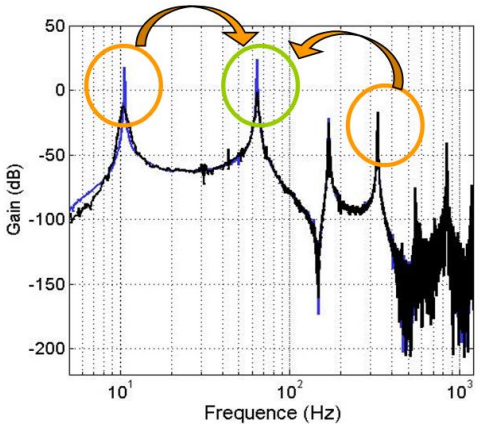

Figure 1.29 Concept of the research: energy transfer between modes

This concept was firstly proposed by Wu but applied to some specific cases (mode 4 is targeted with a lot of energy on the other modes). The purpose here is to increase the damping of a low frequency mode (as mode 1 for example) thanks to the energy of the other modes but in realistic configurations in terms of energy distribution. For that, we will choose an experimental and a current case which will be the thread of this work.

Various scientific questions and challenges are addressed in this thesis:

1. How to use a piezoelectric element to harvest energy or control vibration?
2. How to design a self-powered efficient interface circuit to transfer the energy between modes? Or: How to recover mechanical energy from the uncontrolled modes and use this energy to create a better damping on the targeted mode?
3. How to implement this power self-supplied interface circuit to realize energy transfer between modes?

The outline of this thesis is as following.

Chapter 1: Introduction
In this first chapter, we will introduce the current techniques of vibration control, energy harvesting, and energy transferring.

Chapter 2: Smart Structure
The objective of this chapter is to construct a modal model of our smart structure thanks to experimental identification. All the simulation works will be done according to that realistic and current model: it's our thread.

Chapter 3: Energy transfer between modes – Damping circuit
In this chapter, the idea of a new vibration modal control technique named Modal *SSDV on Capacitor* (Modal *SSDVC*) is firstly proposed. Two different behaviors are modeled: constant voltage or discharge of a capacitor. The electrical circuit and the associated control law are presented. The aim is to add energy during the inversion process occurring on the piezoelectric element in order to enhance the vibration damping.

Chapter 4: Energy transfer between modes – Harvesting circuit
In this chapter, four energy harvesting techniques are proposed to obtain the needed energy that will be used to enhance the control performances of the *SSDVC* circuit presented in chapter 3.

Chapter 5: Global architecture SSDH: simulation and discussions
This chapter focuses on the global architecture that links modal control and modal harvesting circuits to realize our self-powered vibration control. This architecture will be called Modal Synchronized Switching Damping and Harvesting (Modal *SSDH*) which represents the main originality of this work. The electrical circuit and the control laws will be introduced to explain how the mechanical energy can be transferred between different modes of one structure to achieve damping effect on a target mode.

Chapter 6: Other SSDH operating modes
The objective of this chapter is to present other new control functions of our SSDH circuit, and to understand each control technique though simulation implements. These variants of Modal *SSDH* controls introduce different control laws of the switches, leading to various performances of our Modal SSDH.

Chapter 7: Conclusion

This chapter presents the main conclusions of the thesis work, as well as a discussion in the light of the original requirements that have been formulated at the beginning of the self-powered combinative techniques.

2 Smart Structure

2.1 Introduction

The main goal of this work is to damp the vibration of target modes helped by the harvested energy from other modes. To achieve this goal, the research work of this thesis is to provide a link between the modal energy harvesting techniques and the modal vibration control techniques.

The objective of this chapter is to construct a model to carry out this research and to provide an experiment model for the simulation works. This model takes into account the structure with its piezoelectric elements. The necessary data are issued from direct measurements and identification methods. These parameters are the mechanical characteristics, the electromechanical coupling coefficients of the piezoelectric elements and the modal damping factor.

The basic model of the smart structure is presented in section 2.1. The identification of the parameters are explained in section 2.2. The real structure will be presented in section 2.3.

2.2 Model of the smart structure

2.2.1 Behavior law of piezoelectric effect

The piezoelectric material has two reversible process effects: direct effect and inverse effect. The mathematical constitutive equations are issued from thermodynamics and are used to describe the constitute law of piezoelectric material in particular the coupling effect.

$$\begin{cases} D_m = d_{im} T_i + e_{ik}^T E_k \\ S_i = s_{ij}^E T_j + d_{mi} E_m \end{cases} \tag{2.1}$$

where the indexes i, j = 1, 2,…, 6 and m, k = 1,2,3 refer to different directions within the material coordinate system and where the terms of the constitutive equations are summarized in **Erreur ! Source du renvoi introuvable.**1.

Table 2.1 Summarized terms of the constitutive equation

Matric symbol	Matric symbol	Dimension(line×column)
S	Material strain	6×1
D	Electric displacement (*C/m²*)	3×1
T	Material stress (*N/m²*)	6×1
E	Electric field (*V/m*)	3×1
s^E	Elastic compliance (*m²/N*)	6×6
d	Piezoelectric strain constant (*C/N*)	3×6
ε^T	Permittivity of the material (*F/m*)	3×3

In matrix form, these equations can be written as:

$$\begin{bmatrix} D_1 \\ D_2 \\ D_3 \end{bmatrix} = \begin{bmatrix} 0 & 0 & 0 & 0 & d_{15} & 0 \\ 0 & 0 & 0 & d_{15} & 0 & 0 \\ d_{31} & d_{31} & d_{33} & 0 & 0 & 0 \end{bmatrix} \begin{bmatrix} T_1 \\ T_2 \\ T_3 \\ T_4 \\ T_5 \\ T_6 \end{bmatrix} + \begin{bmatrix} \varepsilon_{11}^T & 0 & 0 \\ 0 & \varepsilon_{11}^T & 0 \\ 0 & 0 & \varepsilon_{33}^T \end{bmatrix} \begin{Bmatrix} E_1 \\ E_2 \\ E_3 \end{Bmatrix} \tag{2.2}$$

and

$$\begin{Bmatrix} S_1 \\ S_2 \\ S_3 \\ S_4 \\ S_5 \\ S_6 \end{Bmatrix} = \begin{bmatrix} s^E_{11} & s^E_{12} & s^E_{13} & 0 & 0 & 0 \\ s^E_{12} & s^E_{11} & s^E_{13} & 0 & 0 & 0 \\ s^E_{13} & s^E_{13} & s^E_{33} & 0 & 0 & 0 \\ 0 & 0 & 0 & s^E_{44} & 0 & 0 \\ 0 & 0 & 0 & 0 & s^E_{44} & 0 \\ 0 & 0 & 0 & 0 & 0 & 2(s^E_{11}-s^E_{12}) \end{bmatrix} \begin{Bmatrix} T_1 \\ T_2 \\ T_3 \\ T_4 \\ T_5 \\ T_6 \end{Bmatrix} + \begin{bmatrix} 0 & 0 & d_{31} \\ 0 & 0 & d_{31} \\ 0 & 0 & d_{33} \\ 0 & d_{15} & 0 \\ d_{15} & 0 & 0 \\ 0 & 0 & 0 \end{bmatrix} \begin{bmatrix} E_1 \\ E_2 \\ E_3 \end{bmatrix} \tag{2.3}$$

Furthermore, the superscripts *E* and *T* specify that the corresponding characteristics are given with constant electric field (volts/meter) and constant stress (force/area), respectively.

These expressions underline the coupling effect between electricity and mechanic into a piezoelectric element: equation (2.2) shows that a part of the electrical field applied to the material is converted into mechanical stress. Likewise, equation 2.3 shows that a part of the mechanical strain applied to the material is converted into electrical field.

In the absence of electric field E, equation (2.3) is $S=s^E T$ which is basically Hooke's law. And also, in the absence of mechanical stress, the equation (2.2) is $D=\varepsilon^T E$, which only describes the electrical behavior of the material (insulator).

The matrix d represents the direct piezoelectric effect (d_{im}) and the converse piezoelectric effect (d_{mi}).

The energy conversion occurring into a piezoelectric element is proportional to the strain. The efficiency of conversion is mainly dependent on the piezoelectric strain coefficients: d_{31}, d_{33}, d_{15}. In most of piezoelectric materials, d_{15} is the largest coefficient, but it is more difficult to realize a d_{15} mode device. Thus, the two different d_{31} and d_{33} modes are generally used in piezoelectric material which are illustrated in **Erreur ! Source du renvoi introuvable.**1. The x, y, and z axes are labeled as 1, 2, and 3.

Piezoelectric material can operate in the 33 mode, which means that both the electric field and stress act in the 3 direction. However, the material possesses the 31 mode of transduction in which the electric field acts in the 3 direction (i.e. the material is poled in the 3 direction), and the mechanical stress/strain acts in the 1 direction. Therefore, the 31 mode condition is generally used for the bending of a cantilever, and the 33 mode is applied in cases of direct loading, such as impactor with stack transducers.

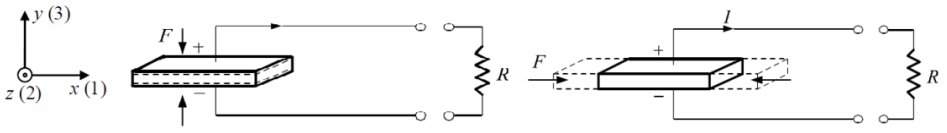

a b

Figure 2.1 Illustration of 33 mode and 31 mode operation of piezoelectric material. a.33mode ; b. 31mode

In this research work, we want to apply all our news technique to a simple and efficient structure. For that purpose, we choose an academic structure: a cantilever, namely a clamped-free beam. Piezoelectric transducers (actuators and sensors) will be bonded onto the structure in strategic locations, as describes in the next sections. One can note that in generator mode (conversion of mechanical energy into electrical one), higher current can be generated form the cantilever structure under a 31 mode, because the deformation of the piezoelectric material is maximized. Thus, in our work, we select the simplest cantilever structure with piezoelectric element under a 31 mode, as shown in Figure 2.2.

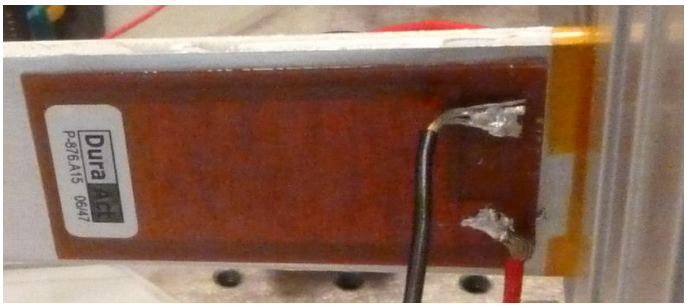

Figure 2.2 Photograph of the piezoelectric element

2.2.2 Electromechanical model of our smart structure

The electromechanical principle of a vibrating structure can be described as a single degree of freedom (DOF) oscillator. In the following section, this representation is used as a reference, considering this DOF as a mode. Indeed, if the mechanical structure vibrates with a linear behavior on a single mode, the electromechanical system can be represented by an equivalent model: mass+piezo+spring+damper, as shown in **Erreur ! Source du renvoi introuvable.**3.

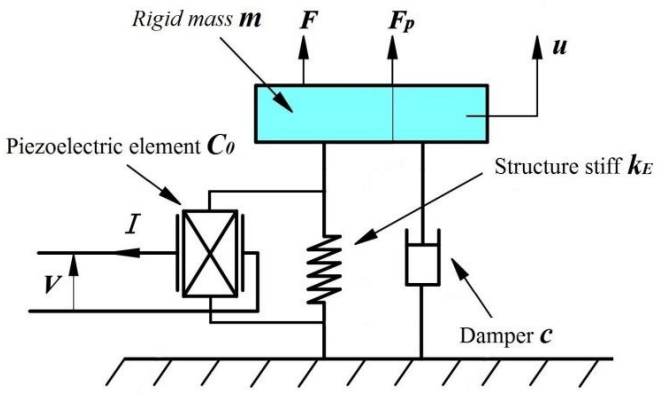

Figure 2.3 Schematic representation of the electromechanical model

By using the equivalent values of the mass m, damping c, and stiffness k^E when the piezoelectric elements are short-circuited, the force equilibrium equation of this system can be expressed as:

$$m\ddot{u} + c\dot{u} + k^E u = F - F_p \tag{2.4}$$

Here, u is the displacement, F is an external force applied to the structure. F_p is the issue from the piezoelectric elements and applied on the structure, given by:

$$F_p = -\alpha V \tag{2.5}$$

$$I = \alpha \dot{u} - C_0 \dot{V} \tag{2.6}$$

where I is the outgoing current from the piezoelectric elements, C_0 is the capacitance of the piezoelectric element, α is the electromechanical coupling of piezoelectric material and V is the voltage across the piezoelectric element.

Integrating over the time variable and multiplying both terms of Eq. (2.4) by the velocity $\dot{u}$, the energy equation could be written as Eq.(2.7):

$$\int m\ddot{u}\dot{u}dt + \int c\dot{u}^2 dt + \int k^E u\dot{u}dt + \int \alpha V\dot{u}dt = \int F\dot{u}dt \tag{2.7}$$

The provided energy $\int F\dot{u}dt$ is distributed into kinetic energy, potential energy, mechanical energy losses and transferred energy.

The integration over a finite number of periods in the steady state leads to Eq.2.8:

$$\left[\frac{1}{2}m\dot{u}^2\right]_0^T + \left[\frac{1}{2}k^E u^2\right]_0^T + \int_0^T c\dot{u}^2 dt + \int_0^T \alpha V\dot{u}dt = \int_0^T F\dot{u}dt \tag{2.8}$$

If we consider as initial conditions that the displacement u and velocity $\dot{u}$ are zero, Eq.(2.8) leads to Eq.(2.9). The structure energy terms are defined in the Erreur ! Source du renvoi introuvable.**2.**

$$\frac{1}{2}m\dot{u}^2 + \frac{1}{2}k_E u^2 + \int_0^T c\dot{u}^2 dt + \int_0^T \alpha V\dot{u}dt = \int_0^T F\dot{u}dt \tag{2.9}$$

Table 2.2 Structure Energy terms

Definition	Energy
$E_f = \int_0^T F\dot{u}\,dt$	Supplied Energy
$E_K = \frac{1}{2}m\dot{u}^2$	Kinetic Energy
$E_P = \frac{1}{2}k_E u^2$	Potential elastic Energy
$E_V = \int_0^T c\dot{u}^2\,dt$	Viscous damping Energy
$E_S = -\int_0^T \alpha V\dot{u}\,dt$	Transferred Energy

The transferred energy $\int \alpha V\dot{u}dt$ corresponds to the part of the mechanical energy which is converted into electrical one.

The transferred energy is also called converted energy or extracted energy. This energy (Eq. 2.10) is the sum of the electrostatic energy stored in an

electrical element (piezoelectric capacitor C_0) and the energy dissipated in the electric circuit connected to the piezoelectric element (dissipated in the circuit by joule effect).

$$\int \alpha V \dot{u} dt = \frac{1}{2} C_0 V^2 + \int V I dt \tag{2.10}$$

2.2.3 Model analysis

2.2.3.1 Modal approach

The modal approach is based on the hypothesis that the structure displacement u can be represented by a linear summation of m modal displacements q_i. The modal displacement vector $\vec{q}$ which is related to $\vec{u}$ by using the transfer modal matrix Φ, of the structure according to Eq.(2.11).

$$\vec{u}(t) = \Phi \vec{q}(t) \tag{2.11}$$

where

$$\Phi = \left[\vec{\Phi}^{(1)} \quad \vec{\Phi}^{(2)} \quad . \quad . \quad . \quad \vec{\Phi}^{(m)} \right] \tag{2.12}$$

$$\vec{q}(t) = \begin{Bmatrix} q_1(t) \\ q_2(t) \\ . \\ . \\ . \\ q_m(t) \end{Bmatrix} \tag{2.13}$$

According to Eq.(2.11), the previous dynamical equations Eq.(2.4) and Eq. (2.6) can be transformed as:

$$m\Phi \ddot{\vec{q}} + c\Phi \dot{\vec{q}} + k^E \Phi \vec{q} = \vec{F} - \alpha V \tag{2.14}$$

$$I = \alpha \Phi \dot{\vec{q}} - C_0 \dot{V} \tag{2.15}$$

Multiplying the Eq. (2.14) and (2.15) throughout by Φ^T, the structural and electrical behaviors become:

$$M\ \ddot{\vec{q}} + C\ \dot{\vec{q}} + K^E \vec{q} = \Phi^T \vec{F} - \theta V \tag{2.16}$$

$$I = \theta^T \dot{\vec{q}} - C_0 \dot{V} \tag{2.17}$$

with the modal electromechanical coupling matrix θ defined as:

$$\theta = \Phi^T \alpha \tag{2.18}$$

and where, M, C, K^E are the generalized modal mass, generalized modal damping coefficient and generalized modal short circuit stiffness coefficient of the structure respectively.

2.2.3.2 State space Model

Assuming that there is no mechanical or electromechanical coupling effect between modes and the damping is weak, the three matrices *M, C,* K^E are diagonal.

This condition allows writing the dynamic behavior and observation equations of a structure with *n* piezoelectric patches as:

$$M_{mm}\ddot{q}_m + C_{mm}\dot{q}_m + K_{mm}{}^E q_m = \rho_m F - \sum_{k=1}^{n} \theta_{mk} V_k \tag{2.19}$$

$$I_n = \sum_{i=1}^{m} \theta_{in}{}^T \dot{q}_i - C_{0n}\dot{V}_n \tag{2.20}$$

Where ρ_m matrix is built with the mode shape coefficient corresponding to the location of the applied force *F*. The piezoelectric element *n* generates an outgoing current I_n and a voltage V_n across its blocked capacitance C_{0n}.

To easily model and solve these equations, a state-space representation is used. The state-space method is based on the transformation of the *m* second-order coupled equations into a set of $2m$ first-order coupled equations.

$$\begin{cases} \dot{x}(t) = Ax(t) + Bu(t) \\ y(t) = Cx(t) + \mathrm{D}u(t) \end{cases} \tag{2.21}$$

where *x* is the state vector, *u* is the control vector, *y* is the output vector, *A* is the dynamic system matrix, *B* and *C* are the input and output matrices, respectively.

Here, the state vector *x* and the control vector *u* is chosen as:

$$x(\mathrm{t}) = \begin{bmatrix} q_1 & \dots & q_m & \dot{q}_1 & \dots & \dot{q}_m \end{bmatrix}^T \tag{2.22}$$

$$u(\mathrm{t}) = \begin{bmatrix} F & V_1 & \dots & V_{n_a} \end{bmatrix}^T \tag{2.23}$$

The final matrices *A*, *B*, *C* and *D* can be written as:

$$\begin{aligned} A &= \begin{bmatrix} 0_{m\times m} & I_{m\times m} \\ -\left[M_{m\times m}\right]^{-1} K_{m\times m} & -\left[M_{m\times m}\right]^{-1} C_{m\times m} \end{bmatrix}_{2m*2m} \\ B &= \begin{bmatrix} 0_{m\times 1} & 0_{m\times N_a} \\ \dfrac{\rho_{m\times 1}}{M_{m\times 1}} & \dfrac{-\theta_{m\times N_a}}{M_{m\times N_a}} \end{bmatrix}_{2m*(\mathrm{N}_a+1)} \\ C &= \begin{pmatrix} \dfrac{\theta_{N_s\times m}}{(C_0)} & 0_{N_s\times m} \end{pmatrix}_{N_s*2m} \\ D &= 0 \end{aligned} \tag{2.24}$$

Finally, the modal system can be written as:

$$A = \begin{bmatrix} 0 & I \\ -diag(\omega_i^2) & -2diag(\xi_i\,\omega_i) \end{bmatrix}_{2n,2n}$$

$$B = \begin{bmatrix} 0_{n,N_s} \\ B_i^l \end{bmatrix}_{2n,N_s}$$

$$C = \begin{bmatrix} C_i^k & 0_{N_a,n} \end{bmatrix}_{N_a,2n},$$

where ω_i is the angular frequency in rad/s and ξ_i is the modal damping of the ith mode. N_s and N_a are the numbers of sensors and actuators, and n is the number of modes under consideration. With this type of control system, the values B_i^l and C_i^k are usually estimated from the generalized electromechanical coupling parameters determined for each transducer (sensor k and actuator l) and each mode. The modal state of the structure is reconstructed by adding an observer based on that modelling. Some keys parameters must be determined thanks to an experimental identification, as described in the next sections.

2.3 Design of our Smart Structure

2.3.1 Choice of the smart structure

The research work is carried out by using a simple smart structure: a cantilever beam instrumented with piezoelectric transducers. The main reason of this choice is historical. Many previous studies of the laboratory have work with this kind of structure, they are consequently well known and representative of many dynamical problems. Even if this structure has already be used, all the identification process has to be done for every new project or new series of measure, as these parameters can evolve significantly with the temperature as example. All our future developments and simulations proposed in this study will be based on this structure and its identified model.

The cantilever beam is 40 cm length (L_T), 4 cm width and 0.3 cm thickness, as shown in Fig 2.4. Various piezoelectric material can be used as actuators or sensors. Based on the laboratory experiments, PZT (piezo zircon titanium) material have been chosen as actuators and PVDF (polyvinilydene fluoride) as sensors. Indeed, PZT develop high electromechanical coupling (up to 0.5 in 31 mode) necessary to act on the structure (damp

the vibration or harvest energy). PVDF are light, cheap. They develop a low electromechanical coupling, enough to be used as a sensor.

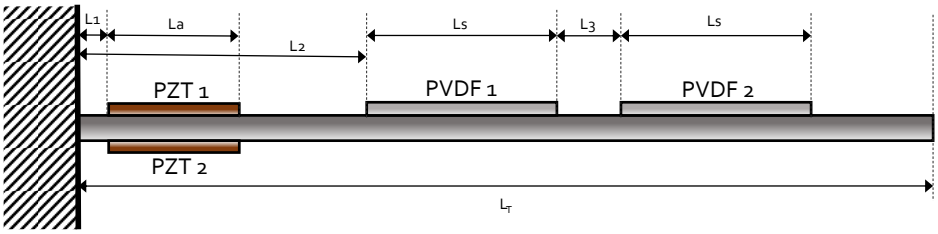

Figure 2. 4 Cantilever smart beam in aluminum

This aluminum beam is clamped at one side on a rigid base, the parameters of this structure are shown in the Table 2.3, the parameters of PZT actuators are shown in Table 2.4 and the parameters of PVDF sensors are shown in Table 2.5.

Table 2.3 Smart structure parameters

Parameter	Value
Thickness	40 e^{-3} m
Length	0.3 e^{-3} m
Width	4 e^{-3} m
Density	2700 $kg.m^{-3}$
Young's modulus	6.9e^{10} Pa
Poisson's ratio	0.3
Position of the first PZT_1	L_1=5 e^{-5} m
Position of the second PZT_2	L_1=5 e^{-5} m
Position of the second $PVDF_1$	L_2=20 e^{-3} m
Position of the second $PVDF_2$	L_2+ L_s +L_3=33 e^{-3} m
Length of PZT_1 and PZT_2	L_a=6.1 e^{-3} m
Length of $PVDF_1$ and $PVDF_2$	L_s=3 e^{-3} m

Table 2.4 Parameters of the PZT

Parameter	Value
Thickness	8e^{-4} m
Length	6.1e^{-3} m
Width	3.5e^{-3} m
Density	7800 $kg.m^{-3}$
Piezoelectric strain constant	d_{31}=1.74e^{-10} m/V
	d_{33}=3.94e^{-10} m/V
Elastic compliance	s^E_{11}=16.1e^{-12} m^2/N
	s^E_{33}=20.7e^{-12} m^2/N
Permittivity of the material (*F/m*)	ε=8.85e^{-12} F/m

Table 2.5 Parameters of the PVDF

Parameter	Value
Thickness	$2.8e^{-5}$ m
Length	$1.5\ e^{-4}$ m
Width	$1.6\ e^{-4}$ cm
Density	1780 $kg.m^{-3}$
Piezoelectric strain constant	$d_{31}=0.22e^{-10}$ m/V
	$d_{33}=-0.33e^{-10}$ m/V
Elastic compliance	$s^E_{11}=3.33e^{-10}$ m^2/N
	$s^E_{33}=3.33e^{-10}$ m^2/N
Permittivity of the material (*F/m*)	$\varepsilon=8.85e^{-12}$ F/m

2.3.2 Modal analysis and transducers locations

It is well known that to obtain the maximum efficiency, the actuators must be placed in high strain regions. The positions of piezoelectric elements have a critical influence on the natural frequencies of smart structures. In order to design the experimental setup, the natural frequencies of the aluminum beams with surface bonded piezoelectric elements have to be estimated as its modal shapes. Modal analysis are carried out using ANSYS 14.5 software in order to estimate the natural frequencies and mode shapes of the cantilever beam. The material property of the cantilever beam is detailed in table 2.6.

Table 2.6 Material properties of the cantilever beam

	Material	Yong 's Modulus	Poisson's ratio	density
cantilever beam	Aluminum	69GPa	0.295	2770kg/m^3

Our target is to enhance the damping on low frequency modes thanks to energy transfer. Thus, the actuators dedicated to these task (harvest and damp) must be located near the clamped boundary to present good efficiency (see Figure 2.5). We arbitrary chose to observe and model the five first modes of our structure. After several numerical tests, PVDF are located to measure as well as possible the five first mode, knowing that the best locations are occupied by the PZT actuators. Note that the third PZT transducers (visible on the ANSYS model or on the pictures) won't be used in this study.

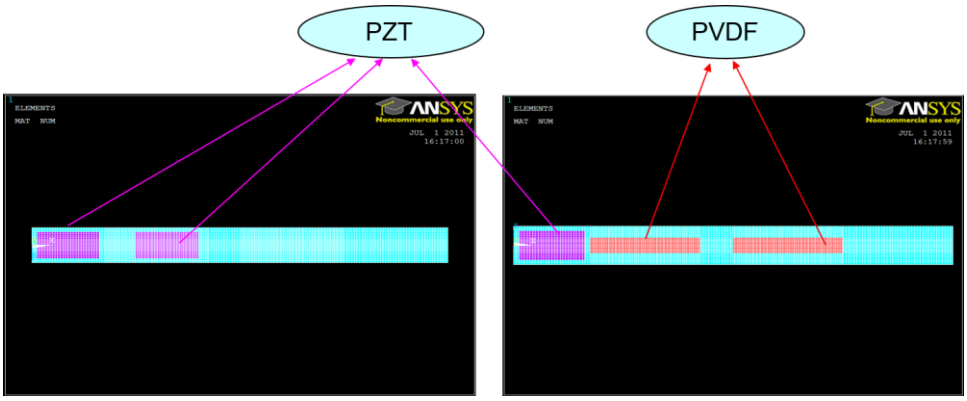

Figure 2.5 Finite element model of cantilever beam with piezoelectric elements

The deformation mode of our cantilever beam with its transducers are shown in Figure (2.6).

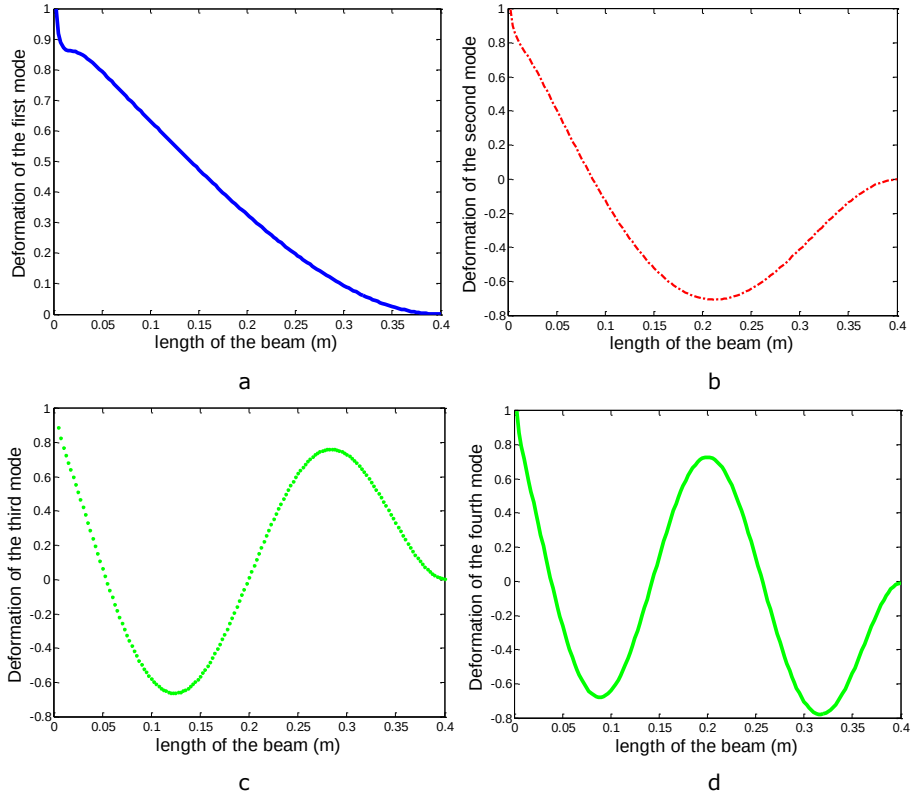

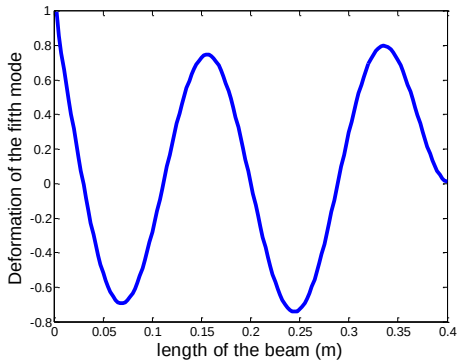

e

Figure 2. 6 Deformation mode shapes of cantilever beam

a. Deformation Mode shape ; b. Second Deformation Mode shape ; c. Third Deformation Mode shape; d. Fourth Deformation Mode shape; e. Fifth Deformation Mode shape

The deformation fields shown in Figure 2.6, validates that the chosen transducers locations is the more relevant to obtain the best actuation and sensing capability. Indeed it can be seen that sensors and actuator are located near high deformation domains.

2.4 System parameter identification

Figure 2.7 shows the pictures of the real beam structure. The beam is equipped with several independent piezoelectric elements.

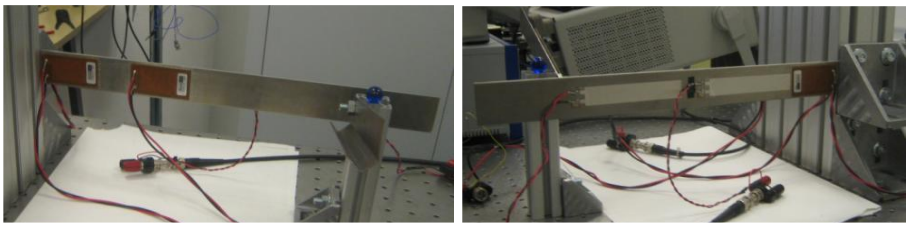

Figure 2.7 The cantilever smart beam

The first five natural frequencies numerically calculated and experimentally measured are shown in the Table (2.7). The low percentage error confirms the validity of our model. Even if it is not perfect, it is sufficiently accurate.

Table 2.7 Natural frequencies in Hz of cantilever beam with piezoelectric elements

Mode	Frequency of numerical (HZ)	Frequency of experimental (HZ)	Percentage error(%)
1	17.760	17.1906	3.2
2	101.40	94.45	6.8
3	276.65	262.1656	5.2
4	531.14	496.287	6.5
5	867.82	835.5075	3.7

In order to develop and simulate the control/harvesting technics, an accurate and realistic model of the smart structure has to be built as described in section 2.2. Many parameters cannot be directly measured and has to be identified. Figure 2.8 shows the overview of our experimental setup used to construct the model. The identification of the coupling coefficient is the most difficult task in that process. We will present in the next two section reliable technics developed in our laboratory to do so.

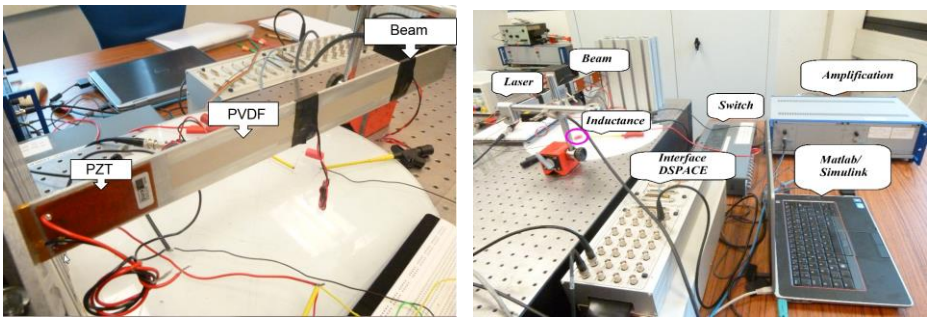

Figure 2.8 Overview of experimental setup

2.4.1 Coupling coefficient of the PZT piezoelectric actuators

The electromechanical coupling coefficient k can be defined according to Equation (2.25) [80].

$$k^2 = \frac{\omega_D^2 - \omega_E^2}{\omega_D^2} = \frac{K^D - K^E}{K^D} \tag{2.25}$$

where ω_E and ω_D are the frequency of the structure when the piezoelectric elements are in short-circuit and in open-circuit respectively. K^D and K^E are the modal open-circuit and short-circuit stiffness of the structure, respectively.

One can remember that the modal matrices are defined from the mode shape matrix norm:

$$\Phi^T M \Phi = I_m \tag{2.26}$$

Where Φ is the mode shape matrix, I_m is the identity matrix, and m is the number of modes.

With this normalization, the matrix C and K can be written as:

$$K^E = diag\left(\left(\omega^E\right)^2\right) = diag\left(\left(2\pi f_{cc}\right)^2\right) \tag{2.27}$$

$$C = 2diag\left(\xi\right) diag\left(\omega^D\right) = 2diag\left(\xi\right) diag\left(\left(2\pi f_{co}\right)^2\right) \tag{2.28}$$

With f_{cc} and f_{co} the resonance frequencies in short-circuit and in open-circuit respectively.

These resonance frequencies are measured with a Dynamic Signal Analyzer (Agilent 4395A) as shown in figure 2.9. Due to the very narrow difference between the short-circuit frequency and open-circuit frequency (typically <1Hz), these frequency shifts are estimated through various very accurate swept sine analyses (step of 1mHz is possible).

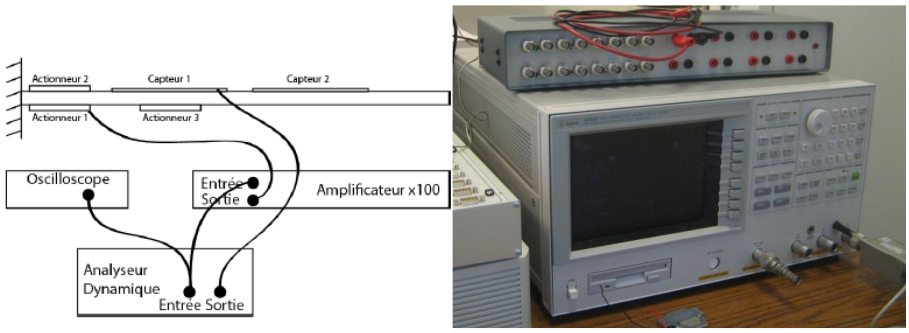

Figure 2.9 Overview of Dynamic Signal Analyzer and the results of an example

The smart structure includes three PZT piezoelectric elements. To identify the coupling coefficient of a PZT patch, the other two PZT are both short circuited. For example, to identify the PZT1, the PZT3 is connected in short circuit and PZT2 is used as an actuator (see table 2.8).

In this table, "actuator" means that the piezoelectric element patch is used to stimulate the structure, "CC" means the piezoelectric element is short-circuited, and "CO" presents that the piezoelectric element is open circuit. The figure 2.10 shows a typical curve in CC configuration.

Table 2.8 The necessary measurements for the electromechanical coupling coefficients

Measurement type	PZT1	PZT2	PZT3
1	Actuator	CC	CC
2	Actuator	CO	CC

3	Actuator	CC	CO
4	CC	Actuator	CC
5	CO	Actuator	CC

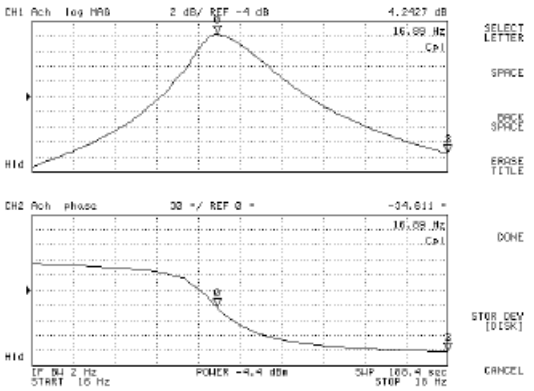

Figure 2.10 Typical response curves in the CC configuration

The modal damping factor ξ of each mode is obtained from the mechanical quality factor (Q_M) which can be easily evaluated by the -3 dB method.
with:

$$\xi = \frac{1}{2Q_M} \tag{2.29}$$

Remark:

The temperature influences lightly the resonant frequencies. Thus, average values calculated by multiple measurements will be used in the simulation.

Table 2.9 shows the results of the identification of the dynamic characteristics in the smart structure in terms of resonance frequencies (F_{CO}: the piezoelectric element is in open circuit; F_{CC}: the piezoelectric element is short-circuited) and damping factor (ξ).

Table 2.9 Identification of the dynamic characteristics of PZT actuators

Piezoelectric element PZT_1			
Mode	F_{CC} (Hz)	F_{CO}(Hz)	Damping factor ξ
1	17.15	17.24	7.88e-3
2	94.05	94.20	4.21e-3
3	262.00	263.23	3.13e-3
4	496.30	496.50	7.02e-3
5	834.13	836.90	3.45e-3

Piezoelectric element PZT_2

Mode	F_{CC} (Hz)	F_{CO}(Hz)	Damping factor
1	17.16	17.23	9.85e-3
2	94.21	94.77	4.43e-3
3	259.71	263.63	4.94e-3
4	495.80	496.78	7.54e-3
5	835.10	836.10	3.55e-3

2.4.2 Coupling coefficient of the *PVDF* sensors

PVDF sensors have a very weak stiffness. So the difference between the open-circuit and short-circuit frequencies resonance are too weak to be measured. For determining the electromechanical coupling coefficients of the *PVDF* sensors, we cannot use the same way as the *PZT* actuators.

A measuring method [81] developed by the LaMCoS laboratory is chosen here. It is based on the transfer functions between the first actuator PZT_1 and the two sensors $PVDF_1$ and $PVDF2$.

The relation between the state-space and the transfer function is given by:

$$H(\mathrm{s}) = \frac{y(\mathrm{s})}{u(\mathrm{s})} = C(\mathrm{sI} - \mathrm{A})^{-1} B \tag{2.30}$$

where:
y(s) is the output signal
u(s) is the input signal
A is the evolution matrix (n×n)
B is the activation matrix (n×nPZT)
C is the observation matrix (nPVDF×n)

Thus, the transfer functions between the voltage across the actuator *PZT* and the voltage of sensor $PVDF_1$ and $PVDF_2$ are composed by the algebraic fraction of the second order with the RFP [82] algorithm.

$$H^{ident}_{C_k, A_l}(\mathrm{s}) = \sum_{i=1}^{n/2} \left[\frac{M^i_{k,l} e^{j\phi^i_{k,l}}}{s^2 + 2\xi^i \omega^i s + \left(\omega^i\right)^2} \right] \tag{2.31}$$

where:

$M_{k,l}^{i}$ is the modal amplitude of the transfer function for the frequency corresponding to the mode *i* of the actuator l and sensor *k*;

$\phi_{k,l}^{i}$ is the modal phase of the transfer function for the frequency corresponding to the mode *i* of the actuator l and sensor *k*;

ω^{i} is the angular frequency of the mode *i*;

ξ^{i} is the modal damping factor of the mode *i*.

with *i* is the mode number, *k* is the sensor number and l is the actuator number.

The state matrix A is obtained through the denominator of Eq(2.32). The "modal amplitude" and the "modal phase" of the transfer function for the frequency corresponding to the mode i of the actuator l and sensor k, and the coefficients of the matrices B and C are linked by the following relationship:

$$M_{k,l}^{i} e^{j\phi_{k,l}^{i}} = C_{k}^{i} B_{l}^{i} \tag{2.32}$$

When the structure is weakly damped, the phase shifts measurements are near 0 or π. Therefore, the input matrix B and output matrix C are considered as real matrices.

The "modal amplitude" $M_{k,l}^{i}$ and the "modal phase" $\phi_{k,l}^{i}$ are calculated by ¨curve fitting¨ [82][83] and the activation matrix B is constituted by the electromechanical coupling coefficients of the *PZT* actuators identified previously.

Then, the coefficients of the output matrix C_{k}^{i} is determined by:

$$C_{k}^{i} = \frac{M_{k,l}^{i} e^{j\phi_{k,l}^{i}}}{B_{l}^{i}} \tag{2.33}$$

So the matrices C and B can be determined.

Concretely, dSPACE and ControlDesk interface are used to save the output signal y(s) of each sensors and the input excitation u(s) "white noise" applied via the actuator PZT_l. Figure 2.11 give the schematic of the experiments and the typical obtained curves.

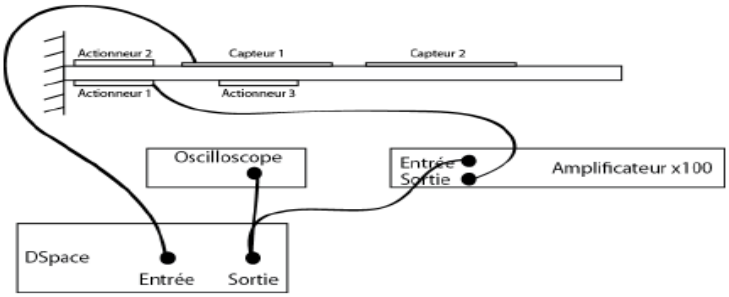

a

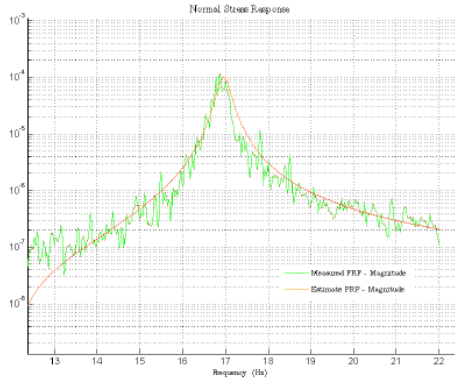

b

Figure 2.11 Shematic of the experiments and the curves obtained by curve fitting

a. Measurement configuration ; b.Typical response curves

The transfer function H(s) can be calculated from the ratio of the *FFT* of the sensor response and the *FFT* of the actuator signal. According to the transfer function and by using the Curve Fitting method, the resonance frequencies, the modal amplitudes and the modal phases can be estimated. Thus, the electromechanical coupling coefficients of $PVDF_1$ and $PVDF_2$ contained in the output matrix C, can be determined.

Table 2.10 shows the results of the electromechanical coupling coefficients of $PVDF_1$ and $PVDF_2$ sensors. These characteristics are the average values obtained from ten experiments and associated curves fitting.

Table 2.10 Electromechanical coupling coefficients of $PVDF_1$ and $PVDF_2$

Mode	$PVDF_1$	$PVDF_2$
1	6.86e-2	11.95e-2
2	2.52e-2	4.82e-2
3	2.79e-2	4.84e-2
4	9.23e-2	11.87e-2
5	1.55e-2	1.80e-2

2.5 Final description and characteristics of the smart structure

The geometric parameters of the cantilever and the piezoelectric element are summarized in table 2.3 and 2.4 and 2.5.

Once this 3D multiphysic model established it is interesting to construct its equivalent modal model for the first mode. It will be used as a reference to tune and optimize the smart system. Indeed, in the literature and the theoretical equation allowing the optimization are written for a single degree of freedom. In our case this DoF will be the first mode (for the control part) and the second mode (for the harvesting part). This simple model are built using the experimental setup and the mechanical parameters. In practice, the tip displacement of the cantilever beam is set to 2mm without control. This tip displacement leads to an induced voltage on the piezoelectric elements PZT_1 and PZT_2 with an amplitude value of 10V. The link between temporal quantities (tip displacement, voltage) and modal quantities (modal displacement…) on this structure would be created.

Our research focus on enhancing the damping of low frequency modes than to the energies of other modes. A structure in generally excited thanks to a pulse, noise or multi-sinus and the low frequency mode will develop the higher response (in terms of amplitude of the vibration). Controlling these low frequency modes without any external power is difficult. Thus, we decide to target these low frequency mode for our enhanced vibration control technique, and especially the first mode of our structure. The needed energy will thus be harvested on the higher modes (mode 2 to 5). As, one of our goal is to propose a realistic technique that can work even if there is a small amount of energy on the others modes, we chose to limit the harvesting process only on the energy of the mode 2. As it, we harvest energy on mode 2 to better control the mode 1. If this configuration work, it will be easy to add others modes (mode 3 to 5) on which the energy could be harvested.

Table 2.11 and table 2.12 summarize the various parameters identified on the structure for the energy harvesting system and damping control system, respectively.

Table 2.11 Mechanical characteristics data for the energy harvesting system

Parameter	Symbol	Value
Short-circuit resonance frequency(Hz)	f_{2cc}	94.05
Open-circuit resonance frequency(Hz)	f_{2co}	94.21
Mechanical quality factor	Q_M	150
Modal damping factor	ξ	0.00432
Equivalent damping**(**$Nm^{-1}s^{-1}$**)**	c_2	5.14
Electromechanical coupling coefficient	k_2	0.0122
Equivalent stiffness**(**kNm^{-1}**)**	K^E	3.49e2

Table 2.12 Mechanical characteristics data for damping control system

Parameter	Symbol	Value
Short-circuit resonance frequency(Hz)	f_{1cc}	17.16
Open-circuit resonance frequency(Hz)	f_{1co}	17.24
Mechanical quality factor	Q_M	100
Modal damping factor	ξ	0.00886
Equivalent damping **(**$Nm^{-1}s^{-1}$**)**	c_1	1.92
Electromechanical coupling coefficient	k_1	0.002
Equivalent stiffness **(**Nm^{-1}**)**	K^E	11.6e2

2.6 Conclusion

In this chapter, modal analysis and experimental measurements are carried out in order to construct a representative modal model of the structure. Some parameters, as the electromechanical coupling coefficient, necessitate the use of an indirect approach to be determined. The global modal model will be use to simulate and understand the proposed approach in this work, combining harvesting and control. In parallel, as a first step, simple 1DoF models are also built in order to use the theoretical formulae of control and harvesting proposed in the literature, as explained in the following chapters.

3 General SSDH Modal principles

3.1 The idea of energy transfer between modes for semi-active control

As underlined in chapter 1, the semi-active/passive vibration control technics are promising solutions to control embedded structures leading to a drastic reduction of on-board weight of the overall structure. Indeed, Synchronized Switch Damping techniques (*SSD*), have demonstrated interesting properties in vibration control with a low power consumption, high efficient, energetically autonomous ability, low weight and low cumbersome.

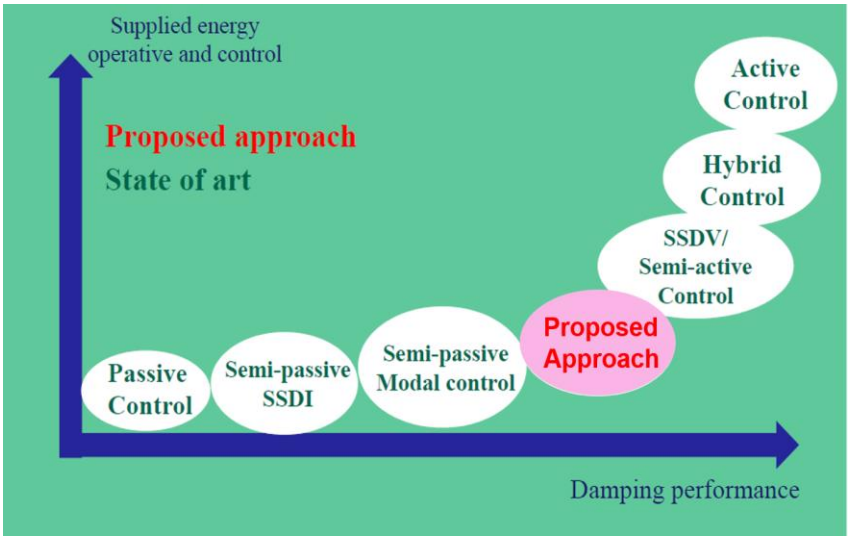

Figure 3.1 Relation between the damping performance and the corresponding energy requirements for various techniques.

As shown in figure 3.1, among all the *SSD* technique, *SSDV* can lead to a better damping effect and don't need many energy. However, external constant voltage is needed. We propose here to develop a self-powered architecture able to supply this extra voltage namely this extra energy.

Our research is based on the idea of modal energy transfer between modes. The goal is to increase the damping effect of targeted mode by harvesting energy on non-controlled mode, as shown in figure 3.2. As we will see, this implies also a small damping of the non-controlled modes as the corresponding modal energy is reduced by the energy transfer. This idea can be used between several structures or the same structure. In this PhD research work, the same structure is used.

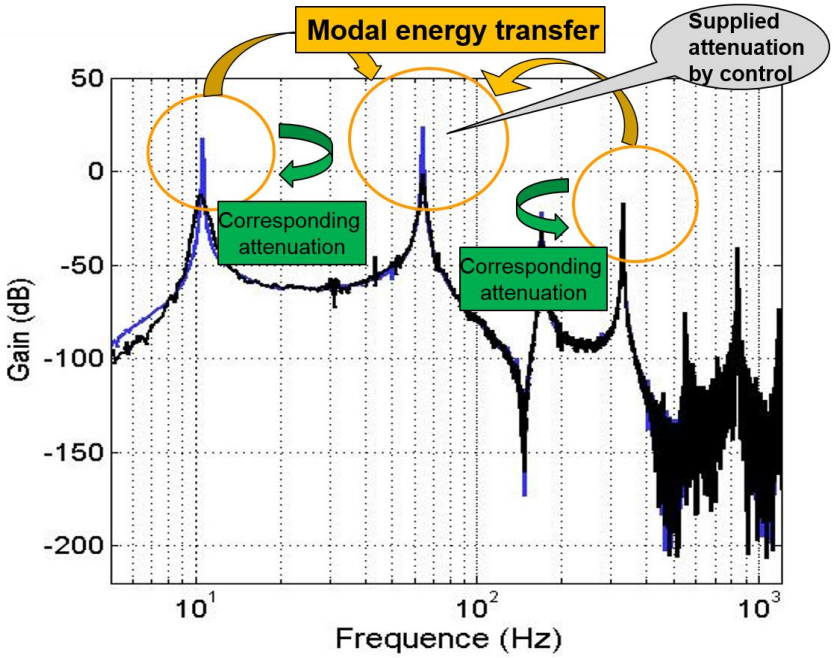

Figure 3.2 Energy transfer between modes

The proposed electrical architecture is so called Modal Synchronized Switching Damping and Harvesting (Modal *SSDH*), which is a self-powered system.

A general view for Modal *SSDH* technique can be depicted in Figure 3.3.

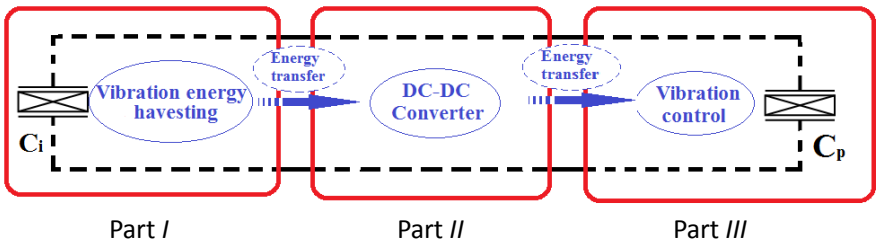

Figure 3.3 Three energy flow parts of Modal *SSDH*

As shown in Figure 3.3, the system is composed of three parts. Part *I* refers to the harvesting part which convert mechanical energy from the vibrations into electrical one. This electrical energy is then formatting thanks to a converter (Part *II*), as a *DC/DC* converter, to reach the requirements of the vibration control part in term of voltage, current and storage capacitor. Part *III* is vibration control circuit based on modal *SSD* technics

to enhance the damping of the targeted mode. In the following, this modal vibration control will be called "*SSDVC*" (SSDV on Capacitor).

In order to clearly present our technique, all the developments and associated theories will be related to the smart structure detailed in chapter 2. The chosen practical example consists in harvesting mechanical energy from the second mode of the structure, in order to enhance the vibration damping of the first mode and reduce consequently the second mode.

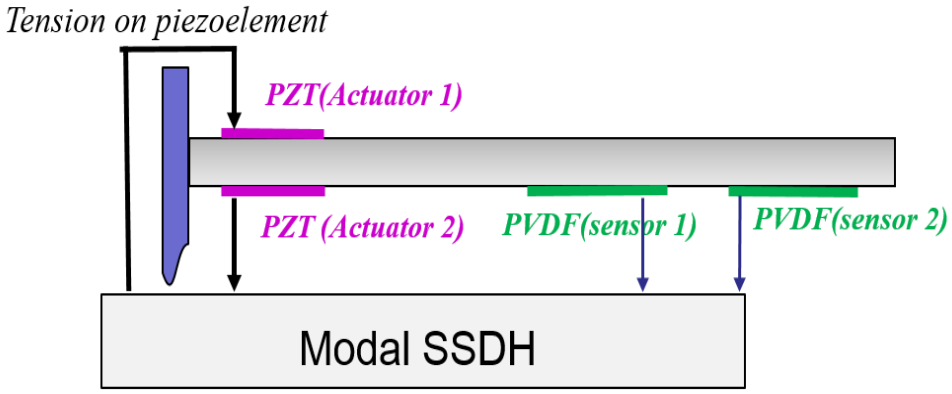

Figure 3.4 A schematic of energy transferring between different modes of a same structure

The figure 3.4 illustrates the setup. The excitation is a distributed modal force not represented in the figure. This non physical excitation allows a good understanding of the smart system by simply tuning the contribution of each modes in the response, avoiding the question about the effect of the source type. The mechanical energy is partially extracted by the piezoelectric element (*PZT 2*) and maximized thanks to Modal *SSH*, then transferred via a converter to another piezoelectric element (*PZT 1*) which control the target mode by Modal SSD control algorithm. Indeed, by increasing the voltage amplitude on the target controlled piezoelectric, it will also increase the damping effect on that targeted mode.

3.2 Details of Modal *SSDVC* circuit

We propose a new simple architecture to add an energy during the inversion process of the piezoelectric element. Classic *SSDV* or $SSDV_a$ uses an

external constant voltage. We replace this external source by a storage capacitor which is able to create the desired voltage increase.

Two main operating principles are developed and studied. In a first operating principle, the voltage across the storage capacitor C_B remains constant or slightly decrease. This condition is insured by the amount of scavenged energy coming from the energy harvesting part (part *I* and part *II* in figure 3.3). This mode will be called *SSDVC (I):* "constant intermediate voltage". In a second operating principle, all the charges stored into the capacitor are fully transferred to the piezoelectric element during a switching phase. This second mode is named *SSDVC (II):* "capacitor discharge".

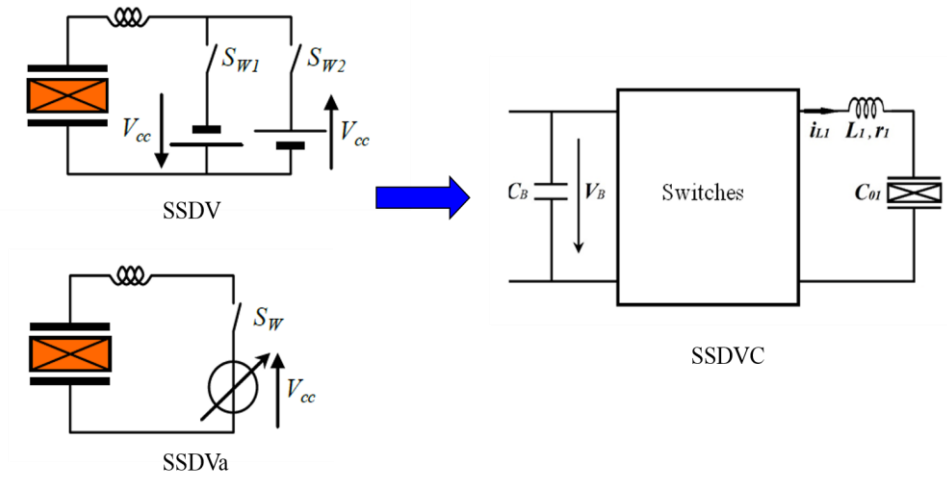

Figure 3.5 Proposed new SSD control techniques

The Modal *SSDVC* technique consists of a *LCR* circuit which contains an inductor L_1, an equivalent resistor r_1 and the capacitance of piezoelectric element C_{01}. V_{C01} is the voltage on the piezoelectric element C_{01}. Four switches (T_1 to T_4) insure to rightly connect the capacitor and the piezoelectric element. When a maximum of displacement is reached, the voltage on the piezoelectric element is positive leading to add a negative voltage. When a minimum displacement is reached, it is basically the inverse: the voltage on the piezoelectric element is negative and the added one must be positive. Figure 3.6 shows the two studied configurations: *SSDVC* at constant voltage and *SSDVC* capacitor discharge.

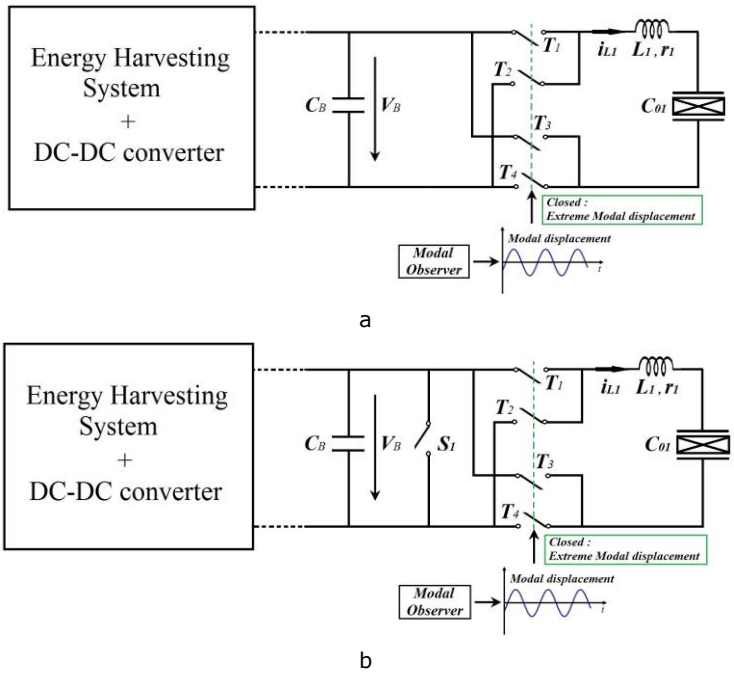

Figure 3. 6 The Modal SSDVC technique scheme

a. SSDVC (I): Constant intermediate voltage; b. SSDVC (II): Capacitor discharge

The switch S_1 is used only on the "capacitor discharge" mode to insulate the piezoelectric element C_{01} and the storage capacitance C_B when the energy transferring from C_B to C_{01} is completed.

The five switches are in open state most of the time and only switched on when the modal displacement of the first mode reaches either a maximum or a minimum. The detail control law of the energy transfer for these two operating modes will be explained in the next sections. In order to present the details of the implementation of the modal *SSDVC* technique, it is assumed that the structure is excited at the first resonance frequency.

3.2.1 SSDVC(I) - Constant intermediate voltage

For the first function mode *SSDVC (I),* the value of the intermediate capacitor C_B must be great enough in comparison with the other capacitors. Consequently the ripple can be neglected and the voltage V_B on the capacitor C_B can be considered as constant. Thus, a positive voltage (V_B) or a negative voltage ($-V_B$) source can be added to the piezoelectric element during the

inversion process. This operation mode is similar as classic *SSDV* technique. The relationship between the voltages of the piezoelectric element (V_{C01_m} and V_{C01_M}) before and after inversion can be expressed as Eq.(3.1).

$$V_{C01\_m} - V_B = \gamma(V_{C01\_M} + V_B) \tag{3.1}$$

With γ the inversion coefficient and V_B the constant voltage across the storage capacitor.

Control law of the switches

In this part of the study, we assume sinusoidal voltage on the piezoelectric element that brings up maximum (positive voltage) and minimum (negative voltage). Two cases of voltage inversion will be considered. Therefore, it is important to control the direction of the voltage thanks to the four switches of *SSDVC (I)* technique.

When the sign of the V_{C01} is positive (a maximum of modal displacement occurs corresponding to a maximum of voltage), the added voltage should be negative which will increase the inverted voltage on the piezoelectric element. Inversely, when the sign of the V_{C01} is negative (a minimum of modal displacement correspond to a minimum of voltage occurs), the added voltage should be positive. Four switches (T_1, T_2, T_3, T_4) are thus needed (see Figure 3.5) to accomplish this goal (two are used to add the positive voltage and the two other are used to add the negative voltage). Then, an amount of energy is transferred from the capacitor C_B to the piezoelectric element C_{01} though these switches. The switches should be closed for a half of an electric oscillation period, which roughly equals to $\pi\sqrt{L_1 C_{01}}$ in the energy transfer process. The sequence control law of the switches as shown in the table 3.1.

Table 3.1 Sequence control law of the switches of Modal *SSDVC (I)*

	Modal displacement q_1 : maximum			Modal displacement q_1 : minimum	
STEP	**1 to 2**	**2 to 3**	**3 to 4**	**4 to 5**	**6**
T_1,T_4	**OFF**	**ON**	**OFF**	**OFF**	**OFF**
T_2,T_3	**OFF**	**OFF**	**OFF**	**ON**	**OFF**

The waveforms of the voltages are the same as the one depicted in figure 1.15.

3.2.2 SSDVC (II) – Capacitor discharge

In this second function mode *SSDVC (II),* there is no constraint on the value of the capacitor C_B.

Control law of the switches

The control law is almost similar as previous operation. The four switches (T_1, T_2, T_3 and T_4) are used to control the direction of the voltage which will be added on the piezoelectric element C_{01}. The corresponding additional energy driven through the switches has been scavenged by the energy harvesting system (part I and II in figure 3.3). The switch S_1 is used to insulate the piezoelectric element C_{01} from the storage capacitance C_B after that the energy transferring between C_{01} and C_B has occurred. The five switches are in the opened state most of the time and only switched on when the modal displacement of the first mode reaches either a maximum or a minimum. Then the energy is transferred from the capacitor C_B to the piezoelectric element C_{01} through these switches. The sequence control law of the switches and the waveforms in *SSDVC (II)* control circuit are given in the table 3.2 and figure 3.7, respectively.

Table 3.2 Sequence control law of the switches of Modal *SSDVC (II)*

	Modal displacement q_1:maximum			Modal displacement q_1: minimum			
		t_1	t_2		t_1	t_2	
	1 to 2	2 to 3	3 to 4	4 to 5	5 to 6	6 to 7	8
S1	OFF	OFF	ON	OFF	OFF	ON	OFF
T1,T4	OFF	ON	ON	OFF	OFF	OFF	OFF
T2,T3	OFF	OFF	OFF	OFF	ON	ON	OFF

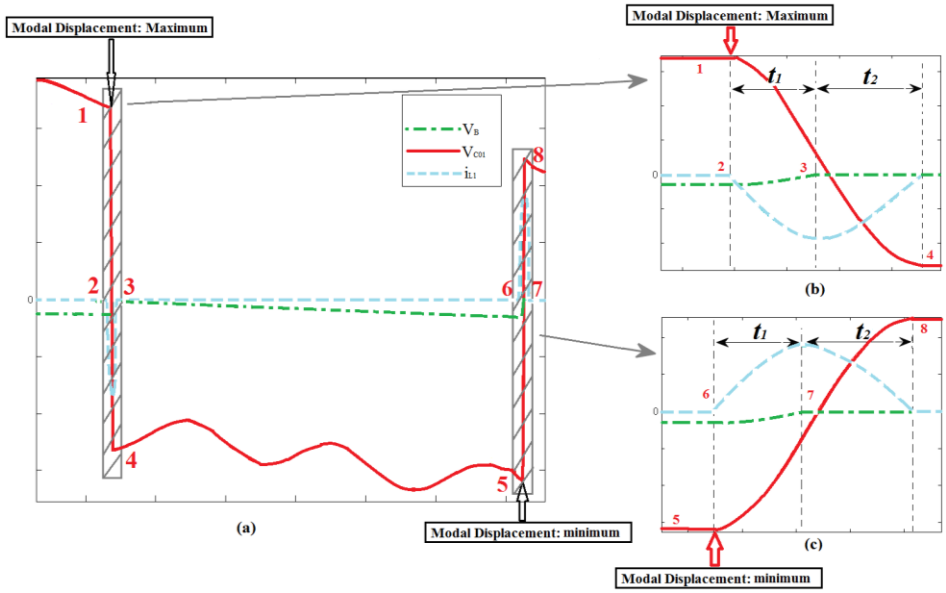

Figure 3.7 The waveforms in Modal *SSDVC (II)* control circuit

The different phases can be detailed as follows:

1 to 2: The switches are opened. The energy is accumulated and stored on the capacitor C_B. The piezoelectric element is in the open state.

2 to 3: T_1 and T_4 are closed when the modal displacement reaches the maximum. Then, the energy stored on the capacitor C_B is transferred to the piezoelectric element C_{01} during t_1.

3 to 4: When the voltage across the capacitor C_B reduces to zero, S_1 is closed, while T_1, T_4 are still closed. S_1, T_1 and T_4 are closed during t_2 (oscillating LC circuit). V_{C01} is inverted. Closing S_1 on a zero-voltage value reduces the losses and the breaking failures.

4 to 5: All switches are opened. Energy can be accumulated and stored on the capacitor C_B. The piezoelectric element is in the open state. The control of the minimum displacement is the same as aforementioned.

5 to 6: T_2 and T_3 are closed when the modal displacement reach a minimum. Then, the energy on storage capacitor C_B is transferring to the piezoelectric element C_{01}.

6 to 7: Then S_1 is closed when the voltage across C_B reduces to zero, and T_2, T_3 are still closed. V_{C01} is thus inverted (oscillating LC circuit).

8 : All switches are open.

Theoretical development

Contrary to the *SSDVC (I)* where the timing for the aperture or the closure of the switch are constants and simples, the timing for the *SSDVC (II)* depends on the state and the charges present in the circuit. It necessitates consequently a theoretical analysis. The analytic laws describe the be-

havior of the *SSDVC (II)* architecture in "capacitor discharge" mode are detailed and discussed in this section.

The two steps occurring during the energy transfer are shown in the figure 3.8.

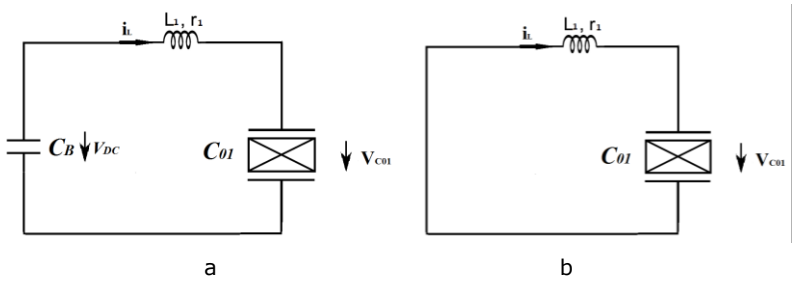

Figure 3.8 Equivalent circuit of two energy transfer steps. a.step1 ; b.step2

Step 1:

When the modal displacement of target mode reaches its maximum (minimum), T_1 and T_4 (or T_2 and T_3) are switched on, and S_1 is always open. As shown in figure 3.8 (a), the equivalent circuit is a *LCR* circuit which contains an inductor L_1, an equivalent resistor r_1, the piezoelectric element C_{01} as well as the capacitance C_B. During this period, the energy which has been stored in the capacitance C_B is transferred to the piezoelectric element C_{01}. A current flow i_1 appears as described by equation 3.2:

$$L_1 \frac{d^2 i_1}{dt^2} + r_1 \frac{di_1}{dt} + \frac{i_1}{C_{series}} = 0 \tag{3.2}$$

with:

$$C_{series} = \frac{C_B + C_{01}}{C_B C_{01}} \tag{3.3}$$

The expression of the current in the inductor L_1 is given by:

$$i_1(t) = I_{1M}\, e^{-\alpha_1 t} \sin(\omega_{1d}\, t + \varphi_1) \tag{3.4}$$

Giving the amount of transferred charge:

$$\begin{aligned} q_1(t) &= -I_{1M} \frac{e^{-\alpha_1 t}}{\omega_{10}} \sin(\omega_{1d}\, t + \varphi_1) \\ I_{1M} &= -\frac{\left(V_{C_{01}}(0) - V_{C_B}(0)\right) C_{series}\, \omega_{10}}{\sqrt{1-\xi_1^2}} \end{aligned} \tag{3.5}$$

.

The phase φ_1 is nul. $V_{C01}(0)$ and $V_{CB}(0)$ are respectively the value of the voltage across the piezoelectric element and the capacitor just before the switching event.

Thus, the current is expressed as:

$$i_1(\mathrm{t}) = -\frac{C_{series}\left(V_{C_{01}}(0) - V_{C_B}(0)\right)\omega_{10}}{\sqrt{1-\xi_1^2}} e^{-\omega_1\xi_1 t}\sin(\omega_{1d}t) \tag{3.6}$$

with:

$$\omega_{10} = \sqrt{\frac{1}{L_1\frac{C_B C_{01}}{C_B + C_{01}}}}$$

$$\omega_{1d} = \omega_{10}\sqrt{1-\xi_1^2}$$

$$\xi_1 = \frac{1}{2} r_1 \sqrt{\frac{\frac{C_{01}C_B}{C_{01}+C_B}}{L_1}}$$

ω_{10} is the natural angular frequency of the damping circuit
ω_{1d} is the angular frequency of oscillation circuit
ξ_1 is the damping coefficient of the damping circuit

During step 1, the voltage on the two capacitors (piezoelectric element C_{01} and capacitor C_B) will oscillate around an equilibrium voltage $V_B^{equ} = V_{01}^{equ}$:

$$V_{C_B}^{equ} = -\frac{C_{01}V_{C_{01}}(0) - C_B V_{C_B}(0)}{C_{01}+C_B} \tag{3.7}$$

$$V_{C_{01}}^{equ} = \frac{C_{01}V_{C_{01}}(0) - C_B V_{C_B}(0)}{C_{01}+C_B} \tag{3.8}$$

Considering an equivalent capacitor C_{series} (equation 3.3), the voltage oscillations V_{series} across this equivalent capacitor can be defined thanks to Kirchhoff's circuit laws:

$$V_{series}(\mathrm{t}) + r_1 i_1(\mathrm{t}) + L_1\frac{di_1(\mathrm{t})}{dt} = 0 \tag{3.9}$$

leading to:

$$V_{series} = I_{1M}e^{-\alpha_1 t}\left[\left(-r_1 + L_1\alpha_1\right)\sin(\omega_{1d}t) - L_1\omega_{1d}\cos(\omega_{1d}t)\right] \tag{3.10}$$

The amount of transferred charges is thus determined by the following equation:

$$\Delta q = C_{series}V_{series} \tag{3.11}$$

The corresponding voltage oscillation across the piezoelectric element C_{01} and across the intermediate capacitor C_B are given by the equation 3.12 and 3.13.

$$V_{C_{01}}^{osc}(\mathrm{t}) = \frac{\Delta q}{C_{01}} \tag{3.12}$$

$$V_{C_B}^{osc}(\mathrm{t}) = \frac{\Delta q}{C_B} \tag{3.13}$$

Finally, the voltage across the piezoelectric element C_{01} and intermediate capacitor C_B at the end of *step 1* is the sum of the equilibrium state and the oscillating one. It can be expressed as:

$$V_{C_B}(\mathrm{t}) = V_{C_B}^{equ}(\mathrm{t}) + V_{C_B}^{osc}(\mathrm{t}) \tag{3.14}$$

$$V_{C_{01}}(\mathrm{t}) = V_{C_{01}}^{equ}(\mathrm{t}) + V_{C_{01}}^{osc}(\mathrm{t}) \tag{3.15}$$

The energy transfer process is stopped when all the energy from the storage capacitor is collected across the piezoelectric element. Without this condition, charge stored into the capacitor C_B and on the piezoelectric element will oscillate until an equilibrium (charge transfer is not unidirectional). Due to our control strategy of the switches, the first step is finished when the voltage across the capacitor C_B drops to zero.

$$V_{C_B}(\mathrm{t}_1) = 0 \tag{3.16}$$

By using Eq.(3.7) to Eq.(3.13), Eq.(3.15) and (3.16) leads to:

$$\begin{aligned} &\frac{C_{series} I_{1M} e^{-\alpha_1 t_1}}{C_B}((-r_1 + L_1\alpha_1)\cdot\sin(\omega_{1d}t_1) - L_1\omega_{1d}\cos(\omega_{1d}t_1)) \\ &+ \frac{C_B V_{C_B}(0) - C_{01} V_{C_{01}}(0)}{C_B + C_{01}} = 0 \end{aligned} \tag{3.17}$$

with :

t_1 the end time of step 1. S_1 is closed at $t=t_1$.

I_{1M} the value of the current at $t=0$,

$\alpha_1 = \frac{r_1}{2L_1}$ the neper frequency (attenuation) of the first energy transfer step circuit

With the damping factor : $\xi_1 = \frac{\alpha_1}{\omega_{10}}$

$\omega_{10} = \sqrt{\frac{1}{L_1 C_{series}}}$, the resonant angular frequency of the first step circuit (figure 3.5.a)

$\omega_{1d} = \sqrt{\omega_{10}^2 - \alpha_1^2}$, the angular frequency of the first energy transfer step circuit

As there is no simple analytic solution, the time t1 must be find numerically solving equation 3.17.

Step 2:

As shown in figure 3.8 (b), the equivalent circuit is also a *LCR* which consists of L_1, r_1 and the capacitance of the piezoelectric element

C_{01}. The voltage across the piezoelectric element will be inversed. The initial conditions are the voltages and the current at the end of step 1 ($V_{C01}(t_1)$ and $i_1(t_1)$). The electric equation corresponds to the circuit is given by equation (3.18)

$$L_1 \frac{\partial^2 i_1}{\partial t^2} + r_1 \frac{\partial i_1}{\partial t} + \frac{i_1}{C_{01}} = 0 \tag{3.18}$$

The expression of the current in the inductor L_1 is given by

$$i_2 = I_M \sin(w_{d2} + \phi_2) \tag{3.19}$$

With I_{M2} the amplitude of the current during this second step, given by

$$I_{M2} = \frac{I_{M1}}{\sin(\phi_2)} \tag{3.20}$$

The phase phase φ2 is given by

$$\tan \phi_2 = \frac{-L_1 w_{2d}}{V_{C01}(t_1) + (r_1 - \alpha_2 L_1) i_2(t_1)} \tag{3.21}$$

The closing time t_2 correspond to the time when current i_1 in the inductor at the end of the step 2 is equal to zero: $i_1(t_2)=0$. One has to keep in mind that the definition of t_2 is positive. So the condition is:

$$\begin{cases} t2 = \pi - \dfrac{1}{w_{2d}} arctg\left[\dfrac{w_{2d} i_1(t_1) L_1}{V_{C01}(t_1) + (r_1 - \alpha_2 L_1) i_i(t_1)}\right] \\ \quad for \quad arctg\left[\dfrac{w_{2d} i_1(t_1) L_1}{V_{C01}(t_1) + (r_1 - \alpha_2 L_1) i_i(t_1)}\right] > 0 \\ t2 = -\dfrac{1}{w_{2d}} arctg\left[\dfrac{w_{2d} i_1(t_1) L_1}{V_{C01}(t_1) + (r_1 - \alpha_2 L_1) i_i(t_1)}\right] \\ \quad for \quad arctg\left[\dfrac{w_{2d} i_1(t_1) L_1}{V_{C01}(t_1) + (r_1 - \alpha_2 L_1) i_i(t_1)}\right] < 0 \end{cases} \tag{3.22}$$

where:

$\alpha_2 = \dfrac{r_1}{2L_1}$, neper frequency of the second energy transfer step circuit

With the damping factor: $\xi_2 = \dfrac{\alpha_2}{\omega_{20}}$

$\omega_{20} = \sqrt{\dfrac{1}{L_1 C_{01}}}$, the resonant angular frequency of the second energy transfer step circuit

$\omega_{2d} = \sqrt{\omega_{20}^2 - \alpha_2^2}$, angular frequency of the second energy transfer step circuit

The closing time t_1 is a constant value but the closing time t_2 is a variable one due to the possible variation on the initial conditions (voltage and current).

Comparison between *SSDI* and *SSDVC* (II)

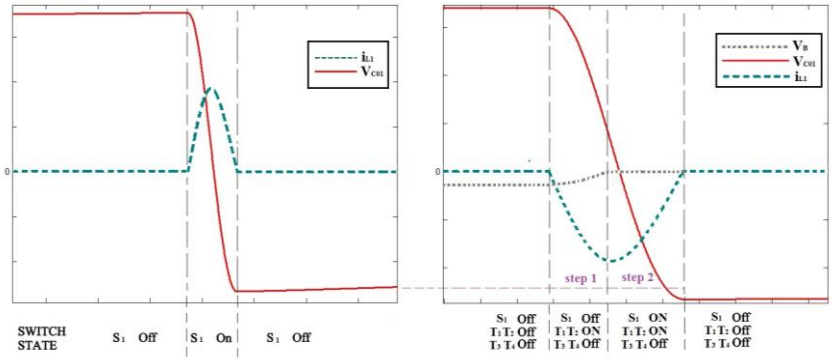

a b

Figure 3.9 Comparisons between *SSDI* and *SSDVC* (II) techniques
a. *SSDI* waveforms ; b. SSDVC (II) waveforms

In order to compare the efficiency of *SSDI* and *SSDVC* (II) techniques, simulations are done as presented in chapter 4. We can expect that the efficiency of *SSDVC* (II) would be better than *SSDI*: the inversed voltage of *SSDVC* (II) is larger than *SSDI*, which should provide a better control performance. Indeed, compared with *SSDI* technique, the proposed *SSDVC* (II) method contains two steps. In the step 1, the charges on the capacitance C_B are cut off at zero, and the energy is transferred to the piezoelectric element. The operation in step 2 is the same with *SSDI*, but begins with an initial inductor current and thus gives rise to a greater inversion.

3.3 Optimization of the SSDVC concept

This section will focus on the optimization of our damping circuit *SSDVC* for its two operating modes. In order to clarify and simplify our analytic equations, we will firstly consider the simple case of mono-sinusoidal excitation at the first resonance frequency of the structure. Bi-sinusoidal excitation will be considered in a second step.

3.3.1 Optimization of *SSDVC* (I): "Constant intermediate voltage"

As illustrated in the previous section, the *SSDVC (I)* is working as SSDV technique.

For the *SSDV* control technique, if the structure is driven around one of its resonance frequency, the critical value of the extra voltage is [59]:

$$\left(V_B\right)_{\max} = \frac{\pi}{4\alpha_1}\frac{1-\gamma}{1+\gamma}F_M \tag{3.23}$$

With F_M the maximal amplitude of the output mechanical force applied to the structure, γ the inversion coefficient and α_1 the coupling factor in V/N.

Indeed, above this maximal value, the voltage inversion process will introduce too much energy in the system and can generate stability problems [59].

In the case studied in this work for a mono harmonic excitation, this value is V_{Bmax}=1.1V for the considered displacement (+/-2mm at the free boundary of the beam). In our final case, the structure is excited around the first and second frequencies excitation (bi harmonic excitation). In order to find the critical value of this extra voltage, simulations are necessary as analytic development will be too long and too complicated. As a starting point, to find this particular voltage value, the value of V_{Bmax}=1V is chosen. Figure 3.9 shows the damping effect for fixed extra voltage V_B of 0.5V, 1V, 1.5V, 2V, 2.2V and 3V. For these simulations, an inversion factor of 0.75 was chosen leading to specific values for the inductor L_1 and resistance r_1, as depicted in chapter 2. To insure a constant voltage V_B, the capacitance C_B must be large enough: a value of 10 000µF was selected. Figure 3.10 shows that the critical extra voltage of 2V leads to the best damping performance.

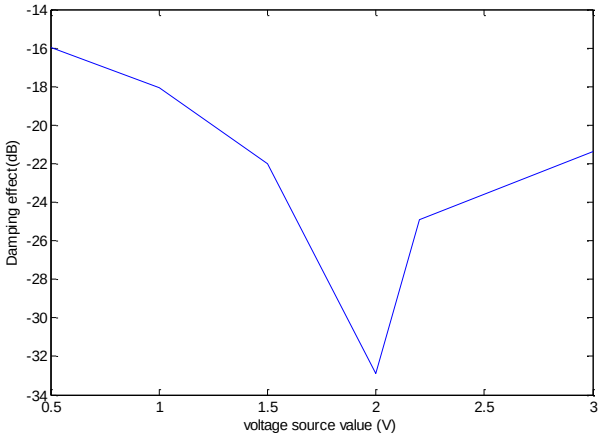

Figure 3.10 Steady state damping versus the voltage source value obtained by simulation with bi-sinusoidal excitation

Local variation around this point (1.9, 1.95, 2.05…) was done and do not improve the damping performances. To conclude, we can observe that the critical value of the extra voltage do not change drastically between its theoretical value for a mono harmonic excitation and a value numerically found with a bi harmonic excitation. This value is 2V.

3.3.2 Optimization of SSDVC (II): "Capacitor discharge"

In this mode, all the energy stored in the capacitor C_B is transferred to the piezoelectric element C_{01}. To enhance the damping performances (i.e. increasing the attenuation and the efficiency), the energy transfer between the capacitor C_B and the piezoelectric element C_{01} must be maximized. The energy transfer presents an optimum which is mainly determined by the value of the capacitance C_B, and the value of the voltage across this capacitance. The goal is thus to maximize the energy transfer during this step. Equation 3.20 expresses this energy transfer: the difference between the electrostatic energy stored into the piezoelectric element C_{01}:

$$\Delta E_{C_{01}} = E_{C_{01}}(\mathrm{t}_1) - E_{C_{01}}(0) \tag{3.24}$$

with $E_{C_{01}}(0)$ and $E_{C_{01}}(\mathrm{t}_1)$ are respectively the energy stored into the piezoelectric element at the beginning (t=0) and at the end (t=t_1) of the first step, defined as:

$$E_{C_{01}}(\mathrm{t}_1) = \frac{1}{2} C_{01} V_{C_{01}}^2(\mathrm{t}_1) \tag{3.25}$$

$$E_{C_{01}}(0) = \frac{1}{2} C_{01} V_{C_{01}}^2(0) \tag{3.26}$$

To compute this energy, the voltage $V_{C_{01}}(t_1)$ must be determined.

We firstly present the optimization for a mono-sinusoidal excitation. As presented in the previous section 3.2.2, the voltage across the piezoelectric element C_{01} during *step 1* can be calculated (equation 3.15) as the time t (resolution of equation 3.17). The amount of energy transferred (equation 3.24) can thus be computed. To find the best value for the storage intermediate capacitor, we chose to express C_B as:

$$C_B = x \cdot C_{01} \tag{3.27}$$

Using equations (3.8) (3.13) (3.15) (3.27), the expression of the piezoelectric voltage is:

$$V_{C_{01}}(\mathrm{t}_1) = \frac{V_{C_{01}}(0) - xV_B(0)}{1+x} - \left(\frac{x}{1+x}\right)^2 C_{01}\Omega \tag{3.28}$$

with:

$$\Omega = \left(V_{C_{01}}(0) - V_{C_B}(0)\right) \frac{\omega_{10}}{\sqrt{1-\xi_1^2}} e^{-\alpha_1 t} \begin{bmatrix} \left(-r_1 + L_1\alpha_1\right)\sin\left(\omega_{1d}t\right) \\ -L_1\omega_{1d}\cos\left(\omega_{1d}t\right) \end{bmatrix} \tag{3.29}$$

Thus, the electrostatic transferred energy is given by the following equation:

$$\Delta E_{C_{01}} = \frac{1}{2} C_{01} \left\{ \left[\frac{V_{C_{01}}(0) - xV_B(0)}{1+x} - \left(\frac{x}{1+x}\right)^2 C_{01}\Omega \right]^2 - {V_{C_{01}}}^2(0) \right\} \tag{3.30}$$

Figure 3.11 shows the transferred energy as a function of the coefficient x and the initial voltage $V_B(0)$ across the capacitor C_B. The parameter x vary from 0 to 100, and the initial potential on C_B from 0V to 10V (constant value). The voltage across the piezoelement C_{01} used to control the vibration is considered as an ideal signal: mono-sinusoidal excitation with a maximal amplitude set to 10V (see chapter 2).

One can note on figure 3.11 that the transferred energy increases with the increase of the capacitance value for a fixed value of the initial voltage V_B, until it reaches a maximum. Then, the transferred energy decreases slowly with the increase of the storage capacitor. In the range of the initial voltage (0-10V), the optimal value for the storage capacitor C_B is between 2 and 4 times the value of C_{01}. In other words, the optimal value of

storage capacitor C_B is not sensitive to the voltage across the capacitors, but depends on the value of the piezoelectric element.

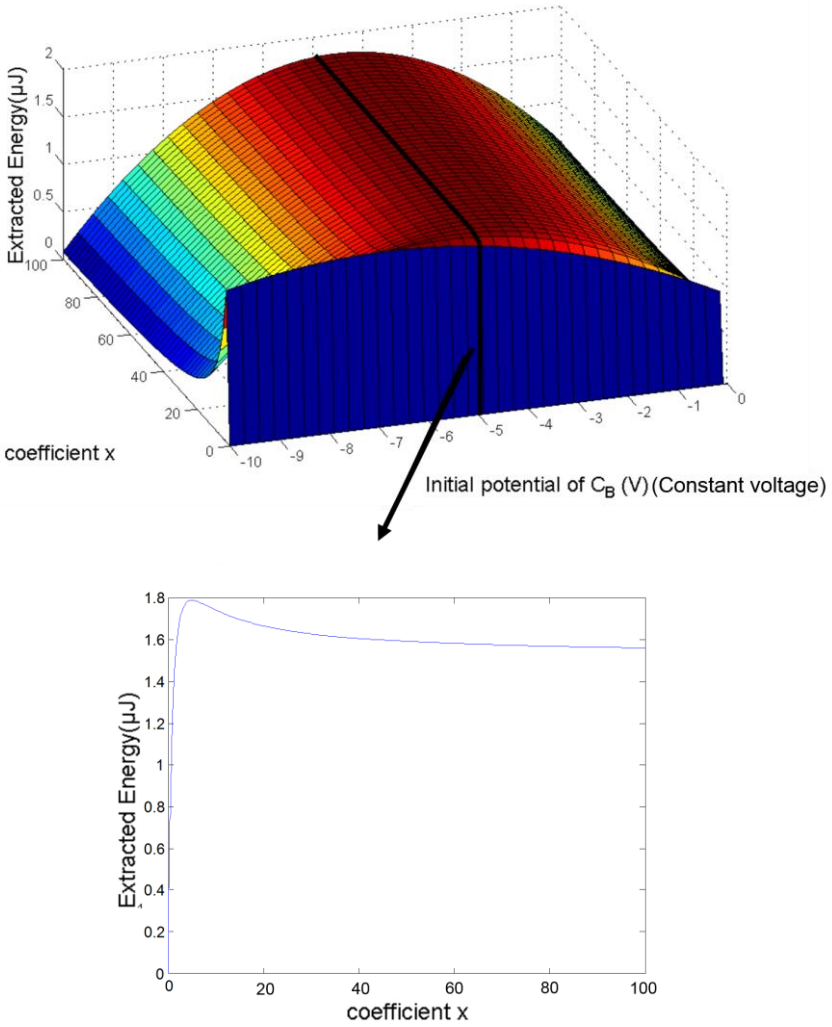

Figure 3.11 Extracted energy as a function of the coefficient x (of capacitor C_B) and the initial potential of the C_B (V_{C01}=5V).

The efficiency of the transferred energy can be defined as the ratio of the transferred electrostatic energy divided by the initial total energy stored into the capacitance C_B and the piezoelectric element C_{01}:

$$\eta_{extra} = \frac{\Delta E_{C_{01}}(t_1)}{E(0)} = \frac{\left[\frac{V_{C_{01}}(0) - xV_B(0)}{1+x} - \left(\frac{x}{1+x}\right)^2 C_{01}\Omega\right]^2 - V_{C_{01}}{}^2(0)}{xV_{C_B}^2(0) + V_{C_{01}}^2(0)} \tag{3.31}$$

with:

$$E(0)=\frac{1}{2}C_B V_{C_B}^2(0)+\frac{1}{2}C_{01}V_{C_{01}}^2(0)$$

the total energy stored into the capacitance and the piezoelectric element.

Figure 3. 12 depicts the variation of the efficiency of the transferred energy as a function of the value of the ratio x between the capacitors for various initial potential on C_B. In figure 3.12, it clearly shows that the efficiency of the transferred energy decreased with the increase of the initial value of the voltage V_B. The efficiency is maximized with an optimal value C_B that is approximately between 2 to 6 times the value of the capacitance C_0, for each value of the initial potential on C_B.

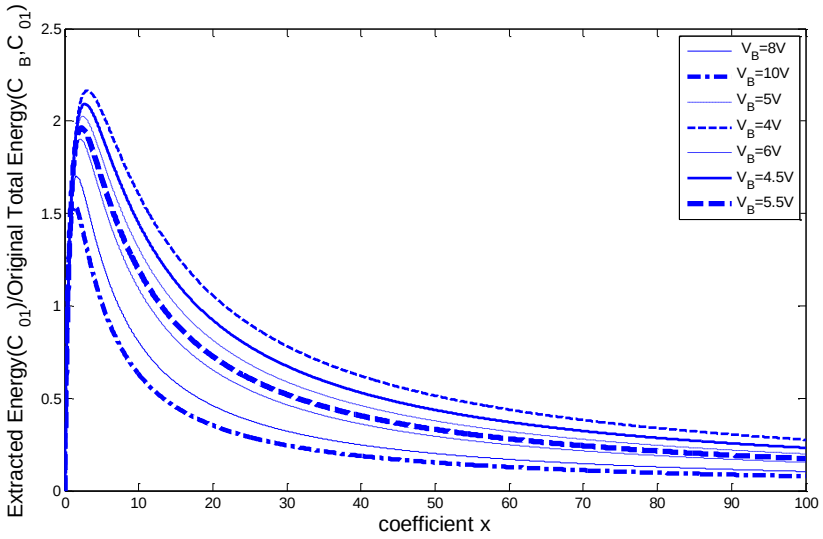

Figure 3.12 Efficiency of transferred energy as a function of the coefficient x (of capacitor C_B) for various initial value of the voltage V_B (V_{C01}=10V);

For a bi-harmonic excitation, no simple theoretical calculus can lead to the optimal parameters. And even if, these parameters will change on each configuration, especially they depends on the ratio of the response amplitude of each sinus.

The optimal operating values are then found by simulations. By changing the searched values around their optimal value for a mono harmonic excitation. The figure 3.13 show the resulting attenuation as a function of the capacitance ratio for a given voltage 3.13(a), and as a function of different voltage for a given capacitance ratio 3.13(b). These values are the optimal ones for the damping circuit alone. As shown in the following

chapter (chapter 6), a voltage V_B =5.2V, is not easy to reach and depends greatly on the ratio of the amplitude of the excitation sinus.

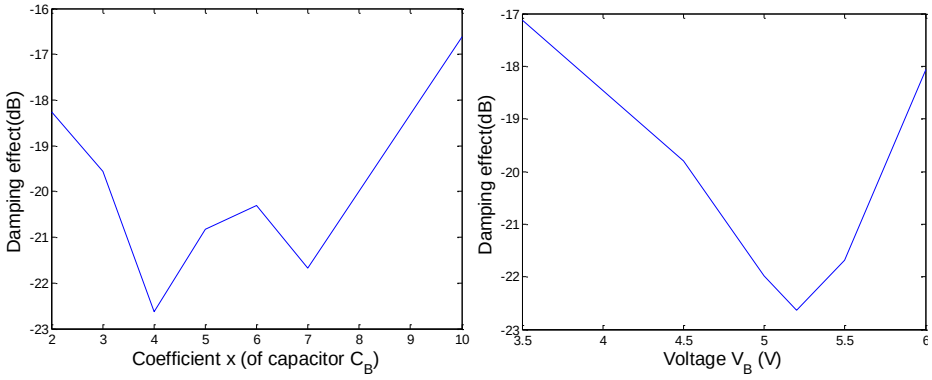

a b

Figure 3.13 Resulting attenuation of the first mode for different coefficient x (give, V_B =5.2V) and for different voltages (given x=4).

3.4 Performance discussion of Modal SSDVC: Energy transfer and damping effect

The aim of this section is to analyze the performance of the Modal *SSDVC* technique, including the energy transfer performance, the damping performance and the relationship between the extra energy and the damping effect.

In order to understand the energy transfer in the *SSDVC*, the general energy analysis of *SSD* technique is recalled firstly:

In the *SSDS* technique, the transferred energy E_T (See chapter 2) is:

$$E_T = \int_0^T \alpha V \dot{u} dt = \int \alpha V d\dot{u}$$

It corresponds to the part of the mechanical energy, which is converted into electrostatic energy by the piezoelectric element.

In the *SSDI* technique, the voltage on the piezoelectric element is divided into two components, one is proportional to the displacement, and another one is a piecewise constant function. The transferred energy E_T depends on the piecewise constant function which is related to the performance of piezoelectric voltage inversion process.

In the *SSDV* technique, the energy transfer is related with the amplitude of the vibration and the extra voltage V_{cc} (See chapter 1).

Thus, regarding one period of mechanical vibration, the transferred energy of these three techniques are summarized in table 3.3[84].

Table 3.3 Transferred energy with different *SSD* techniques

E_{SSDS}	$4\frac{\alpha^2}{C_0}u_M^2$
E_{SSDI}	$4\frac{\alpha^2}{C_0}\cdot\frac{1+\gamma}{1-\gamma}u_M^2$
E_{SSDV}	$\left(4\frac{\alpha^2}{C_0}u_M^2+4\alpha u_M V_{CC}\right)\cdot\frac{1+\gamma}{1-\gamma}$

γ is the inversion factor, α is the coupling factor, u_M is the maximal of displacement, C0 is the value of the capacitance of the piezoelectric element. It can be seen that the transferred energy of *SSDV* technique is the maximum of the three *SSD* control techniques. Damping effect in *SSDI* technique is closely related to the electromechanical coupling coefficient. In *SSDV* technique, not only the electromechanical coupling coefficient is related in the damping effect, but also the applied voltage source *Vcc*. This applied voltage lead to a larger inversion factor than *SSDI* and *SSDS* (the inversion factor of *SSDS* is zero). Enlarging the inversion factor means that more energy is extracted from the structure which can be achieved by increasing the inversion voltage. Thus, *SSDV* shows the better damping effect than *SSDI* and *SSDS*. Figure 3.14 shows an example of the different attenuations induced by these non-linear techniques on an academic structure: camped-free beam submitted to a 1N force at the free end, with an inversion coefficient about 0.8[84].

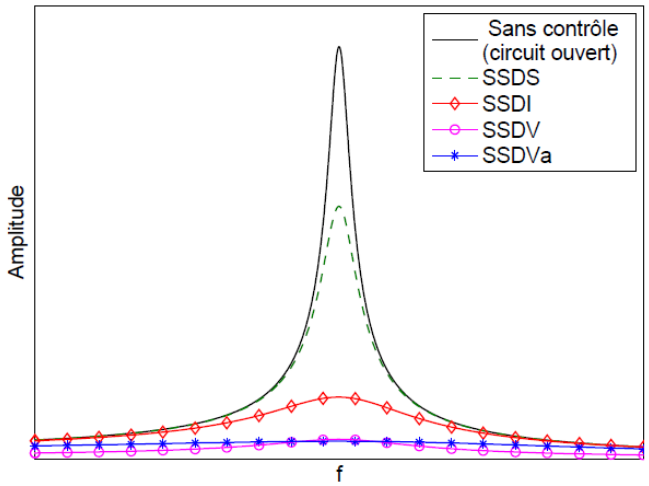

Figure 3.14 Different attenuations via different non-linear techniques

Energy transfer in the case of SSDVC (I) (constant voltage):

It is assumed that the modal displacement of the target mode under *SSDVC* control is sinusoidal with the first vibration frequency ω_1.

$$q_m(\mathrm{t}) = q_{1M}\sin\left(\omega_1 t + \varphi_1\right) \tag{3.32}$$

with q_{1M} the modal amplitude of the target mode
Thus the expression of the energy transferred of Modal SSDVC (I) is:

$$\left(E_T\right)_{SSDVC_I} = \left(4\frac{\alpha^2}{C_0}q_{1M}^2 + 4\alpha q_{1M}V_B\right)\cdot\frac{1+\gamma}{1-\gamma} \tag{3.33}$$

with V_B the voltage on the capacitor C_B. It is obviously very similar to the expression of the energy transfer for SSDV technique.

Energy transfer in the case of SSDVC *(II)* (capacitor discharge):

In the case considered here, the piezoelectric element in the vibration control circuit is excited by a single sinusoidal excitation at its first natural frequency.

Details of the energy transfer: figure 3.15

The voltage on the storage capacitor C_B, on the piezoelectric element C_{01} and displacement q_1 typical waveforms of the target mode 1 are shown in Figure 3.15. At the beginning of the transfer period (*step 1*), the piezoelectric voltages are $V_{01,M}$ on the piezoelectric element C_{01} and V_{BM} on the storage capacitor C_B respectively. At the end of transfer period (*step 2*), the voltages are $V_{01,m}$ on the piezoelectric element C_{01} and V_{Bm}=0 on capacitor C_B respectively. The switching time occurs at each extreme modal displacement of the target mode. Thus, during one period of the target mode, there are two transfers at the maximum (q_{1M}) and minimum ($-q_{1M}$) modal displacement instant. The inversion process is in two step so the switch time t_i is $t_i=t_1+t_2$ with t_1 and t_2 introduced in Eq.(3.17) and Eq.(3.22).

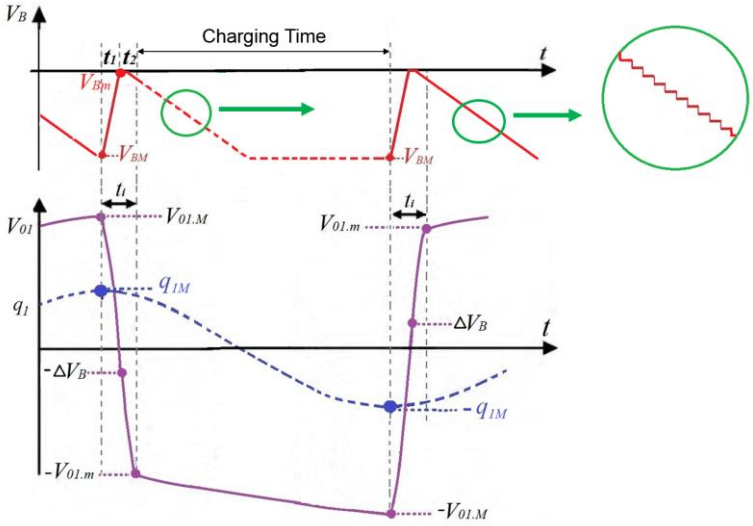

Figure 3.15 Voltages and displacements typical waveforms

Theoretical analysis:

As for the *SSDVC* (I) case:

$$q_m(\mathrm{t}) = q_{1M}\sin\left(\omega_1 t + \varphi_1\right)$$

So, the total transferred energy on C_B in one energy transfer period is:

$$E_B = \frac{1}{2}C_B\left(V_{BM}^2 - V_{Bm}^2\right) \tag{3.34}$$

The total transferred energy on C_{01} in one energy transfer period is:

$$E_{C_{01}} = \frac{1}{2}C_{01}\left(V_{01.M}^2 - V_{01.m}^2\right) \tag{3.35}$$

So the total dissipated energy during one transfer cycle is

$$E_{dis} = \frac{1}{2}C_B\left(V_{BM}^2 - V_{Bm}^2\right) + \frac{1}{2}C_{01}\left(V_{01.M}^2 - V_{01.m}^2\right) \tag{3.36}$$

In open circuit, voltage variation are proportional to modal displacement with a factor $\frac{\alpha_1}{C_{01}}$, so the voltage on the piezoelectric element after two voltage inversion processes can be given by (Eq.3.34), where q_{1M} is the modal displacement amplitude.

$$V_M = V_m + \frac{2\alpha_1}{C_{01}}q_{1M} \tag{3.37}$$

The voltage of the piezoelectric element C_{01} can be expressed as the sum of two functions, one being the image of the displacement $\frac{\alpha_1}{C_{01}}q_{1M}$ and the other one is a piecewise constant function $\tilde{V}$. So the voltage of the piezoelectric element is given by (Eq.3.38), when shunt circuit operates.

$$V_{01} = \frac{\alpha_1}{C_{01}} q_{1M} + \tilde{V} \tag{3.38}$$

Combining Eq. (3.34) and Eq. (3.35), $V_{01,M}$ and $V_{01,m}$ can be expressed in Eq. (3.36) and Eq. (3.37).

$$V_{01.M} = \left|\tilde{V}\right| + \frac{\alpha_1}{C_{01}} q_{1M} \tag{3.39}$$

$$V_{01.m} = \left|\tilde{V}\right| - \frac{\alpha_1}{C_{01}} q_{1M} \tag{3.40}$$

The crenel function $\tilde{V}$ can be expressed as Fourier series and written as:

$$\tilde{V} = \left|\tilde{V}\right| sign(\dot{u}) = \left|\tilde{V}\right| \sum_{n=0}^{\infty} \left\{ \frac{4}{\pi(2n+1)} \cos\left[(2n+1)\omega_1 t + \varphi_1\right] \right\} \tag{3.41}$$

It is possible to define an energy transfer efficiency factor η_{SSDH} of our *SSDVC(II)* during one energy transfer period by the ratio of the stored energy in the capacitor C_B and C_{01} at the end and at the beginning of the process, as shown in (Eq.3.39)

$$\eta_{SSDVC(II)} = \frac{\frac{1}{2} C_B V_{Bm}^2 + \frac{1}{2} C_{01} V_{01.m}^2}{\frac{1}{2} C_B V_{BM}^2 + \frac{1}{2} C_{01} V_{01.\mathrm{M}}^2} \tag{3.42}$$

By Eq.(3.35),(3.36),(3.37),(3.39), $\left|\tilde{V}\right|$ can be obtained as :

$$\left|\tilde{V}\right| = \sqrt{\frac{C_B(\mathrm{V}_{Bm}^2 - \eta_{SSDVC(II)} \cdot \mathrm{V}_{BM}^2)}{C_{01}(\eta_{SSDVC(II)} - 1)} - \left[1 - \left(\frac{\eta_{SSDVC(II)} + 1}{\eta_{SSDVC(II)} - 1}\right)^2\right] \left(\frac{\alpha_1}{C_{01}}\right)^2 q_{1M}{}^2} - \frac{\alpha_1}{C_{01}} \cdot \left(\frac{\eta_{SSDVC(II)} + 1}{\eta_{SSDVC(II)} - 1}\right) \cdot q_{1M} \tag{3.43}$$

Combining Eq.(2.4), (2.5) and (3.35), only the first harmonic of the crenel can be considered, which leads to Eq. (3.42) and (3.43):

$$\begin{aligned} &-Mq_{1M}\omega_1^2 \sin(\omega_1 t + \varphi) + Cq_{1M}\omega_1 \cos(\omega_1 t + \varphi). \\ &+\left(K^E + \frac{\alpha_1^2}{C_{01}}\right) q_{1M} \sin(\omega_1 t + \varphi) = F \sin(\omega_1 t) - \alpha_1 \left|\tilde{V}\right| \end{aligned} \tag{3.44}$$

$$
\begin{aligned}
&-Mq_{1M}\omega_1^2\sin(\omega_1 t+\varphi_1)+Cq_{1M}\omega_1\cos(\omega_1 t+\varphi_1)\\
&+\left(K^E+\frac{\alpha_1^2}{C_{01}}\right)q_{1M}\sin(\omega_1 t+\varphi)\\
&=F\sin(\omega_1 t)-\frac{4\alpha_1}{\pi}\cdot\left(\sqrt{\frac{C_B(\mathrm{V}_{Bm}^2-\eta_{SSDVC(II)}\cdot\mathrm{V}_{BM}^2)}{C_{01}(\eta_{SSDVC(II)}-1)}-\left[1-\left(\frac{\eta_{SSDVC(II)}+1}{\eta_{SSDVC(II)}-1}\right)^2\right]\left(\frac{\alpha_1}{C_{01}}\right)^2 {q_{1M}}^2}-\frac{\alpha_1}{C_{01}}\cdot\left(\frac{\eta_{SSDVC(II)}+1}{\eta_{SSDVC(II)}-1}\right)\cdot q_{1M}\right)\cdot\cos(\omega_1 t+\varphi_1)
\end{aligned}
\tag{3.45}
$$

For a given angular frequency ω_1, the modal displacement magnitude q_{1M} as well as the phase shift φ_1 can be obtained by solving the system (Eq.3.46):

$$
\begin{aligned}
&\left[Cq_{1M}\omega_1+\frac{4\alpha_1}{\pi}\left(\sqrt{\frac{C_B(\mathrm{V}_{Bm}^2-\eta_{SSDVC(II)}\cdot\mathrm{V}_{BM}^2)}{C_{01}(\eta_{SSDVC(II)}-1)}-\left[1-\left(\frac{\eta_{SSDVC(II)}+1}{\eta_{SSDVC(II)}-1}\right)^2\right]\left(\frac{\alpha_1}{C_{01}}\right)^2 {q_{1M}}^2}-\frac{\alpha_1}{C_{01}}\cdot\left(\frac{\eta_{SSDVC(II)}+1}{\eta_{SSDVC(II)}-1}\right)\cdot q_{1M}\right)\right]\cos\varphi_1\\
&+q_{1M}\left(K^E+\frac{{\alpha_1}^2}{C_{01}}-{\omega_1}^2M\right)\sin\varphi_1=0
\end{aligned}
\tag{3.46}
$$

$$
\begin{aligned}
&-\left[Cq_{1M}\omega_1+\frac{4\alpha_1}{\pi}\left(\sqrt{\frac{C_B(\mathrm{V}_{Bm}^2-\eta_{SSDVC(II)}\cdot\mathrm{V}_{BM}^2)}{C_{01}(\eta_{SSDVC(II)}-1)}-\left[1-\left(\frac{\eta_{SSDVC(II)}+1}{\eta_{SSDVC(II)}-1}\right)^2\right]\left(\frac{\alpha_1}{C_{01}}\right)^2 {q_{1M}}^2}-\frac{\alpha_1}{C_{01}}\cdot\left(\frac{\eta_{SSDVC(II)}+1}{\eta_{SSDVC(II)}-1}\right)\cdot q_{1M}\right)\right]\sin\varphi_1\\
&+q_{1M}\left(K^E+\frac{{\alpha_1}^2}{C_{01}}-{\omega_1}^2M\right)\cos\varphi_1=F_M
\end{aligned}
\tag{3.47}
$$

For $\varphi = -\frac{\pi}{2}$, then the angular resonance frequency is given by: $\omega_d = \sqrt{\frac{K^E + \frac{\alpha^2}{C_o}}{m}}$.

then,

$$C q_{1M} \omega_d + \frac{4\alpha}{\pi}\left(\sqrt{\frac{C_B(V_{Bm}^2 - \eta_{SSDVC(II)} \cdot V_{BM}^2)}{C_{01}(\eta_{SSDVC(II)} - 1)} - \left[1 - \left(\frac{\eta_{SSDVC(II)} + 1}{\eta_{SSDVC(II)} - 1}\right)^2\right]\left(\frac{\alpha_1}{C_{01}}\right)^2 {q_{1M}}^2} - \frac{\alpha_1}{C_{01}} \cdot \left(\frac{\eta_{SSDVC(II)} + 1}{\eta_{SSDVC(II)} - 1}\right) \cdot q_{1M}\right) = -F_M \qquad (3.48)$$

In this case, the modal displacement amplitude can be expressed as (Eq.3.49)

$$q_{1M} = \left| \sqrt{\frac{F_M^2 \hat{A}^2}{\left(\hat{A}^2 + \hat{B}^2 \hat{D}\right)^2} + \left(\frac{\frac{\hat{B}^2 \hat{C}}{F_M^2} - 1}{\hat{A}^2 + \hat{B}^2 \hat{D}}\right) \cdot F_M^2} - \frac{F_M \hat{A}}{\hat{A}^2 + \hat{B}^2 \hat{D}} \right| \qquad (3.49)$$

with

$$\hat{A} = C\omega_d - \frac{4\alpha_1^2}{C_{01}\pi} \cdot \frac{\eta_{SSDVC(II)} + 1}{\eta_{SSDVC(II)} - 1}$$

$$\hat{B} = \frac{4\alpha_1}{\pi}$$

$$\hat{C} = \frac{C_B\left(V_{Bm}^2 - \eta_{SSDVC(II)} \cdot V_{BM}^2\right)}{C_{01}\left(\eta_{SSDVC(II)} - 1\right)}$$

$$\hat{D} = \left[1 - \left(\frac{\eta_{SSDVC(II)} + 1}{\eta_{SSDVC(II)} - 1}\right)^2\right]\left(\frac{\alpha_1}{C_{01}}\right)^2$$

Thus, *SSDVC* Modal damping can be expressed by the ratio between the modal displacement q_{1M} after control and $(q_{1M})_{no}$ before control.

$$\frac{q_{1M}}{(q_{1M})_{no}} = \frac{C\omega_D}{\sqrt{\frac{\hat{A}^2}{\left(\hat{A}^2+\hat{B}^2\hat{D}\right)^2}+\left(\frac{\hat{B}^2\hat{C}-1}{F_M^2\left(\hat{A}^2+\hat{B}^2\hat{D}\right)}\right)}-\frac{\hat{A}}{\hat{A}^2+\hat{B}^2\hat{D}}} \tag{3.50}$$

Therefore, the theoretical value of the *SSDVC* Modal damping can be expressed as:

$$A_{SSDVC(II)} = 20\log_{10}\left(\frac{C\omega_D}{\sqrt{\frac{\hat{A}^2}{\left(\hat{A}^2+\hat{B}^2\hat{D}\right)^2}+\left(\frac{\hat{B}^2\hat{C}-1}{F_M^2\left(\hat{A}^2+\hat{B}^2\hat{D}\right)}\right)}-\frac{\hat{A}}{\hat{A}^2+\hat{B}^2\hat{D}}}\right) \tag{3.51}$$

It is possible to compute the energy transferred during a period of vibration. The expression of the energy transferred of *SSDVC (II)* Modal technique is given by Eq.(3.52).

$$\begin{aligned}(E_T)_{SSDVC_{II}} &= \frac{4\alpha_1}{C_{01}}\cdot\frac{1+\eta_{SSDVC(II)}}{1-\eta_{SSDVC(II)}}\cdot {q_{1M}}^2 \\ &+4\alpha_1 q_{1M}\sqrt{\frac{C_B\left(V_{Bm}^2-\eta_{SSDVC(II)}\cdot V_{BM}^2\right)}{C_{01}\left(\eta_{SSDVC(II)}-1\right)}-\left[1-\left(\frac{\eta_{SSDVC(II)}+1}{\eta_{SSDVC(II)}-1}\right)^2\right]\left(\frac{\alpha_1}{C_{01}}\right)^2 {q_{1M}}^2}\end{aligned} \tag{3.52}$$

This theoretical equation clearly shows that the energy transferred by *SSDVC* (II) can be more than one obtained with *SSDI* and *SSDS* techniques. A better damping performance can be achieved by the *SSDVC* (I) or (II) technique thanks to the energy transfer from the source mode.

3.5 Conclusion

In this chapter, the idea of a new vibration modal control technique named *Synchronized Switching Damping and Harvesting* (*SSDH*) was proposed firstly. The first step of analysis is presented, focusing on the damping part. A new simple architecture so called "*SSDVC*" is designed, to add an energy during the inversion process of the piezoelectric element. The electrical circuit and the associated control law are introduced to explain that the mechanical energy can be transferred between different modes of one structure to achieve damping effect on the target mode.

The principles of Modal *SSDVC* technique are presented in three main aspects.

Firstly, two operating modes of Modal *SSDVC* are proposed: the first Modal *SSDVC (I)* is seen as "Constant intermediate voltage", which operates approximatively as SSDV; the second Modal *SSDVC (II)* is seen as "Capacitor discharge". The simple electric circuits and control laws illustrate the process of the vibration control.

Secondly, a detailed switch control law is presented to analyze two steps of the energy transfer in period of the vibration control by Modal *SSDVC (II)*: energy transferring process and inverse process. Modal *SSDVC* (II) show promising result in term of voltage inversion compared to Modal *SSDI* thanks to energy transfer.

Thirdly, theoretical equations of the energy transfer and the damping effect are expended. It reveals that Modal *SSDVC* technique is theoretically more efficient to reduce vibration than the usual *SSDI* technique.

These good results are obtained thanks to the added harvested energy. The following chapter will detail the energy harvest steps, to supply and charge the capacitor used in the vibration control part.

4 Energy transfer between modes – Harvesting circuit

4.1 Introduction

As mentioned in the previous chapter, the proposed Modal SSDH technique consists in harvesting energy from the uncontrolled modes, in order to use this energy to enhance the control performances on targeted modes. In the previous chapter, new techniques SSDVC (I) and (II) were presented, explaining how the harvested energy is used. In this chapter, energy harvesting techniques are proposed to reach the requirements in term of voltage, energy for the SSDVC technics. One of the originality of this work is the modal point of view, indeed the harvesting techniques have to be redefined in the modal basis.

This chapter is organized as follow: Section 4.2 recalls the basic energy harvesting circuits and power converter which will be combined. Section 4.3 discusses the principles of different proposed energy harvesting topologies based on modal description. The corresponding circuit topologies will be described by the electromechanical equations. Lastly, a comparison between the output powers of the different proposed topologies will be presented in section 4.4.

4.2 Basic circuit

In our proposed Modal SSDH technique presented in chapter 3, the energy extracted has to be transferred to a corresponding piezoelectric patch to achieve damping effect of the target mode. In this work, we suppose that the energy source is the second mode and the target mode is the first mode. The energy harvesting architectures include two parts.

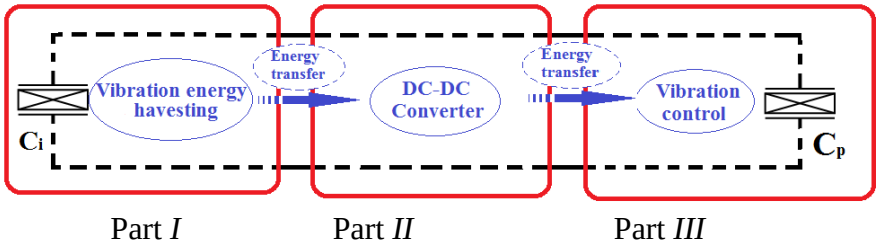

Figure 4.1 Three energy flow parts of *Modal SSDH*

The first one is the basic harvesting interface corresponding to the transformation of the mechanical strain energy into electrical energy via the

direct piezoelectric effect. The voltage delivered by the piezoelectric element is not constant but alternative and must be rectified as SSDVC (I) need a constant voltage for example. Thus an electronic power conversion interface (AC/DC) is placed between the piezoelectric element and the terminal electric load. Moreover, another converter (DC-DC converter) can be added to control the maximal output power flow. We choose a buck-boost static converter, for its ease design, implementation and good performances (high efficiency).

The basic harvesting interfaces will be explained firstly. Then four new different topologies will be proposed, explained, modeled and detailed. A final choice will be realized according to comparisons of their respective harvesting energy effectiveness.

4.2.1 Choice of the harvesting circuit

As presented in the chapter 1, the non-linear techniques were proposed to increase the electric power extracted from the piezoelectric element, via performing a non-linear treatment on the piezoelectric voltage. In order to get good electromechanical power conversion performance of the weakly electromechanical coupling system which is used in the following sections, the basic harvesting interface circuit series are considered. Figure 4.1 presents the three basic configuration and the associated waveform of voltage and strain compared to the standard classic solution [84].

The series-SSHI interface is composed of a dipole (switch + inductor in series) connected in series with the piezoelectric element and the rectifier bridge, as shown in 4.2(b). In the case of parallel-SSHI interface, the dipole is connected in parallel with the piezoelectric element and the rectifier, as shown in Figure 4.2(c). The last architecture named SECE is a converter in which the switch is synchronized on the charge available on the active element.

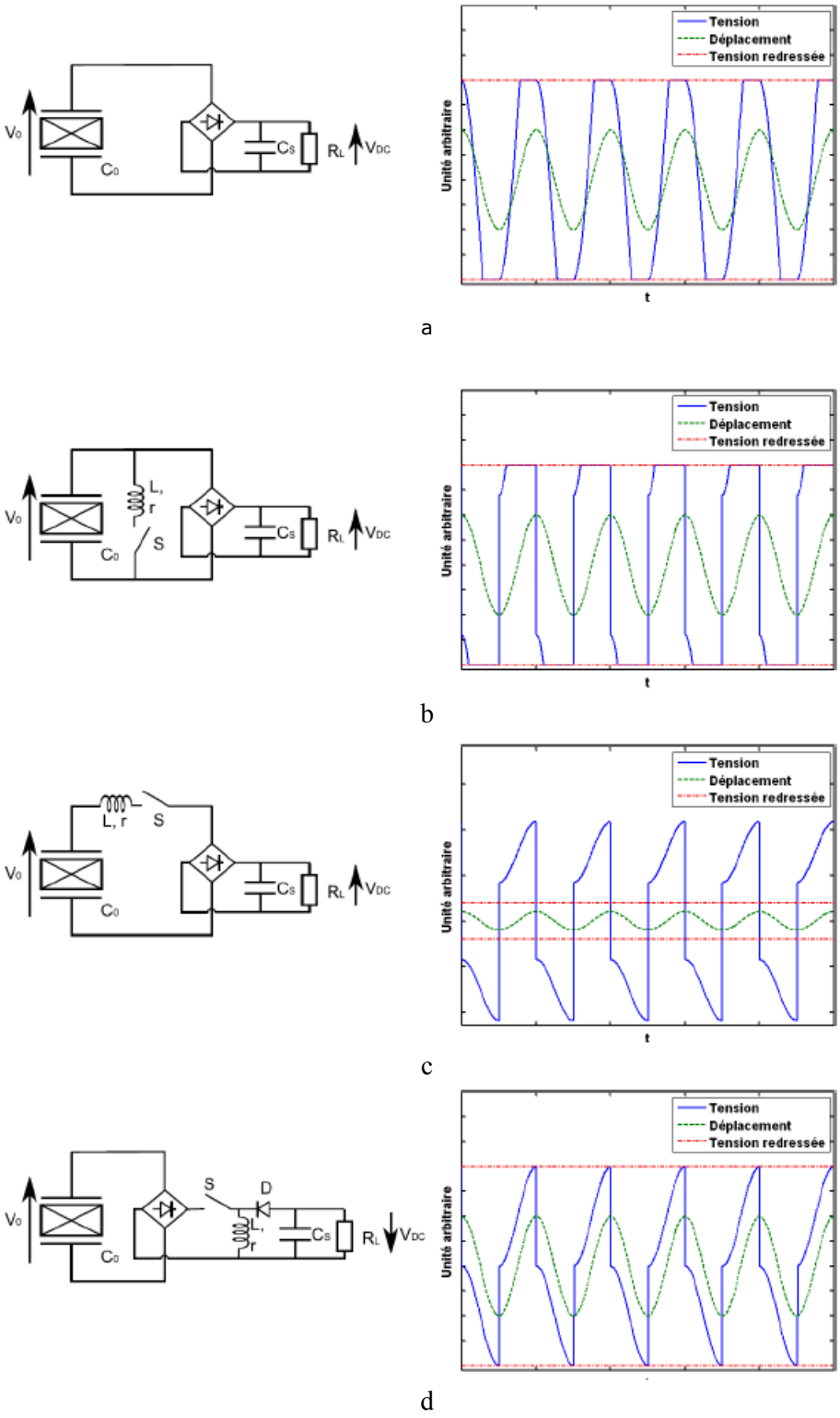

Figure 4.2 Harvesting circuit et associated waveform [84]

a. Standard; b. SSHI parallel; c. SSHI series; d. SECE

The table 4.1 and the figure 4.3 summarize the extracted and scavenged powers for these methods.

Table 4.1 Harvested power for various interfaces with constant displacement amplitude [84]

Technique	Maximum harvested power
Standard	$\frac{\alpha^2}{C_0} f_0 u_M^2$
SSHI parallel	$\frac{2}{1-\gamma}\frac{\alpha^2}{C_0} f_0 u_M^2$
SSHI series	$\frac{1+\gamma}{1-\gamma}\frac{\alpha^2}{C_0} f_0 u_M^2$
SECE	$4\gamma_c \frac{\alpha^2}{C_0} f_0 u_M^2$

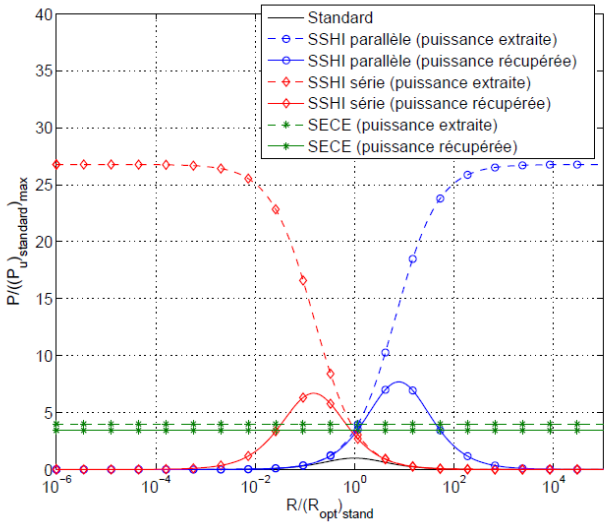

Figure 4.3 Extracted and harvested power for the various interfaces in the case of vibration with constant amplitude [84]

In the case of SSHI series or parallel, the extracted and scavenged powers are much higher than the one in the standard case (simple rectifier). The SECE gain is lower than the two others techniques but the extracted and scavenged energies remains constants as a function of the load R. The extracted energies with the parallel or series SSHI are equivalent. One can note that the SSHI series develop a lower optimal load than the SSHI parallel. On an optimal load, the SSHI parallel scavenge more energy than the other techniques with a gain around 14.5 compared to classic standard techniques (13.5 for the series SSHI). In the case of strongly coupled struc-

tures with a low k²Qm factor (most of the case), the SECE technique extract the energy in a faster way than the other technics.

In our research case, the goal is to scavenge a maximum of energy to create the useful and necessary conditions to enhance the damping of the targeted modes. Thus, according to the state of art, we will chose to focus on SSHI technics.

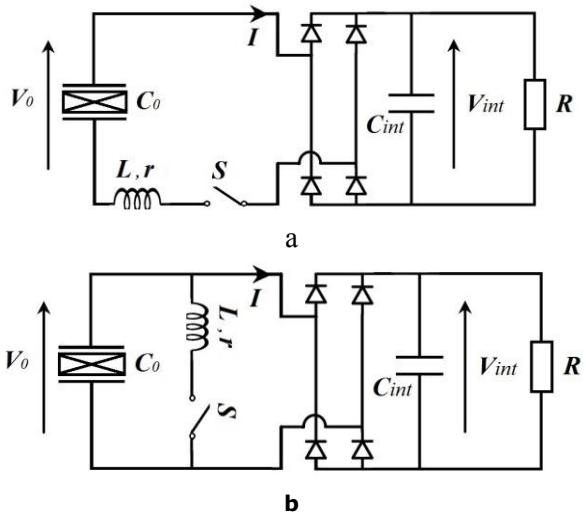

Figure 4.4 SSHI circuit

a. series-SSHI ; b. parallel-SSHI

Several simplification and hypothesis are taken in order to give an insight of SSHI circuit. The piezoelectric element is modeled as a controlled current source i in parallel with its blocked capacitor C_0. The switch and inductor here are regarded as an ideal switch S, and as an inductor L with a purely resistive r (represents the loss of inductor) in series/parallel. A full-wave diode bridge rectifier and an intermedia capacitor C_{int} are also used. The voltage on the load R is constant and remain constant. The capacitance C_{int} is thus enough large to minimize the ripple effect.

If the inversion coefficient is large enough, the performances of *series-SSHI* and *parallel-SSHI* are very similar. But the *series-SSHI* technique has better performance to harvest energy under the low voltage level [59].

The series-SSHI and the parallel-SSHI circuit have the same switch control law. By closing the switch S on each extreme mechanical displacement, the inductance L will be connected to the circuit for a short time Δt. The capacitance C_0 of the piezoelectric element and the inductance L constitute an oscillator circuit. It results in a quick inversion of the piezoelectric voltage on the piezoelectric element C_0. Repetition of this process

will obtain a magnified voltage and increased related transferred energy to supply a load impedance.

The short time Δt is equal to a semi-pseudo-period of the oscillation circuit.

$$\Delta t = \pi\sqrt{LC_0} \tag{4.1}$$

The energy stored on the piezoelectric element capacitance is partially lost in the switching operation. Indeed, the voltage inversion is not perfect. These losses can be simulated as a resistance r in series with the inductance L. The value of r can be calculated by the inversion quality factor Q_i.

$$r = \frac{1}{Q_i}\sqrt{\frac{L}{C_0}} \tag{4.2}$$

With Q_i the electric quality factor

The voltage of the piezoelectric element before and after the inversion process is given by:

$$V_{after} = -V_{before} \cdot e^{-\frac{\pi}{2Q_i}} \tag{4.3}$$

An inversion factor γ which represents the ratio between the voltage after inversion and the voltage before inversion can be defined as:

$$\gamma = e^{-\frac{\pi}{2Q_i}} \tag{4.4}$$

4.2.2 DC-DC converter

Regarding the optimization of energy transfer, a DC-DC converter can be used to regulate the DC power supplies and control the maximal output power flow. For its simplicity of adjustment, a buck-boost converter is chosen as shown in **Erreur ! Source du renvoi introuvable.**4.5. It is used between the rectifier and the storage capacitor C_B.

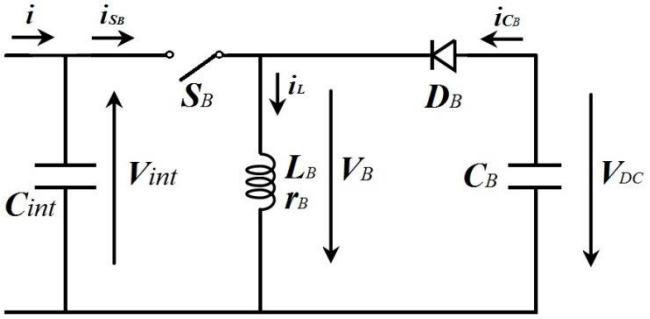

Figure 4.5 Buck-boost converter

This circuit is composed of a switch S_B, an inductor L_B, r_B and a diode D_B; can be used in two different ways: continuous mode and discontinuous current mode (DCM). Working in the discontinuous mode allows to easily tune the input impedance of this converter to match the output of the previous circuit, i.e. the harvesting one. Namely, an impedance match can be basically and simply done to extract more energy. For that practical reasons, the buck-boost converter will be used in this DCM mode.

One can underline, regarding figure 4.2, that this circuit can also be used to transfer electrical charges from the capacitor C_{int} to the capacitor C_B in two steps through the inductor L_B. This behavior was recently used by Lallart in his DSSH circuit. Let's develop this two behavior: DCM modes and DSSH mode.

Buck-boost (step-down/step-up) control command

The buck–boost (step-down/step-up) converter is a type of *DC-to-DC* converter which has an output voltage magnitude that is either greater than or less than the input voltage magnitude. As the result, the main application of the buck-boost converter is to regulate *DC* power supplies.

The basic principle of the buck–boost converter is fairly simple:

- while in the switch S_B is closed, the input voltage source is directly connected to the inductor L_B. This results in accumulating energy in L_B.
- while in the switch S_B is open, the inductor is connected to the output load and capacitor, so energy is transferred from L_B to C_B.

The polarity of the output voltage is opposite to that of the input; and the output voltage can vary continuously from 0 to infinite value (for an ideal converter). The others DC-DC converter such a boost or buck topology have limits in their output range.

If the current through the inductor L_B never falls to zero during a commutation cycle, the converter is said to operate in continuous mode. In some cases, the amount of energy required by the load (which could be a simple load R) is small enough to be transferred in a time smaller than the whole commutation period. Thus, the current through the inductor falls to zero during a part of the period: the converter works in a discontinuous mode. The only difference in the principle described above (the sequence of the switch S_B) is that the inductor is completely discharged at the end of the commutation cycle. Figure 4.6 shows the currents i_L, i_{SB} and i_{CB} respectively in the inductor L_B, switch S_B, capacitor C_B and voltages waveforms of the buck-boost in the DCM. The control unit of the buck-boost circuit is to

turn on and off the MOSFET transistor S_B at the switching frequency f_B, with a duty cycle D.

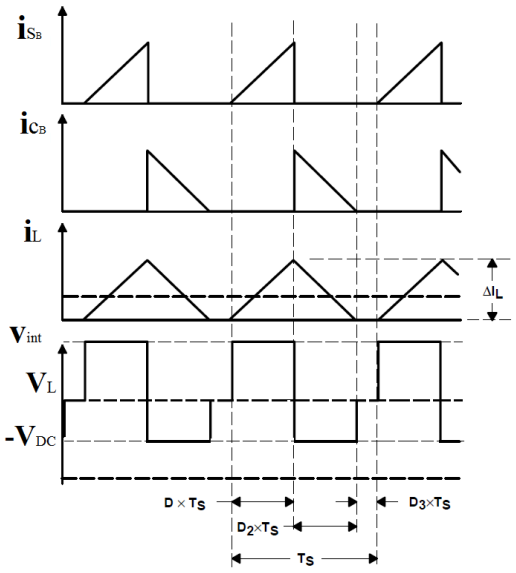

Figure 4.6 Waveforms of current and voltage in a buck–boost converter operating in discontinuous current mode

The current through the inductor L_B falls to zero during part of the period. The inductor is completely discharged at the end of the commutation cycle.

The steady state voltage conversion relationship between the input voltage (V_{int}) and output voltage (V_{DC}) for the *DCM* buck-boost becomes:

$$\frac{V_{DC}}{V_{\text{int}}} = \frac{D}{D_2} \tag{4.5}$$

with duty cycle D, corresponding to the time where the switch is closed. D_2 corresponds to the time necessary to i_L to fall to zero (see Fig. 4.6).

Thanks to Kirchhoff laws, the output voltage gain can be written as:

$$\frac{V_{DC}}{V_{\text{int}}} = -\frac{V_{\text{int}} D^2 T}{2LI_{out}} \tag{4.6}$$

Compared to the expression of the output voltage gain obtained in the continuous mode (D-1/D), the output voltage is much more complicated in DCM mode. Indeed, the output voltage depends on the duty cycle, but also on the inductor value, the input voltage and the output current.

For constant values of the switching frequency f_B and the duty cycle D, buck-boost converter in a DCM mode, has a constant input average resistance R_{in}, which is expressed as:

$$R_{in} = \frac{2 \cdot L_B \cdot f_B}{D^2} \tag{4.7}$$

The output voltage and the input resistance of the converter can be easily tuned thanks to a judicious choice of components and duty cycle.

DSSH control command

This topology, used in *DSSH* (Double synchronized switch harvesting) control command, can be described as: When there is enough energy on the capacitor C_{int}, the switch S_B is closed. Thus, the energy is transferred from the capacitor C_{int} to the inductor L_B. Then, when the energy is maximal on the L_B (maximum current and no charge on C_{int}), S_B is open and the diode D_B conducts, transferring the energy from L_B to the smoothing capacitor C_B. The key issue to control the switch depend on the current in the circuit and charge on C_{int}. In a way, it can be seen as a full charge transfer.

4.3 Association of circuits

The proposed techniques are based on modal control methods applied to the different energy converting techniques. They derive from the *series-SSHI* Modal and *parallel-SSHI* Modal techniques. Due to the different energy conversion modal techniques and different operative modes of the *DC-DC* converter, four combinations are presented here: *DSSH* [84], *series-SSHI* associated with a buck-boost converter; *parallel-SSHI* associated with a buck-boost converter; *parallel-DSSH*. The architecture principles are presented and comparisons of their respective energy harvesting effectiveness will be illustrated.

Mainly developed in a case of a harmonic motion of a one DOF system, these approaches are rewritten in a modal point of view to extend their applications to realistic mechanical system.

4.3.1 Series-SSHI with buck-boost: Physical and Modal version

The proposed circuit *series-SSHI* harvesting technique with buck-boost converter is shown in **Erreur ! Source du renvoi introuvable.**4.7.

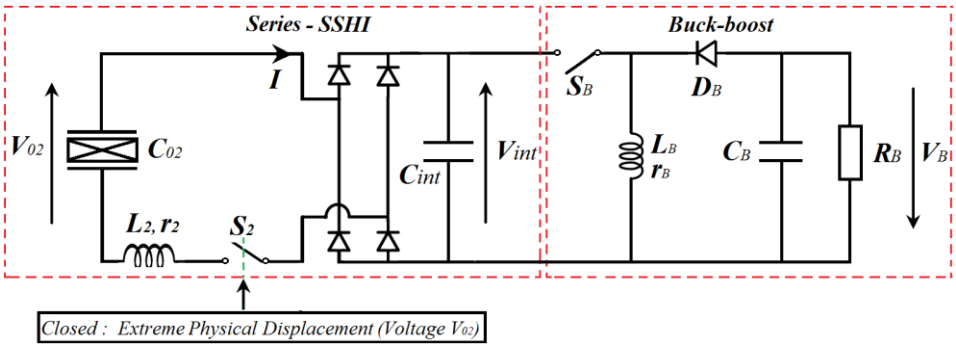

Figure 4.7 Series-SSHI with buck-boost extraction circuit

Based on the energy harvesting *series-SSHI* technique and the buck-boost converter operating in DCM, an optimal duty cycle can be determined where the power flow from the piezoelectric element is maximized.

The circuit in figure 4.7 can be divided into two parts. The first part corresponds to the configuration of the *series-SSHI*, included the piezoelectric element C_{02} connected in series with the switch S_2 and the inductor L_2 (which has an internal resistor r_2), the diode bridge rectifier, and the intermediate capacitor C_{int}. The second part, composed by the switch S_B, the inductor L_B (with an internal resistor r_B) and the diode D, is a buck-boost static converter.

When the displacement u reaches an extreme, the switch S_2 is closed for a very brief time period which corresponds exactly to the half of an oscillation period ($\Delta t = \pi\sqrt{L_2 C_{02}}$).

Thus, energy is transfered from the piezoelectric element C_{02} to the intermediate capacitor C_{int} through the inductor L_2 and the diode bridge rectifier.

Regarding the SSHI series circuit, the constant output voltage V_{int} on a load, equivalent resistor R, during a half of the mechanical period, is expressed as Eq. (4.8)[85].

$$V_{\text{int}} = \frac{2\alpha_2 R(1+\gamma)}{2RC_{02}\omega_2(1+\gamma)+\pi(1-\gamma)}\omega_2 u_M \tag{4.8}$$

Where u_M is the maximal output displacement at the end of the free end of the beam, α2 is the coupling factor in V/N, γ is the inversion

coefficient and w_2 is the natural angular frequency of the electrical oscillating circuit.

According to the power optimization point of view about the *series-SSHI* Modal technique for a constant displacement amplitude u_M, the average harvested power reaches the maximum value for an optimal equivalent load resistance R_{opt}:

$$R_{opt} = \frac{\pi}{2C_{02}\omega_2}\frac{1-\gamma}{1+\gamma} \tag{4.9}$$

and the optimal voltage on the intermediate C_{int} is:

$$\left(V_{\text{int}}\right)_{opt} = \frac{\alpha_2}{2C_{02}}u_M \tag{4.10}$$

One can remember that the buck-boost circuit used here is working in *DCM* (discontinuous current mode), which has been presented in the section 4.1.2. Through closing the switch S_B, the energy transfer process starts. It consists of transferring the energy of the intermediate capacitor C_{int} to the buck-boost inductor L_B. During this time, the inductor will store energy. When the switch S_B is opened, the inductor L_B will be cut off from the input voltage supply. Meanwhile, the capacitor C_B will be charged up by the inductor L_B. For constant values of the switching frequency f_B and duty cycle D, the buck-boost converter has a constant input average resistance R_{in}, which is expressed as:

$$R_{in} = \frac{2 \cdot L_B \cdot f_B}{D^2} \tag{4.11}$$

The load resistance R of the circuit *series-SSHI* can be equivalent to the input average resistance of buck-boost converter, that is:

$$R = R_{in} \tag{4.12}$$

Solving the Eq.(4.8), (4.11) and (4.12), the duty cycle is obtained as:

$$(D^2)_{series} = \frac{4L_B f_B(1+\gamma)\omega_2}{V_{\text{int}}\pi(1-\gamma)}(\alpha u_M - V_{\text{int}}\,\mathrm{C}_{02}) \tag{4.13}$$

The maximization of the power flow from the piezoelectric element can be considered as a resistive impedance matching. In this case, the effective input resistance R_{in} (Eq.(4.11)) should be equal to the optimal resistive load R_{opt} (Eq.(4.9)) of the circuit *series-SSHI*, given in Eq.(4.14).

$$R_{opt} = R_{in} \tag{4.14}$$

Hence, the optimal duty D_{opt} cycle which results in maximum extracted power can be determined as:

$$(D^2{}_{opt})_{series} = \frac{4L_B}{T_B}\cdot\frac{C_{02}(1+\gamma)\omega_{20}}{\pi(1-\gamma)} \tag{4.15}$$

For each switching period T_B, the input voltage of the buck-boost converter is assumed as DC voltage. The input energy charges the inductor during switch on-time and releases the inductor energy completely to the storage capacitor due to the *DCM* operation. The average value of the output voltage is thus:

$$V_B = \frac{2}{1+\sqrt{1+\frac{4K}{\left(D_{opt}^2\right)_{series}}}} V_{\text{int}} \tag{4.16}$$

where

$$K = \frac{2L_B}{R_B T_B} \tag{4.17}$$

Therefore, the average power delivered to the storage capacitor C_B can be expressed as:

$$\left(P_{s\_ssh\_bb}\right)_{out} = \frac{V_B^2}{R_B} \tag{4.18}$$

Thus, the optimal delivered power can be obtained using Equation (4.18) (4.15) (4.16) and (4.17), and is expressed as:

$$\left(P_{s\_ssh\_bb}\right)_{out} = \frac{{\alpha_2}^2 u_M^2}{2R_B C_{02}^2 (1+\Upsilon+\sqrt{1+2\Upsilon})} \tag{4.19}$$

where $\Upsilon = \frac{\pi(1-\gamma)}{R_B C_{02}(1+\gamma)\omega_2}$.

Where u_M is the maximal output displacement at the end of the free end of the beam, α2 is the coupling factor in V/N, γ is the inversion coefficient and w_2 is the natural angular frequency of the electrical oscillating circuit.

The power expression is derived from the energy with the consideration of the vibration frequency f_2 and noting that the energy transfer process occurs twice a period. The harvested energy is:

$$\left(E_{s\_ssh\_bb}\right)_{out} = \frac{\alpha^2 u_M^2}{R_B f_2 C_{02}^2 (1+\Upsilon+\sqrt{1+2\Upsilon})} \tag{4.20}$$

The simulations related to this new technique will be presented at the end of this chapter, and the comparison with the other three following combinations will be discussed.

Modal version

In the physical version, the energy can be extracted by an optimized way for a mechanical displacement u_M. Now, the harvesting energy process focus on a particular mode.

The **Erreur ! Source du renvoi introuvable.**4.8 depicts the modal version, *series-SSHI* Modal with buck-boost.

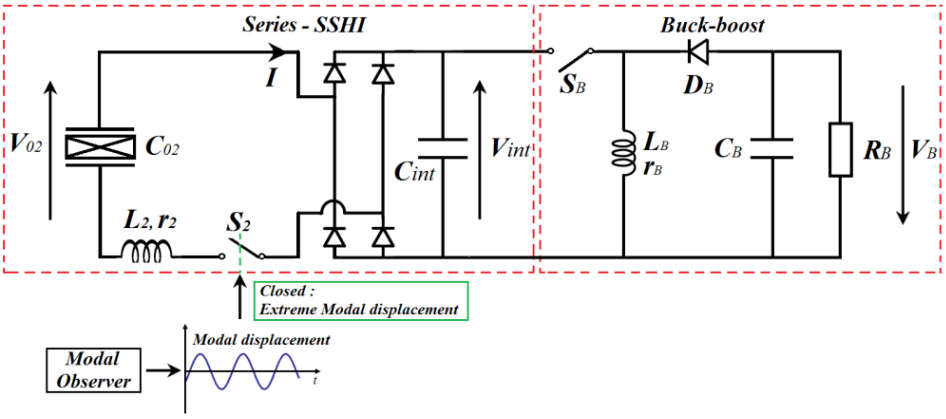

Figure 4.8 Series-SSHI Modal with buck-boost extraction circuit

The modal version of this architecture (*series-SSHI* Modal with buck-boost) is constituted by the same parts of the physical version (*series-SSHI* with buck-boost). For the *series-SSHI*, the difference between modal and physical version only concerns the switching moment: S_2 is now closed when the modal displacement reaches an extreme. The modal displacement can be obtained from a modal observer which was presented in the chapter 2.

All the switching laws, quantities and optimizations presented for the physical version can be transferred, reused in the modal version.

4.3.2 Parallel-SSHI with buck-boost: Physical and Modal version

The second combination is the *parallel-SSHI* circuit with the buck-boost technique. It is similar to the *series-SSHI* with buck-boost technique, but *parallel-SSHI* circuit replace the *series-SSHI* circuit. As the same of the first proposed circuit, an optimal duty cycle can be determined to scavenge a maximum of power from the piezoelectric element.

Physical version

The scheme of *parallel-SSHI* technique with the buck-boost converter is shown in **Erreur ! Source du renvoi introuvable.**4.9.

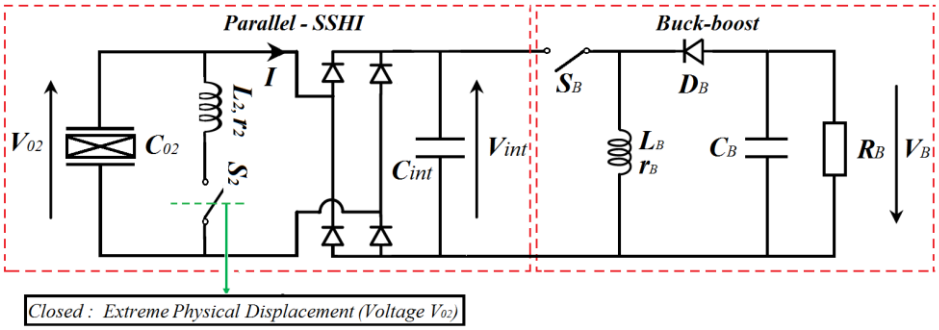

Figure 4.9 Parallel-SSHI with the buck-boost extraction circuit

The scheme can be divided into two parts: the first part corresponds to the configuration of *parallel-SSHI*; the second part is composed by the switch S_B the inductor L_B (with an internal resistor r_B) and the diode D. The switching control command of this technique is operated as *series-SSHI*. When the displacement reaches an extreme, switch S_2 is closed for a very brief time period. A smoothing voltage is collected on the capacitor C_{int}, so the input voltage to the buck-boost converter is assumed as *DC* voltage for each switching period T_B.

As presented in the previous sections, buck-boost converter has a constant input average resistance R_{in} when it is operating in *DCM* (discontinuous current mode), which is expressed as Eq.(4.11). Thus, the expression of the voltage V_{int} as a function of the displacement amplitude u_m and input resistance of the buck-boost converter R_{in} can be given by Eq.(4.21).[85]

$$V_{\text{int}} = \frac{2R_{in}\cdot\alpha_2}{R_{in}C_{02}(1-e^{\xi})\omega_2+\pi}\cdot\omega_2\cdot u_m \tag{4.21}$$

With ξ the damping factor, α_2 the inversion coefficient, ω_2 the natural angular frequency

Inserting Eq.(4.11) in Eq.(4.21), the duty cycle D can be expressed as:

$$D^2 = \frac{4L_B}{T_B(t_2-t_1)V_{\text{int}}}\left[2\alpha\cdot u_m - 2C_{02}\cdot V_{\text{int}} + C_{02}\cdot V_{\text{int}}\cdot\left(1+e^{\xi}\right)\right] \tag{4.22}$$

Regarding the power optimization of the *parallel-SSHI* Modal technique, an optimization resistor (R_{opt}) can be found to obtain the maximum of the output power.

$$R_{opt} = \frac{\pi}{C_{02}(1-\gamma)\omega_2} \tag{4.23}$$

and the optimal voltage on the intermediate C_{int} is:

$$\left(V_{\text{int}}\right)_{opt} = \frac{\alpha_2}{(1-\gamma)C_{02}} u_M \tag{4.24}$$

As discussed in the previous section, the maximization of the power flow from the piezoelectric element is a function of the resistive impedance matching. The optimal duty cycle D_{opt} for *parallel-SSHI* with buck-boost can thus be expressed as:

$$(D^2{}_{opt})_{parallel} = \frac{2L_B}{T_B} \cdot \frac{C_{02}(1-\gamma)\omega_2}{\pi} \tag{4.25}$$

For each switching cycle, the input energy charges the inductor during switch on-time and releases the inductor energy completely to the storage capacitor due to the *DCM* operation. The average value of the output voltage is:

$$V_B = \frac{2}{1+\sqrt{1+\frac{4K}{\left(D_{opt}^2\right)_{parallel}}}} V_{\text{int}} \tag{4.26}$$

where $K = \dfrac{2L_B}{R_B T_B}$

The extracted power for an energy transfer event is given by:

$$\left(P_{\text{p\_ssh\_bb}}\right)_{out} = \frac{V_B^2}{R_B} \tag{4.27}$$

Thus the optimal delivered power can be obtained using Equation (4.24) (4.25) (4.26), and is given by:

$$\begin{aligned} \left(P_{\text{p\_ssh\_bb}}\right)_{out} &= \frac{2}{R_B(1+\Upsilon+\sqrt{1+2\Upsilon})} \cdot \left(\frac{\alpha u_M}{C_{02}(1-\gamma)}\right)^2 \\ \Upsilon &= \frac{2\pi}{R_B C_{02}(1-\gamma)\omega_2} \end{aligned} \tag{4.28}$$

The harvested energy according to vibration period, can be expressed as:

$$\left(E_{\text{p\_ssh\_bb}}\right)_{out} = \frac{4}{R_B f_2(1+\Upsilon+\sqrt{1+2\Upsilon})} \cdot \left(\frac{\alpha u_M}{C_{02}(1-\gamma)}\right)^2 \tag{4.29}$$

Modal version

The modal version of *parallel-SSHI* Modal with buck-boost is shown in **Erreur ! Source du renvoi introuvable.**4.10.

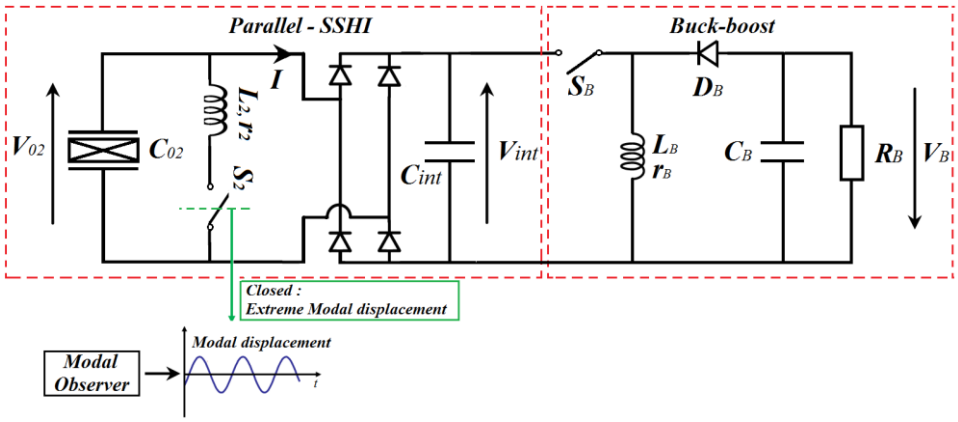

Figure 4.10 *Parallel-SSHI* Modal with the buck-boost extraction circuit

As illustrated in the section 4.2.1, the difference between the physical and the modal version is the conditions of the switching moment: S_2 is closed when the modal displacement reaches an extreme. Otherwise, all the parameters optimization are the same.

4.3.3 Series-DSSH: Physical and Modal version

Lallart [84] proposed an energy extraction circuit so called series-DSSH, shown in **Erreur ! Source du renvoi introuvable.**4.11. This technique is based on an intermediate energy storage unit using a capacitor C_{int}, the control strategy of the switch is determined by the energy harvesting and energy transfer process.

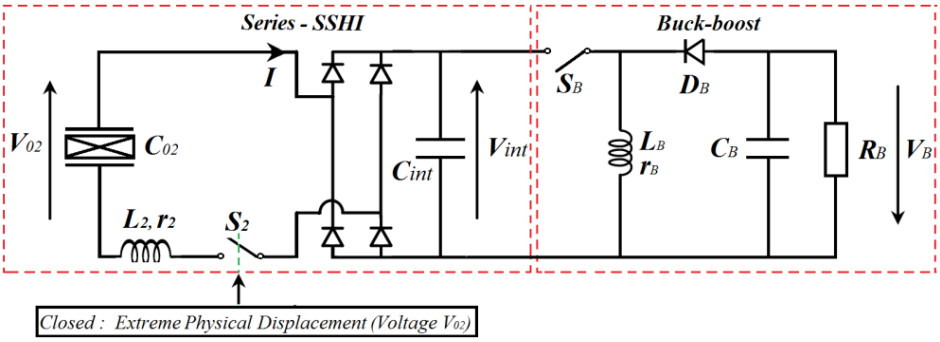

Figure 4.11 Series-DSSH extraction circuit

The scheme of this circuit is the same as *series-SSHI* with buck-boost technique, but the operating principle is different.

Most of the time, the piezoelectric element is in open circuit: S_2 and S_B are open, D_B is blocked. The switch S_2 is closed when the displacement u reaches an extreme u_M. There is thus an energy transfer from the piezoelectric element to the intermediate capacitor C_{int} through the inductor L_2 and the diode bridge rectifier. This oscillating circuit (C_{02} in series with L_2, r_2 and C_{int}) develop the following governing equation:

$$L_2\ddot{q}_0 + r_2\dot{q}_0 + \frac{q_0}{\frac{C_{02}C_{\text{int}}}{C_{02}+C_{\text{int}}}} = 0 \tag{4.30}$$

Where q_0 is the charge of the piezoelectric element, thus giving the current flow:

$$\dot{q}_0 = -\frac{C_0 C_{\text{int}}}{C_0 + C_{\text{int}}} V_0 \frac{\omega_2}{\sqrt{1-\xi_0^2}} \cdot e^{-\omega_2 \xi_0 t} \sin(\omega_2 \cdot \sqrt{1-\xi_0^2} \cdot t) \tag{4.31}$$

V_0 is the voltage across the piezoelectric element just before the switching event. The natural angular frequency and the damping coefficient of the system are defined as:

$$\omega_2 = \sqrt{\frac{1}{L_2 \frac{C_{02}C_{\text{int}}}{C_{02}+C_{\text{int}}}}} \tag{4.32}$$

$$\xi_0 = \frac{1}{2} r_2 \sqrt{\frac{\frac{C_{02}C_{\text{int}}}{C_{02}+C_{\text{int}}}}{L_2}} \tag{4.33}$$

This first switching event stops when the current i is null, giving the amount of transferred charges,

$$\Delta q_0 = \int_0^{\pi/\left(\omega_2 \cdot \sqrt{1-\xi_0^2}\right)} \dot{q}_0 dt = -\frac{C_{02}C_{\text{int}}}{C_{02}+C_{\text{int}}}(1+\gamma_0)V_0 \tag{4.34}$$

where the inversion factor γ_0 is defined as:

$$\gamma_0 = e^{-\pi\xi_0/\sqrt{1-\xi_0^2}} \tag{4.35}$$

The voltage across the capacitors C_{int} and C_B can be detailed as:

$$\left(V_{C_{02}}\right)_{end} = V_0 + \frac{\Delta q_0}{C_0} = \left(1 - \frac{C_{\text{int}}}{C_{\text{int}} + C_{02}}(1+\gamma_0)\right)V_0 \tag{4.36}$$

$$\left(V_{C_{\text{int}}}\right)_{end} = \frac{\Delta q_0}{C_{\text{int}}} = \left(\frac{C_{\text{int}}}{C_{\text{int}} + C_{02}}(1+\gamma_0)\right)V_0 \tag{4.37}$$

When the energy transfer is complete, the switch S_2 is opened and the switch S_B is closed. Thus, an energy transfer from the intermediate capacitor C_{int} to the buck-boost inductor L_B is occurring. The expression of the current in the inductor (oscillating C_{int}, L_B, r_B circuit) is:

$$L_B\ddot{q}_B + r_B\ddot{q}_B + \frac{q_B}{C_{\text{int}}} = 0 \tag{4.38}$$

Leading to

$$i_B = \dot{q}_B = C_{\text{int}}(\mathrm{V}_{C_{\text{int}}})_{end}\frac{\omega_B}{\sqrt{1-\xi_B{}^2}}e^{-\omega_B\xi_B t}\sin(\omega_B\sqrt{1-\xi_B{}^2}t) \tag{4.39}$$

where

$$\omega_B = \sqrt{\frac{1}{L_B C_{\text{int}}}} \tag{4.40}$$

$$\xi_B = \frac{1}{2}r_B C_{\text{int}}\omega_B \tag{4.41}$$

If the damping coefficient $\xi_B \gg 1$, the expression of the current at the end of the transfer can be defined as:

$$I_B = (\dot{q}_B)_{end} = C_{\text{int}}(\mathrm{V}_{C_{\text{int}}})_{end}\frac{\omega_B}{\sqrt{1-\xi_B{}^2}}e^{-\xi_B\pi/2} \tag{4.42}$$

Then, when the energy is maximal on the L_B (current maximal and no charge on C_{int}), S_B is opened and D_B conducts, transferring the energy from L_B to the smoothing capacitor C_B. Then the lastly governing equation for this energy transfer yields:

$$L_B\ddot{q}_{B_2} + r_B\dot{q}_{B_2} = -V_B \tag{4.43}$$

At the end of the transfer process, the current is null and the amount of transferred charges can be expressed by:

$$\Delta q_{B_2} = \frac{L_B}{r_B}I_B - \frac{V_B L_B}{r_B^2}\ln(1+\frac{r_B I_B}{V_B}) \tag{4.44}$$

With V_B the constant output voltage. Using (4.37) (4.42), equation (4.44) leads to:

$$\Delta q_{B_2} \approx \frac{1}{2}\frac{L_B}{V_B}I_B^2 \tag{4.45}$$

The expression of the harvested energy for a single operation cycle is given by:

$$\left(E_{s\_DSSH}\right)_{out} = \int V_B \dot{q}_{B_2} dt = V_B q_{B_2} \tag{4.46}$$

$$\left(E_{s\_DSSH}\right)_{out} = \frac{1}{2}\gamma_B C_{\text{int}} \left(V_{C_{\text{int}}}\right)^2_{end} \tag{4.47}$$

with the efficiency of the converter γ_B, given by:

$$\gamma_B = e^{-\xi_B \pi} \tag{4.48}$$

Thus the optimal harvested power is given by:

$$\left(P_{s\_DSSH}\right)_{out} = \frac{1}{2}\gamma_B \frac{(1+\gamma)^2}{1-\gamma}\frac{\alpha^2}{C_{02}} u_M^2 f_2 \tag{4.49}$$

Modal version

As illustrated in previous section, the principle of the modal version is that the switch S_2 is closed when the modal displacement reaches an extreme. The modal displacement is obtained from a modal observer (see chapter 2). The **Erreur ! Source du renvoi introuvable.**4.12 shows new *series-DSSH* Modal.

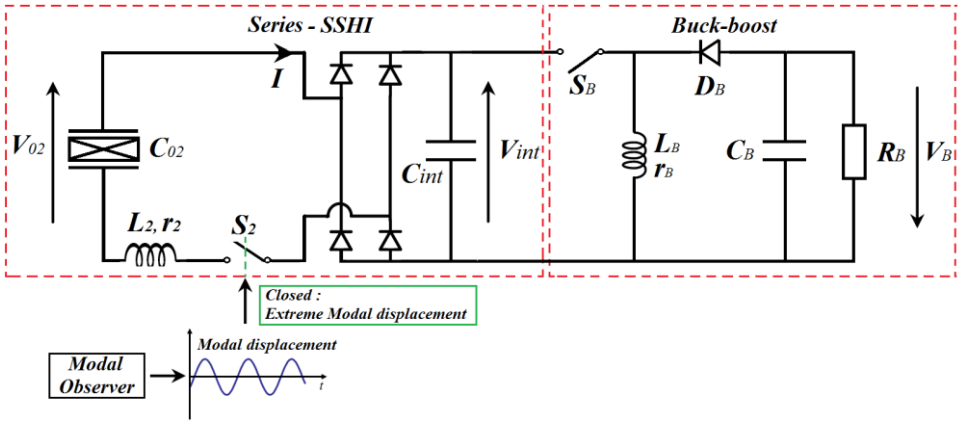

Figure 4.12 Series-DSSH Modal extraction circuit

4.3.4 Parallel-*DSSH*: Physical and Modal version

This new technique is similar to the *series-DSSH* technique, but *parallel-SSHI* circuit is in place of *series-SSHI* circuit.

Physical version

The scheme of the circuit is shown in **Erreur ! Source du renvoi introuvable.**13. The sequence of the switches for this technique is similar to the one of *series-DSSH*.

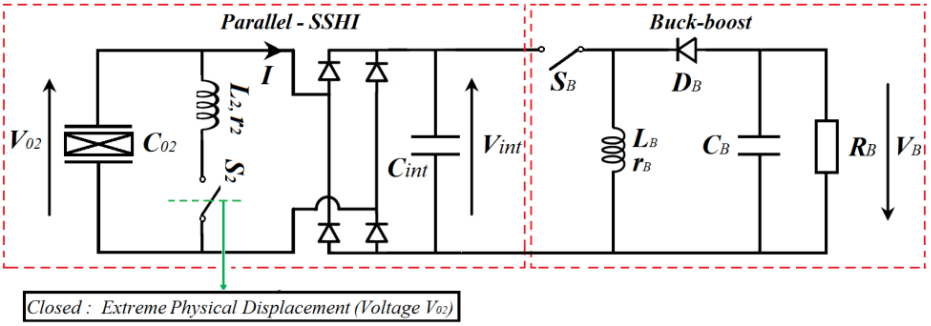

Figure 4.13 Parallel-DSSH extraction circuit

As the voltage across the piezoelectric increases due to the increase of the mechanical strain (the bending of the beam), the diodes in the rectifier conduct the charges, and both the piezoelectric capacitance C_{02} and the intermediate capacitance C_{int} are charged simultaneously. The switch S_2 is closed when the displacement reaches an extreme. Then the voltage of piezoelectric element is inversed. During this inversion, the diodes are blocked because the voltage V_{02} is smaller than the voltage V_{int}.

Considering that the voltage across the piezoelectric element is V_0 just before the switching event, the voltage after the switching event can be expressed as:

$$\left(V_{C_{02}}\right)_{end} = -V_0\gamma \tag{4.50}$$

where γ is the inverse factor.

As in the previous section, the charges q_B transferred during this step can be calculated (oscillating $C_{02}//L_2$, $r_2//C_{int}$). At the end of the inversion process, the switch S_2 is open. The second energy transfer process can start. It consists in transferring the charges stored into the intermediate capacitor C_{int} to the inductor L_B by closing the switch S_B. The governing equation is:

$$L_B\ddot{q}_B + r_B\dot{q}_B + \frac{q_B}{C_{\text{int}}} = 0 \tag{4.51}$$

The expression of the current in the inductor is:

$$i_B = \dot{q}_B = -C_{\text{int}}V_0\frac{\omega_B}{\sqrt{1-\xi_B^{\,2}}}e^{-\omega_B\xi_B t}\sin(\omega_B\sqrt{1-\xi_B^{\,2}}t) \tag{4.52}$$

The switch S_B is open at time t_C when the voltage across the capacitance C_{02} is equal to the one on the capacitance C_{int}. To find this time tc, equation (4.53) must be solved:

$$\left(V_{C_{02}}\right)_{t_C} = \left(V_{C_{\text{int}}}\right)_{t_C} \tag{4.53}$$

The voltage across the capacitance C_{int} can be written as:

$$\left(V_{C_{\text{int}}}\right)_{t_C} = V_M e^{-\alpha_B t} \sin(\omega_B \, \text{t} + \phi_B) \tag{4.54}$$

$$\begin{aligned} \omega_B &= \sqrt{\frac{1}{L_B C_{\text{int}}}} \\ \phi_B &= \arctan(\frac{\omega_B}{\alpha_B}) \end{aligned} \tag{4.55}$$

$$V_M = \frac{V_{C_{\text{int}}}(\text{t}_B)}{\sin(\phi_B)} \tag{4.56}$$

And, the voltage across the capacitance C_{02} is given by:

$$V_{C_{02}} = \frac{\alpha_2}{C_{02}} u$$

With α_2 the coupling coefficient in V/N and u the displacement.

Finally, as discussed in the previous section, the last step consists of transferring the energy stored in L_B to the capacitor C_B through the diode D_B. The governing equation for this energy transfer yields:

$$L_B \ddot{q}_{B2} + r_B \dot{q}_{B2} = -V_B \tag{4.57}$$

Thus lead to:

$$q_{B2} \approx \frac{1}{2} \frac{L_B}{V_B} (i_B(\text{t}_i))^2 \tag{4.58}$$

The extracted energy for an energy transfer event is given by:

$$\left(E_{\text{p\_DSSH}}\right)_{out} = V_B \Delta q_{B2} = \frac{1}{2} \frac{(\text{C}_0 + \text{C}_{\text{int}}) \alpha^2 \gamma_B}{C_0^2 (1-\gamma)^2} u_M^2 \tag{4.59}$$

Thus the optimal power harvested in one vibration period is given by:

$$\left(P_{\text{p\_DSSH}}\right)_{out} = \frac{f_2 (\text{C}_0 + \text{C}_{\text{int}}) \alpha^2 \gamma_B}{C_0^2 (1-\gamma)^2} u_M^2 \tag{4.60}$$

Modal version

The **Erreur ! Source du renvoi introuvable.**4 shows the modal version of *parallel-DSSH* Modal technique. The principle of the modal version is that the switch S_2 is closed when the modal displacement reaches an extreme.

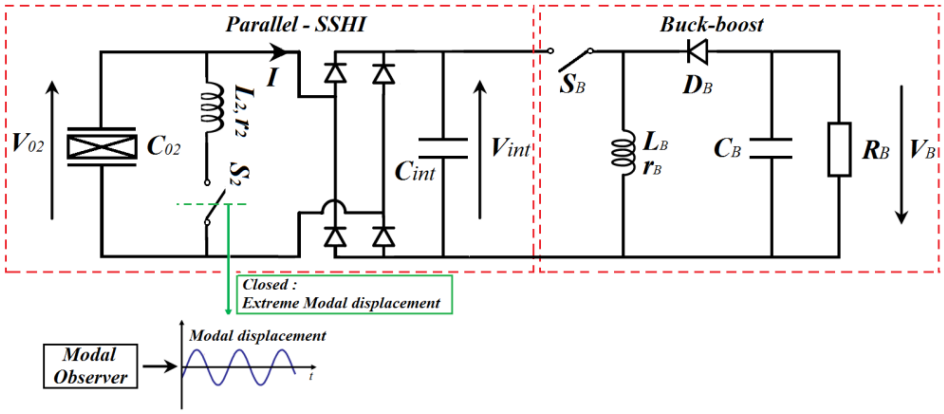

Figure 4.14 Parallel-DSSH Modal extraction circuit

These four combinations present different performances. The theoretical performances comparison of these four interfaces will be presented in the next section. They are compared in the case of operation with constant mechanical displacement amplitude in order to determine the best performance for our studied structure. The theoretical comparison of modal versions which will be used in the following chapter would give the same results.

4.4 Power performance comparison between the proposed techniques

Previous sections presented the four proposed energy harvesting interfaces. The output voltage is calculated for each topology. Considering constant vibration magnitude, the output energy is obtained using the electrical equation. In this section, the various topologies are compared in terms of total extracted energy and power on output capacitance.

Table 4.2 Summary the performances of our four modal harvesting techniques in terms of harvested energy, advantages and drawbacks

	Harvested Energy (with constant displacement)	Advantage	Drawback
P-SSH-BB	$\left(E_{p\_ssh\_bb}\right)_{out} = \frac{2}{R_B f_2 (1+\Upsilon_1+\sqrt{1+2\Upsilon_1})} \cdot \left(\frac{\alpha u_M}{C_0(1-\gamma)}\right)^2$ $\Upsilon_1 = \frac{2\pi}{R_B C_0 (1-\gamma)\omega}$	High power output	Load matching, Frequency matching

S-SSH-BB	$\left(E_{s\_ssh\_bb}\right)_{out} = \frac{\alpha^2 u_M^2}{2R_B f_2 C_0^2 (1+\Upsilon_2+\sqrt{1+2\Upsilon_2})}$, $\Upsilon_2 = \frac{\pi(1-\gamma)}{R_B C_0 (1+\gamma)\omega}$	High power output	Load matching, Frequency matching
P-DSSH	$\left(E_{p\_DSSH}\right)_{out} = \frac{1}{2}\frac{(C_0+C_{int})\alpha^2\gamma_B}{C_0^2(1-\gamma)^2}u_M^2$, $\gamma_B = e^{-\xi_B\pi}$	Load independent, Frequency independent	Complex circuitry, Complex switch strategy
S-DSSH	$\left(E_{s\_DSSH}\right)_{out} = \frac{1}{4}\gamma_B\frac{(1+\gamma)^2}{1-\gamma}\frac{\alpha^2}{C_0}u_M^2$, $\gamma_B = e^{-\xi_B\pi}$	Load independent, Frequency independent	Complex circuitry, Complex switch strategy

Practically, the comparison is realized on our smart structure, described in section 2.2.1. The smart structure is driven by the piezoelectric element in order to obtain a 2mm constant mechanical displacement amplitude at the beam free-end. The constant mechanical displacement supposes that the mechanical damping effect induced by energy harvesting is neglected. The data set used here (C_0, C_{int}, γ, ξ_B…) is chosen in coherence with the previously and following chapter. The comparison result are obtained with the electromechanical coupling ($k^2=0.0089$) corresponding to the second resonance frequency. The inversion factor γ is set at 0.75.

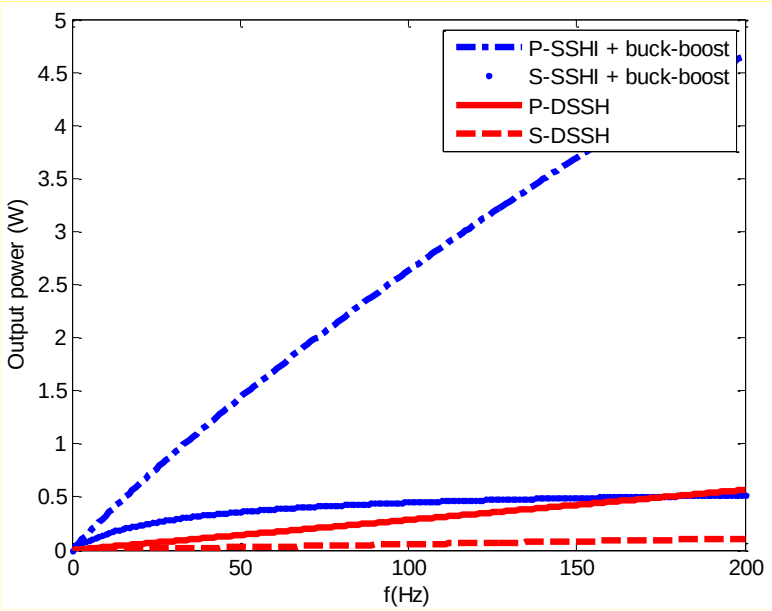

Figure 4.15 Harvested power as a function of the frequency f (Hz)

The first theoretical comparison concerns the variations of the electrical average power delivered by the piezoelectric element as a function of the frequency. The **Erreur ! Source du renvoi introuvable.**15 shows that the harvested energy of series/parallel *SSHI* with buck-boost techniques is strongly influenced by the frequency. In the opposite, the harvested power of series/parallel *DSSH* is undependable on the value of the frequency.

Parallel-*SSHI* with buck-boost obtains the highest power output in our studied frequency range. The Series-*SSHI* with buck-boost scavenge less energy than the previous circuit. The harvested energy increase as a function of the frequency until it reaches a maximum value around 50Hz. When the frequency is between 0Hz and 6Hz, higher power output is obtained with the series/parallel DSSH techniques.

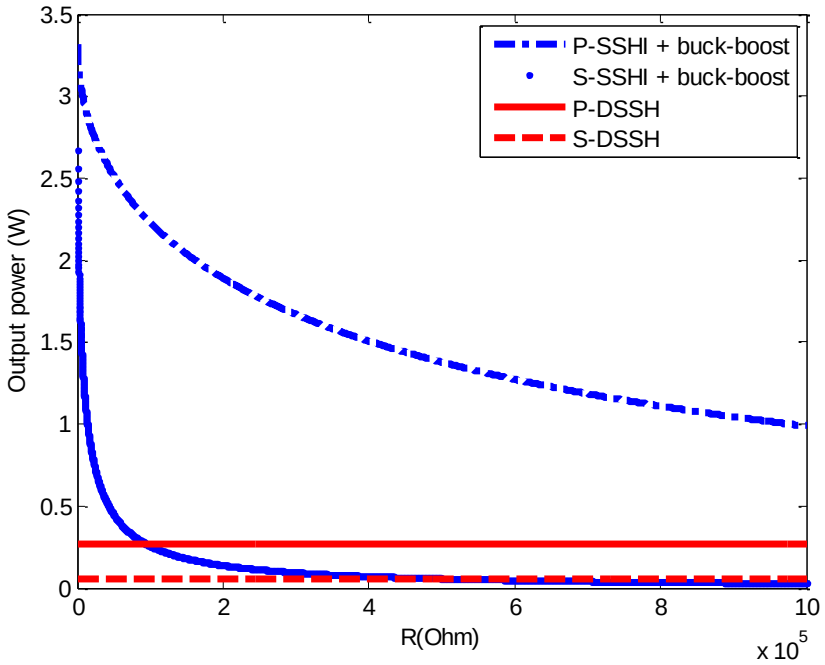

Figure 4.16 Harvested power versus the load resistor (Ohm)

Regarding the impedance adaptation approach, the harvested energy depends on the equivalent load resistance. The second theoretical comparison concerns the harvested energies which are delivered by the piezoelectric element as a function of the load impedance value.

The **Erreur ! Source du renvoi introuvable.**16 shows that the harvested energy is also strongly influenced by the load resistance value.

The series/parallel-*SSHI* with buck-boost techniques could get more energy output than series/parallel *DSSH* techniques. But the harvested energy is decreased with the increase of the load *R*. The series/parallel *DSSH* techniques has a lower power than others techniques and allows an extracted energy independent from the impedance and the frequency resonance of the structure.

As we want to scavenge a maximum of energy on high frequency modes, our development will be based on series or parallel *SSHI* associated with a buck-boost converter. An impressive improvement of the electromechanical energy conversion could be brought, which depend on the load impedance by series/parallel-*SSHI* with buck-boost techniques. In the case of obtaining the same performance, the series-*SSHI* with buck-boost technique leads to low matching load impedances, whereas the parallel-*SSHI* with buck-boost technique leads to higher matching load impedances.

4.5 Conclusion

This chapter presents the principle of four combination of non-linear piezoelectric energy harvesting techniques. Vibration energy is converted into electrical energy using piezoelectric material.

Firstly, all the four topologies have been described with detailed electrical schemes and principles depicted through basic electric equations. The theoretical comparison of four topologies concerns the variations of the electrical output power in term of frequency variations and load impedance values. For this, the generator is driven with constant displacement amplitude and has the same capacitance to convert mechanical energy to electrical energy.

Then, based on these different energy harvesting techniques, the enhanced techniques combining modal method is proposed here. These techniques harvest the energy from a particular mode via modal control. In this case, the results obtained for the physical versions can be extrapolate to the modal versions.

The chapter 5 concerns a method linking the optimal presented harvesting technique with modal control. In order to show its efficiency, an application on the previous smart structure is used. Based on the energy transfer analysis, *SSHI* series with the buck-boost is chosen as harvesting optimal technique for our new method *SSDH* Modal (Modal Synchronized Switching Damping and Harvesting)

5 Global architecture SSDH: Simulation and discussions

5.1 Introduction and simulation context

In the previous chapters, a detailed theoretical analysis about the damping circuit and the harvesting circuit were proposed. This chapter focus on the global architecture that links modal control and modal harvesting circuits. This architecture will be called Modal Synchronized Switching Damping and Harvesting (Modal *SSDH*) which represent the main originality of this work. From the studies previously presented, the best promising new method in terms of damping enhancing is an architecture using a "*SSDVC* (I) - constant intermediate voltage" circuit. From the studied case, the SSHI-series technique associated with a buck-boost converter is the best option to create this constant voltage. The global architecture is thus presented in figure 5.1.

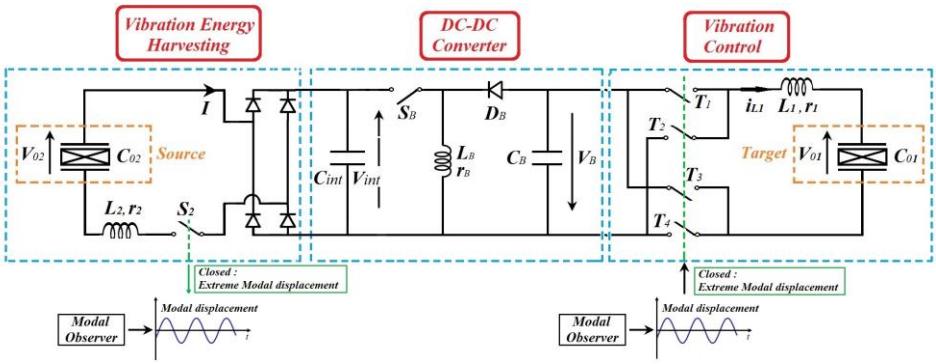

Figure 5.1 Electrical circuit of the Modal *SSDH*

To predict the control performance and choose the optimal values corresponding to a maximal damping, simulations are carried out under Matlab/Simulink™/Simscape™ environment. These optimal values concern the electrical components and the parameters of the control system.

The objective of the simulation is to demonstrate the capacity of modal energy harvesting and quantify the performance of vibration control by the energy transfer system.

Practically, the simulations are realized on the previous structure described in section 2.2.1.

The simulations are carried out with the multi-modal model driven around the first (17Hz) and second (94Hz) resonance frequency of the smart structure with a 2mm constant mechanical displacement amplitude of the beam free-end without control, which is measured by the experiment.

The results are obtained with the electromechanical coupling $k_2^2 = 0.0124$ (corresponding to the second resonance frequency) and $k_1^2 = 0.0082$ (corresponding to the first resonance frequency). In this case, the inversion factor γ is roughly equal to 0.75.

For details regarding the simulations, please refers to annex 1.

5.2 Operating mode of Modal *SSDH*

We remind here that the goal of our global circuit is to harvest energy on the second mode of the structure to enhance the damping of the first mode. Most of the time the switches S_2, T_1, T_2, T_3 and T_4 are in open conditions. Sequences of energy transfer between modes appear only on extremes.

The operating mode of the circuit presented in figure 5.1 is the following: when the modal displacement q_2 reaches an extreme, switch S_2 is closed for a very brief time period which corresponds exactly to half an oscillation period ($\Delta t = \pi\sqrt{L_2 C_{02}}$) of the oscillating circuit composed of L_2C_{02}. As the switch S_2 is closed, an amount of energy is transferred from the piezoelectric element C_{02} to the intermediate capacitor C_{int} through the inductor L_2 and the diode bridge rectifier.

In order to maintain a constant voltage for the operating control circuit, the function of the control unit of the buck-boost circuit is to turn on and off the MOSFET transistor under a very high frequency f_B, with a duty cycle D. When the switch S_B is closed, the capacitor C_{int} provides energy to the inductor. When the switch S_B is open, the energy stored in the inductor L_B is transferred to the second storage capacitor C_B.

The four switches (T_1, T_2, T_3, T_4) are in the open state most of the time and only switched on when the modal displacement of the first mode reaches either a maximum or a minimum. Then, the energy is transferred from the capacitor C_B to the piezoelectric element C_{01} through these switches. The switches should be closed for a half of an oscillation period of the oscillating circuit $L_1C_{01}r_1$, which roughly equals to $\pi\sqrt{L_1 C_{01}}$. The sequence control law of the switches as shown in the table 5.1.

Table 5.1 Sequence control law of the switches of Modal *SSDH*

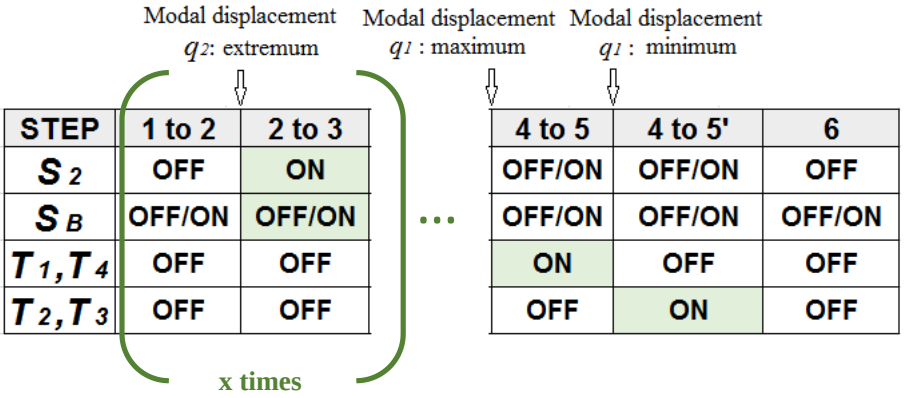

In order to detail the temporal procedure, simulation are carried out.

The figure 5.2 shows the voltage of the two piezoelectric elements (C_{01} and C_{02}), the modal displacement (q_1 and q_2) and the voltage of the intermediate capacitors C_{int} and C_B. The zoom-in waveform of the voltages and modal displacements are shown in figure 5.3. On figure 5.2, it is important to note that the initial conditions are not optimized as the charges on the capacitors start from zero. In the real experimental use of our new SSDH, the initial conditions regarding the electrical charges on the capacitors will be fixed to the one obtained in the steady state. The SSDH circuit starts operating with its two intermediate capacitors fully charged.

The results of the *SSDH* operation with previous switches control law (see number 1 to 6 in table 5.1) are presented here:

During phase 1, the piezoelectric elements are in open circuit and their output voltages are proportional to the displacement of the beam.

During phase 2 to 3: When a maxima of the modal displacement q2 is reached, the switch S2 is closed for a very brief time period which corres ponds exactly to half an oscillation period ($\Delta t = \pi\sqrt{L_2 C_{02}}$). The voltage across the piezoelectric element V_{CO2} is inverted. Energy is transferred from the piezoelectric element C_{02} to the intermediate capacitor C_{int} through the inductor L_2 and the diode bridge rectifier. An amount of ener gy get into the capacitor C_{int} and the voltage across this capacitance slight ly increase. Indeed, the capacitance C_{int} is huge compared to the capaci tance of the piezoelectric element to insure a constant output voltage (low ripple).

These phase 1 to 3 can occurs more than one time as the frequency of the second mode on which the energy is harvested, is higher than the one of the first mode. Here, with our smart structure, at least five inversions on ode 2 are obtained during phase 1 to 3. One can also note that the harvested energy is conditioned thanks to the buck-boost converter in order to insure a constant output voltage V_B. The buck-boost interface is used to adjust the voltage output. The control unit of the buck-boost circuit is to turn on and off the MOSFET transistor under a very high frequency f_B, with a duty cycle D. When the switch S_B is closed, the first rectifier capacitor C_{int} provides energy to the inductor L_B and the diode D_B which is reverse biased. When the switch S_B is open, the energy stored in the inductor L_B is transferred to the second storage capacitor C_B. One can note that the buck/boost converter work al the time but is efficiency only during phase 2 to 3

During phase 4 to 5 (5'): The switches (T_1 *and* T_4) are switched on when the modal displacement of the first mode reaches a maximum and the switches (T_2 *and* T_3) are switched on when the modal displacement of the first mode reaches a minimum. Then, the energy is transferred from the capacitor C_B to the piezoelectric element C_{01} through these switches. The switches should be closed for a half of an oscillation period, which roughly equals to $\pi\sqrt{L_1 C_{01}}$.

Remark: During each switching action of the *DSSH* circuit, the voltage on the intermediate capacitors C_{int} and C_B are viewed as DC voltage.

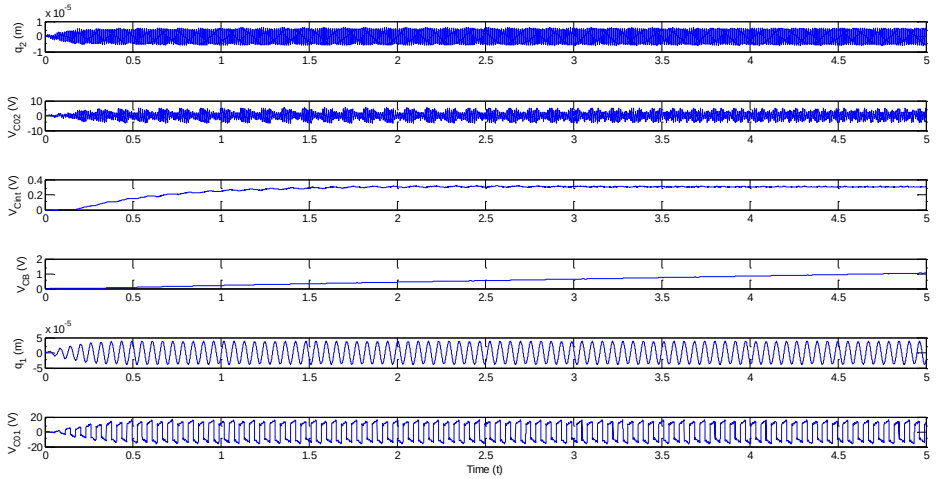

Figure 5.2 Waveforms of Modal *SSDH* without optimized initial conditions

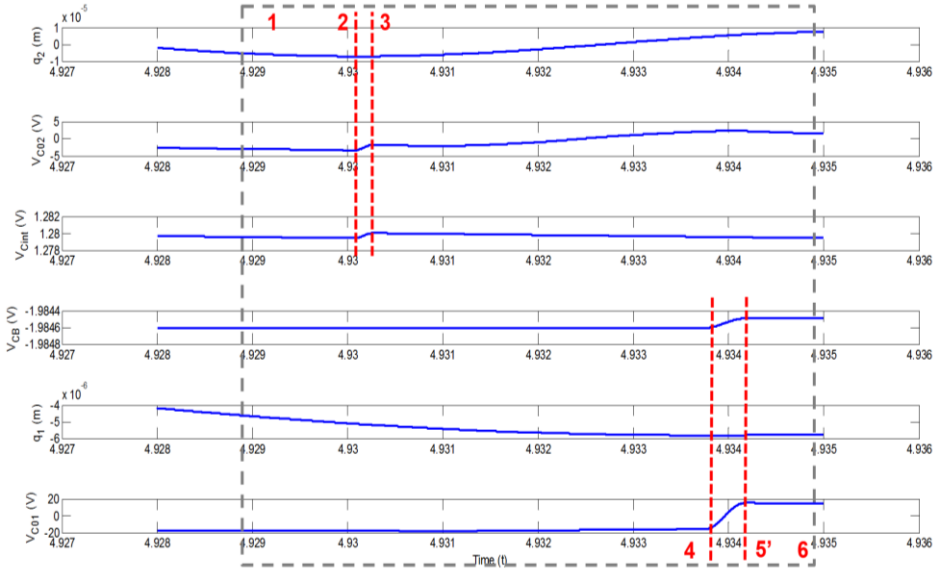

Figure 5.3 Zoom-in waveforms of Modal *SSDH*

5.3 Optimisation of the modal *SSDH*

In order to maximize the damping performance of the first mode, the optimal values of the parameters were found through theory and simulation method.

5.3.1 Theoretical optimization

The theoretical optimization was based on a mono-sinusoïdal excitation of the structure on its first mode for the optimization of the damping circuit and on its second mode for the optimization of the harvesting circuit. It has been mainly presented in the previous chapters where each part of the circuit has been studied.

For the damping circuit, the optimal parameter was found in chapter 3. The value of the capacitor C_B must be great enough to ensure that the output voltage is as a *DC* voltage with a low level of output ripple.

For the harvesting circuit, the optimal parameter was found in chapter 4. This optimization step included also the buck-boost converter, seen as a resistive load.

Nevertheless, the chosen studied case is a bi-sinusoidal excitation. Thus, the theoretical simple equation written in the mono-sinusoidal case

are not correct anymore. As developing theoretical equation in the case of bi-sinusoidal equation is a long and complex, we chose to realize the final global optimization thanks to a simulations process. The previous optimal values were chosen as the initial value to start the parametric analysis.

5.3.2 Simulation optimization of SSHI series parameters

Simulations are realized in two step with a bi-sinusoïdal excitation to adjust the parameters:

- the first step is to simulate only the harvesting circuit (namely the SSHI series circuit)
- the second step is to simulate the harvesting circuit and the DC/DC converter

First step:

According to the energy harvesting circuit *SSHI* series (remind on figure 5.4), the power of a piezoelectric generator strongly depends on the load. In order to find the maximum output power of *SSHI* series technique which is used in SSDH, the voltage on the capacitor C_{int} and the corresponding optimal equivalent load resistance R_{opt} will be determined by simulation. Moreover, the value of the intermediate capacitor C_{int} will be chosen great enough to ensure that the output voltage V_{Cint} is as a DC voltage.

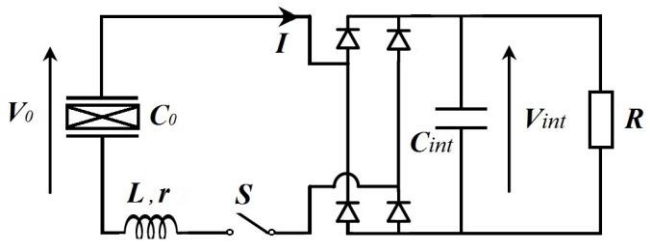

Figure 5.4 SSHI serie used for optimization process.

Figure 5.5 shows the harvested power (V_{Cint}/R^2) as a function of the equivalent load resistance *R*. Figure 5.6 gives the corresponding voltage on the capacitance C_{int} in steady state: approximate to 1.3V, different from the mono-sinusoidal study (around 4V).

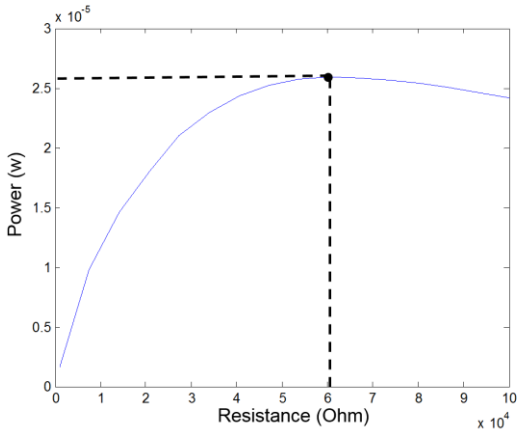

Figure 5.5 Harvested power as a function of resistance R

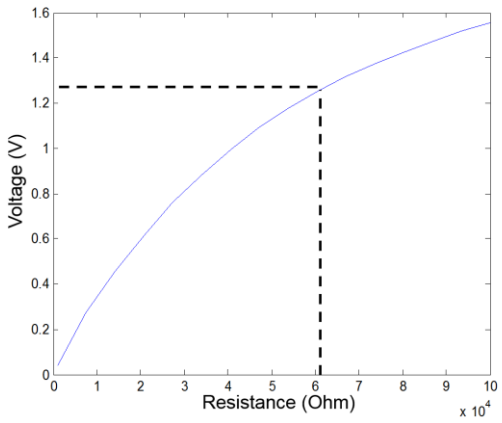

Figure 5.6 Voltage of the C_{int} as a function of resistance R

One can note on figure 5.5 that an optimal value for the load that maximizing the harvested power exist. This value is about 6.02e4 Ohm which is different from the value obtained in mono-sinusoïdal case (1.08e4 ohm). This resistance value is a moderate and reasonable value.

Second step:

As illustrated in chapter 3, for *SSDVC* (I) technique, the damping effect is maximum when the voltage of capacitor C_B is 2V. A buck-boost converter, used in discontinue modes (DCM modes), is associated with the SSHI series circuit to adjust the output voltage. The value of the inductor L_B and the duty cycle D are obtained via theoretical development.

The condition for DCM operation of a buck-boost converter is given by:

$$V_{C_{\text{int}}} < \frac{1-D}{D} V_{C_B} \tag{5.1}$$

This expression allows to practically determine a fixed value of the duty cycle D as a function of the voltage V_{C_B} and as a function of the input voltage $V_{C_{\text{int}}}$.

Using the specific value corresponding to our work, the duty cycle *D* can be calculated from the equation (5.1), which is less than 60.61%.

Then, buck-boost converter has a constant input average resistance R_{in}, which is expressed as:

$$R_{in} = \frac{2 \cdot L_B \cdot f_B}{D^2} \tag{5.2}$$

Assuming that the optimal load resistance R_{opt} of the circuit *series-SSHI* equals to the input average resistance of buck-boost converter, the duty cycle D can be expressed as:

$$D^2 = \frac{2 \cdot L_B \cdot f_B}{R_{opt}} \tag{5.3}$$

The efficiency of the buck-boost converter is defined by:

$$\eta = \frac{V_B \langle i_B \rangle}{V_{\text{int}} \langle i_{\text{int}} \rangle} \tag{5.4}$$

with

$$\frac{V_{\text{int}}}{\langle i_{\text{int}} \rangle} = \left(\frac{1-D}{D} \right)^2 \frac{V_B}{\langle i_B \rangle} \tag{5.5}$$

So, the efficiency decreases with the increase of duty cycle.

According to equations (5.2), (5.3) and (5.4), the inductor and duty cycle can be determined. In this simulation work, switching frequency f_B is fixed at 10 kHz, the corresponding inductor is 0.0144H with a duty cycle D of 6%. This duty cycle value is clearly very low. But in the first step of analysis of the new method we choose to keep it.

One can also underline that boosting a voltage from 1.3V to 2V can be realized with simple topology, such as voltage double, pump charge…, compared to a buck-boost converter. Nevertheless, if the excitation changes in terms of amplitudes or waveforms (noise, pulse…), the buck-boost converter can be adjusted easily by changing the duty cycles to boost or decrease the voltage V_{Cint}, thus insuring an optimal value of the constant voltage V_{CB} for the damping circuit.

5.3.3 Chosen parameters of the complete SSDH circuit

When the three parts of SSDH are connected together, the intermediate capacitances C_{int} and C_B must be sufficiently larger than the capacitor C_{02} and C_{01} of the piezoelectric element, in order to obtain constant voltage of the

C_{int} and C_B. So, 100-μF capacitor (C_{int}) and 10000-μF capacitor (C_B) are used here. Inversion coefficient of 0.75 is taken for the harvesting circuit.
To initiate the simulation, we suppose that the steady state is reached: the voltage across the capacitors C_B and C_{int} are defined initially as 1.3V and 2V, respectively.

Numerical data corresponding to the simulation setup are summarized in Table 5.2.

Table 5.2 Simulation parameters of Modal *SSDH*

Parameter	Symbol	Value
Inductance(*H*)	L_1	0.5
Resistance(*Ohm*)	r_1	667
Inductance(*H*)	L_2	0.1
Resistance(*Ohm*)	r_2	298
Clamped capacitance of the PZT_2 (*F*)	C_{02}	35.8e-9
Clamped capacitance of the PZT_1 (*F*)	C_{01}	35.8e-9
Inductance (*H*)	L_B	0.014
Resistance(*Ohm*)	r_B	10
Duty cycle (*%*)	D	6
Frequency of the switch (*Hz*)	f_B	10000
Clamped capacitance of the intermediate capacitor(*F*)	C_B	10000e-6
Clamped capacitance of the intermediate capacitor(*F*)	C_{int}	100e-6

5.4 Modal SSDH / SSDI simulation results

The simulation are carried out with a Runge-Kutta (ode4) using fixed-step type algorithm. The running time is 10 seconds with a step size of 1e-6 second. The switching time of switch S_2 of the harvesting energy circuit is 3.83e-4 seconds and the switching time of the vibration control circuit is 4.22e-4 seconds.

In order to evaluate the effectiveness of Modal *SSDH* techniques, the simulations of Modal *SSDH* and Modal *SSDI* taken in reference are carried out in two excitations types:

- Bi-Sinusoidal corresponding to the first and second resonance frequencies of the smart structure. This simulation exhibits to show the maximum efficiency of *SSDH*;
- White noise excitation.

The presented results of simulations concern:
- Modal displacement q_1 and q_2 of the first and second mode,
- The voltage on the transducers (V_{02} for the harvesting part on mode 2 and V_{01} for the control of the mode 1).
- The voltage on the intermediate capacitor C_{int} and C_B.

5.4.1 Bi-sinusoidal excitation

The excitation is a bi sinusoidal modal excitation. That mean that each component is perfectly distributed to excite its corresponding mode only. Even if it is not really realistic, it allows a better understanding of the effect of the ratio of the excitation amplitude on the stability as studied in the next part.

For this simulations, we assume that the amplitude of the mode 2 is ten time higher than the amplitude of the first mode, which is a classic vibration case. In our simulation mode, this condition corresponds to an amplitude of the sinus excitation of 0.04 on each mode with the respect of the global displacement of our beam (2mm). The figure 5.7 to 5.12 detailed the obtained curves. As we can note the waveforms of the structure are in perfect adequacy with the theory. The voltages on the piezoelectric element C_{01} and C_{02} are respectively inverted on each mode: mode 1 and mode 2. The ripple on the intermediate capacitors C_{int} and C_B are very low insuring constant voltage.

The figure 5.7 presents the modal displacement q_2 in the case of non-control and modal SSDH control, it shows clearly that the pumped energy reduces the amplitudes of this mode. The attenuation is 0.84dB.

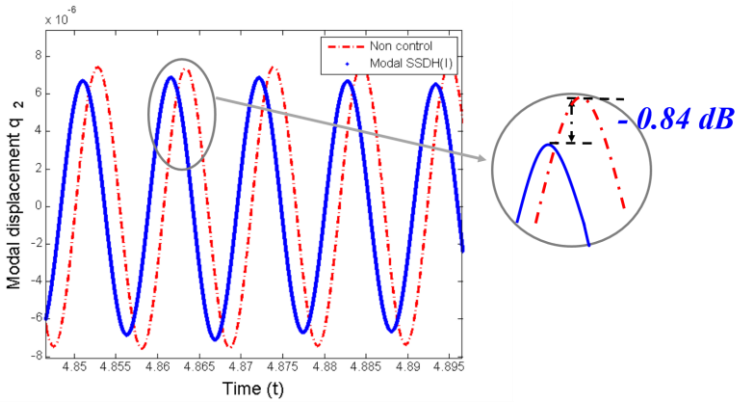

Figure 5.7 Modal displacement of the second mode

The figure 5.8 presents the modal displacement q_1 in the case of non-controlled, controlled by modal SSDI and modal SSDH. It clearly shows that the use of harvested energy with Modal SSDH increases the attenuation in comparison with SSDI Modal technique. Indeed the attenuation with SSDH reaches 26dB versus 13.5dB for the usual SSDI technique.

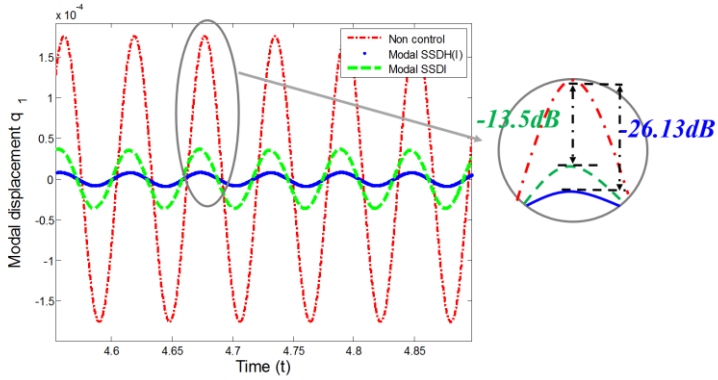

Figure 5.8 Modal displacement of the first mode

These results are obtained thanks to the increase of the voltage induced by the harvested energy from the piezoelectric element C_{02} via Modal SSDH control, as shown in figure 5.9. The voltage on the piezoelectric element C_{01} is inverted at each extreme modal displacement. It can be measured that the inversion coefficient is around 0.96, when the SSDI has an inversion coefficient of 0.75. This explains the very good resulting attenuation.

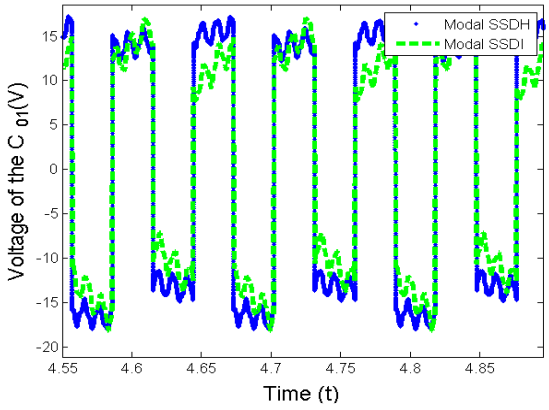

Figure 5.9 Voltage waveforms of Modal SSDI and Modal SSDH control on transducers dedicated to control

Figure 5.10 shows the harvesting part of the SSDH. It can be seen that the voltage V_{C02}, has a complex behavior. Only the modal point of view allows a correct inversion time selection. Note that inversion cannot always happen, due to the fact that on certain times the voltage is very low, and no charges can be transferred to C_{int}.

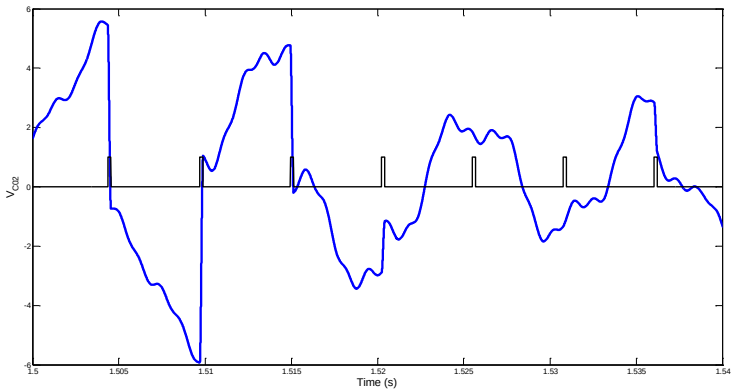

Figure 5.10 Voltage waveforms of Modal SSDH control on transducers dedicated to harvesting. The binary control of the switch is indicated in black.

To invrease the extracted energy, the control law of the switch S2 must be improved. At least two techniques can be developed:

- An enhanced SSHI series. When the modal displacement q_2 reach a maximum, the mechanical energy related to this mode is computed. The inversion process starts only if this mechanical energy is higher than a threshold that the user has to define.
- A SSHI series max. It is based on the technique SSDI max, presented in the first chapter. The fact is that the inversion of the voltage of the

piezoelectric element is triggered when the modal displacement is extreme. Nevertheless, as the excitation of the structure is complex (at least bi-harmonic), the maximal of a modal displacement q_2 do not always reach with a maximum of voltage V_{C02} across the piezoelectric element as we can see in figure 5.10. Thus, the idea, is to wait for a maximum of voltage occurring just after a maximum of modal displacement q_2 to insure a better inversion process leading to more extracted energy.

If we zoom in, Figure 5.11 and 5.12 illustrate the fact that the intermediate voltages are not perfectly constant. Even if they globally oscillate around a constant near their initial value (respectively 1.3V and 2V), this behavior can change depending on the ratio of the excitation amplitude of the two sinus. Basically, if the amplitude of the second mode is too small namely is the mechanical energy of the second mode is to small compared to the one of the first mode, the circuit cannot harvest enough energy to offset, to balance the energy used to damp the vibrations of the structure. The global mechanical and electrical behavior is extremely complex due to the coupling between the modes created by the SSDH circuit. We can only observe that there is no evident equilibrium point. Nevertheless the variation observed on these curves are very small (less the 5e-5V per period), and will very weakly affect the controller.

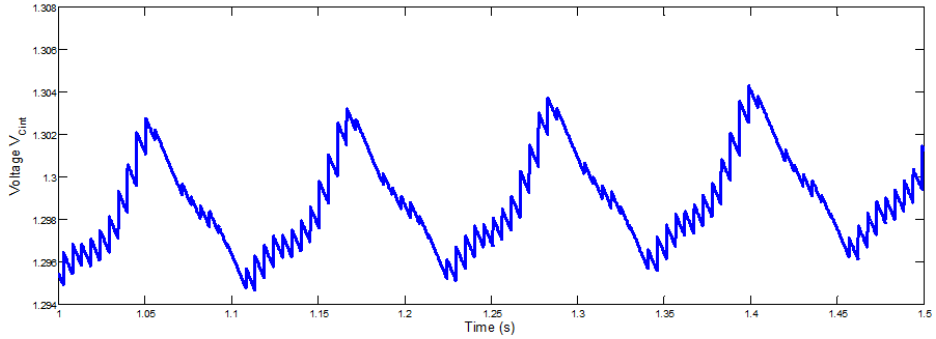

Figure 5. 11 Voltage waveforms of C_{int}

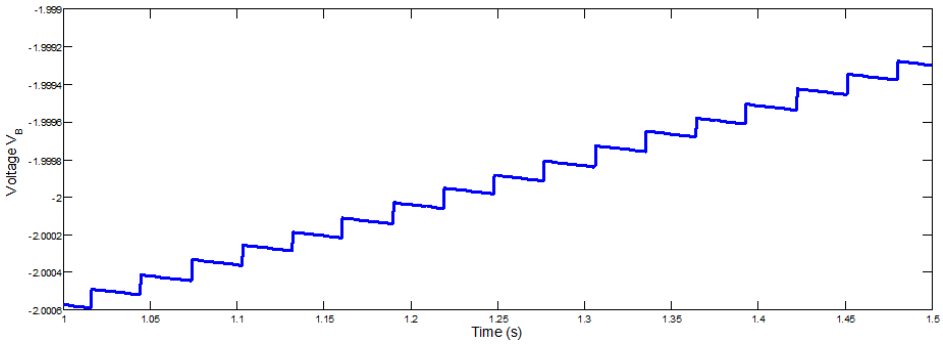

Figure 5. 12 Voltage waveforms of C_B

5.4.2 White noise excitation

To illustrate the method in a more realistic situation, a second type of excitation is tested. It is a spatially distributed White Noise. The same parameter as presented in table 5.2 are used for this simulation.

Figure 5.13 shows the voltage V_{C01} for the two control methods: Modal SSDI and Modal SSDH. In a global way, the inversion correctly occurs on the extreme values of the first mode driven by the modal observer.

Figure 5.14 shows the modal displacement q_1 of the two control methods: Modal SSDI and Modal SSDH. The modal displacement is a bit lower with the SSDH technique compared to SSDI technique.

Figure 5.15 shows the power spectral density of the signal measured on a PVDF sensor. On the first mode, the measured attenuation is approximately 14dB compared to non-controlled, and 5dB compared to Modal SSDI control. Performances of this kind of control are drastically reduced for more complex excitation. The use of the modal basis allows to find the correct time of switch, but the voltage fluctuations are to complex and clearly not sinusoidal. The inversion are no more optimized. Even if our SSDH technique show better performance than the classic SSDI technique, it remains a complex circuit allowing only an enhanced damping of 5dB. However, our SSDH is still promising since the switching control laws can be improve:

- Inversion of the voltage on the piezoelectric insuring the damping on global maximum modal displacement such as $q_2+q_3+q_4$
- Create a SSDH max based on a SSHI max and a SSDVC max, namely we wait for a maximum of voltage on the piezoelectric element occurring after a maximum of modal displacement (for the first and second mode).

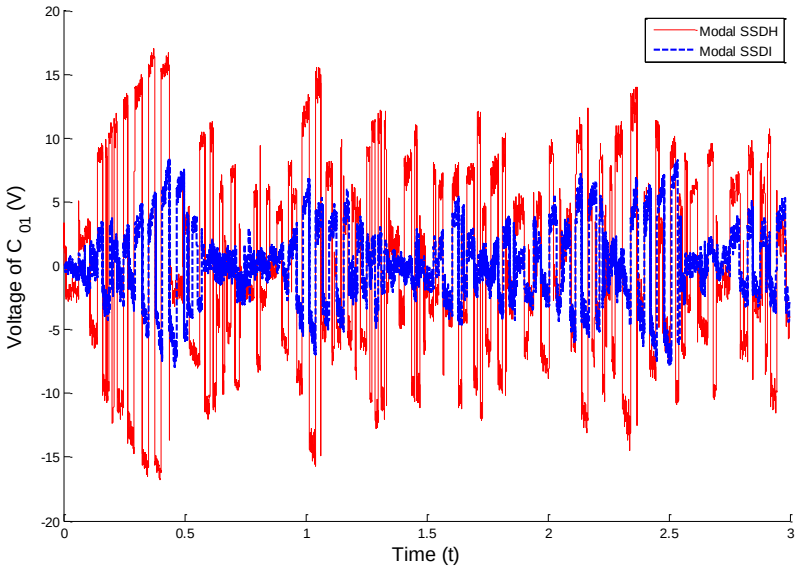

Figure 5.13 Voltage waveforms of Modal SSDI and Modal SSDH control on transducers dedicated to control

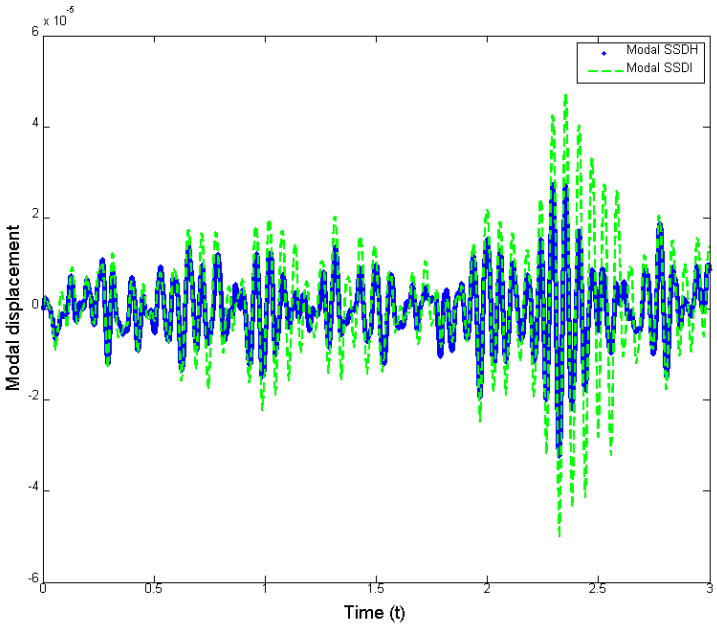

Figure 5.14 The modal displacement of the mode 1

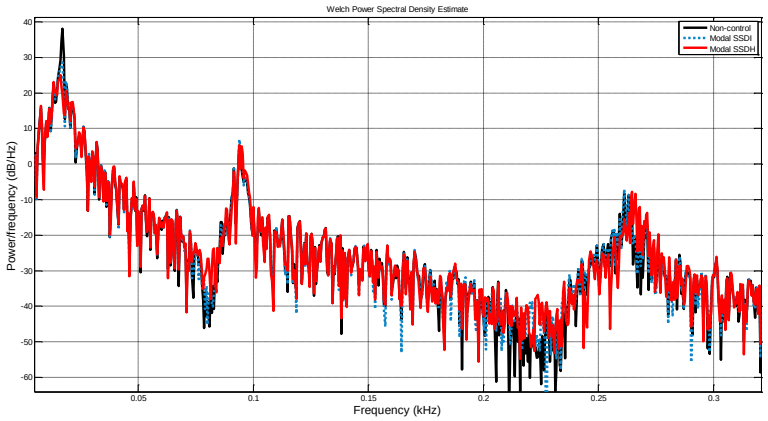

Figure 5.15 Power spectral density for the measured PVDF sensor voltage.

Conclusion

The comparison between Modal *SSDH* and Modal *SSDI* simulations was realized from the damping effect under two type excitations.

Of course, the more interested attenuation (26dB) is obtained by the bi-sinusoidal excitation. The increased damping compared with Modal SSDI is obtained thanks to SSHI circuit included in Modal SSDH method.

With a White Noise excitation, compared with Modal SSDI, a smaller attenuation effect is obtained. This reduction of attenuation is due to the disturbance on the voltage inversion induced by the other non-control modes. An optimization of the inversion moment could be integrated in the approach in order to maximize the voltage inversion of the chosen harvested mode. This kind of optimization has already be studied and is called SSDI-max. [80].

5.5 Robustness test of Modal *SSDH* control

As seen in the previous sections, delays of the modal displacements q_1 and q_2 are observed between non-controlled and Modal *SSDH* controlled curves. As for *SSDV* technic, the added voltage on the inversion can create instabilites, depending on the amplitude vibrations. Moreover, a modal observer is used based on a model of the smart structure. This model is an approximation. For all these reasons, tests of robustness are necessary.

Two main variation have to be studied: (i) a frequency shift on the structure, without updating the observer (ii) variation on the ratio of the amplitude of the bi- sinusoidal excitation.

The robustness of Modal *SSDH* control can be evaluated by parametric variation. An instability or a variation of the modal attenuation can be observed by creating an artificial shift of the frequency employed by the model of the structure.

In our case, the excitation is composed by the first and second frequency resonances of the smart structure (f_1=17Hz, f_2=94Hz).

Fig.5.16 presents the attenuation reduction of the efficiency in the controlled of the first mode in the case of Modal *SSDI* and Modal *SSDH*. The considered variations are -15% to 15% (-15%,-10%, -5%, 0%, 5%, 10%, 15%) of all frequencies of the structure model without update of the observer.

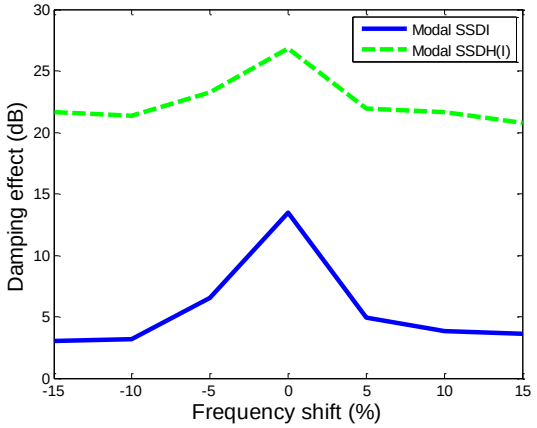

Figure 5.16 Robustness test on the control of the first mode: Modal *SSDH* (green line) and Modal *SSDI* (blue line) - bi-sinusoidal excitation

Result shows that Modal *SSDI* and *SSDH* controls remain perfectly stable but a reduction of attenuation is observed when the frequencies of the structure model go away from those of the observer model. With more than 15% of frequency shift, the attenuation converges towards 21dB. For a variation of 5%, the attenuation decrease to 22dB. The same reduction is observed for Modal *SSDI*: 15%: 3.5dB; 5%: 5dB, but the curve is translated of approximatively 20dB compared to Modal *SSDH* result.

Figure 5.17 shows the attenuation variation depending on the excitation level of mode 1 and mode 2. In previous sections, all the parameters have been optimized for a chosen excitation corresponding to a modal excitation amplitude of 0.04 on both mode. First, the control is unstable if the excitation on the mode 1 is reduced. This is normal, due to the fact that the voltage V_B, added during the inversion is chosen equal to 2V to ensure a coefficient inversion almost equal to 1. It is know that an inver-

sion coefficient superior to 1, will introduce energy in the structure and create instability. Then, we can observe zones, where the attenuation seems very good, but, for these operating conditions, the voltages V_{cint} and V_B fluctuate and cannot ensure stability or performances during a long time without and adaptation of the buck boost operating mode. Globally it appears that the better attenuation ensuring stability corresponds to the chosen excitations (0.04 on both mode), this validates the parameter optimization part of this work.

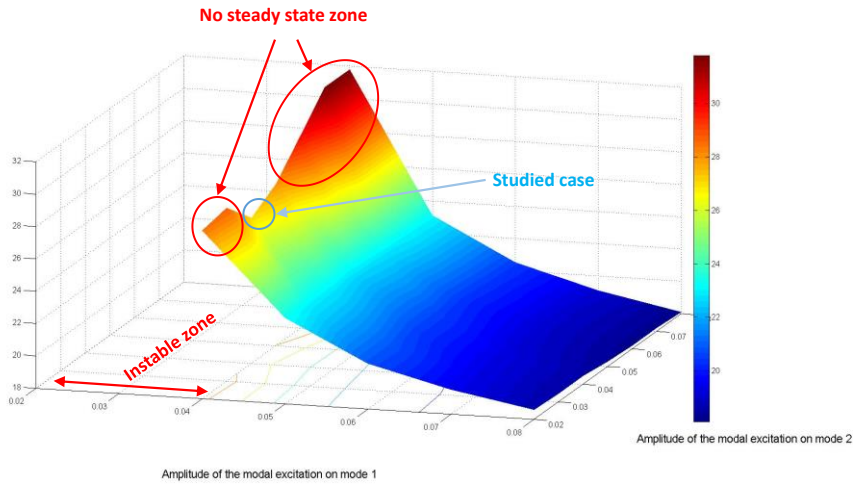

Figure 5.17 Attenuation variation on the first mode, depending on the amplitudes of the excitations

5.6 Energy transfer

The aim of this section is to start the analysis of the performance of the Modal *SSDH* technique, in terms of the energy transfer in the circuit.

The energy transfers in the *SSDH* technique is described in Figure 5.18.

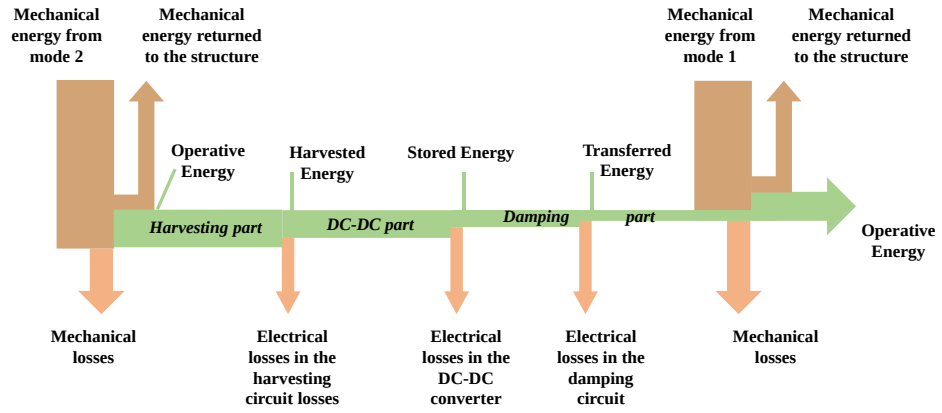

Figure 5.18 Energy flow in *SSDH* technique

The mechanical vibration energy of the second mode is firstly extracted by the piezo-element C_{02} based on Energy Harvesting Circuit (*series-SSHI* technique). This energy is then formatted thanks to a DC-DC converter and store into a capacitor. Finally, an amount of the stored energy is used to enhance the damping of the structure through our SSDVC circuit.

The energy balance equation within the structure for a given modal coordinate is given by equation 5.6.

$$\underbrace{\left[\frac{1}{2}m\dot{q}^2\right]_0^T + \left[\frac{1}{2}k^E q^2\right]_0^T}_{\text{Mechanical energy}} + \underbrace{\int_0^T c\dot{q}^2 dt}_{\text{Damping loss}} + \underbrace{\int_0^T \alpha V\dot{q}dt}_{\text{Extracted energy}} = \underbrace{\int_0^T F\dot{q}dt}_{\text{Provided energy}} \quad (5.6)$$

with

$$\int_0^T \alpha V\dot{q}dt = \left[\frac{1}{2}C_{01,02}V^2\right]_0^T + \int_0^T VIdt \quad (5.7)$$

With F the external force applied to the structure, M, K^E and C respectively the modal matrices of mass, stiffness and viscous damping, α the modal piezoelectric coupling coefficient and q the modal displacement quantities.

The energy described by the equation 5.7 is named extracted energy, and is composed of electrostatic energy stored on the piezoelectric capacitance ($1/2CV^2$) and the energy absorbed by the electric circuit connected with the piezoelectric element. The electrostatic energy, so-called operative energy is related to the harvesting or damping performance (harvesting on mode 2 and damping on mode 1). Increase the available operative energy or increased the voltage results in better damping performance.

All the following energies can be seen as global quantities or computed for one cycle, namely associated to one inversion process (respectively on mode 1 or mode 2). It is small amount of energy as shown in figure 5.11 and 5.12. We define the harvested energy as the energy obtained on the capacitor C_{int}, after the alternative/continuous conversion. During this step, a part of the electrical energy is dissipated into the electrical circuit (losses in the diodes, heat). The harvested energy is given by:

$$E_{C_{\text{int}}} = \frac{1}{2} C_{\text{int}} V_{C_{\text{int}}}{}^2 \tag{5.8}$$

The stored energy is related to the storage capacitor C_B and provided after the power management circuit, i.e. after the buck-boost converter. During this step, a part of energy dissipates into heat due to the switch, the diode as well as the inductor L_B. Thus, the stored energy on the capacitor C_B can be expressed as:

$$E_{C_B} = \frac{1}{2} C_B V_{C_B}{}^2 (5.8) \tag{5.9}$$

Finally, the transferred energy is the amount of energy added to the piezoelectric element during the inversion process. This energy can be simply calculated as:

$$E_T = \frac{1}{2} C_{01} V_{C_{01,after}}^2 - \gamma_N^2 C_{01} V_{C_{01,before}}^2 \tag{5.10}$$

With $V_{C01,after}$ the value of the voltage across the piezoelectric element C_{01} just after the inversion process and $V_{C01,\ before}$ the value just before this process. γ_N is the new improved inversion coefficient obtained thank to the transferred energy.

One can underline that various efficiency can be defined in our *SSDH* process. A global efficient and efficiency for each stage (each part) of our circuit. As an example, the efficiency of the buck-boost converter is calculated by:

$$\eta = \frac{E_{C_B}}{E_{C_{\text{int}}}} \tag{5.11}$$

Comparisons between the various energies and efficiency are feasible, but the relevant comparison remains between the modal energy on mode 1 and 2 and the transferred energy. Table 5.3 summarizes the initial and final mechanical energies (mode 1 and 2), and the transferred energy regarding our studied case. The improved inversion coefficient is 0.96. Initially, the energy of the first mode is eighteen time higher than the one of the second mode. These modal energies are computed for a maximum of modal displacement. After control processing, the first mode is strongly reduced (minus 26dB) leading to a huge decrease of the associated modal en-

ergy (gain of 485). A gain of 12.5dB is notified compared to classic modal SSDI technique thanks to the energy transfer. One can note that during a period of the first mode, at least five energy harvesting cycles have occurred: the capacitance C_B have been fill in five times (five maximum on the modal displacement q_2 leading to five inversion process and so five amount of harvested energy).

Table 5.3 Energy corresponds to the considered items

	Energy
Energy of mode 1 (initial)	354.64 μJ
Energy of mode 2 (initial)	19.52 μJ
Energy transfer	68.36 μJ
Energy of mode 1 (final)	731.01 nJ
Energy of mode 2 (final)	13.57μJ

Regarding table 5.3, the final modal energy of the first mode is lower than the one of the second mode: an energy transfer has occurred between these two modes. Firstly, the energy is pumped on the second mode during our SSDH process (around 6μJ). This energy is then boosted up thanks to the buck-boost converter and transferred to the first mode. The amount of transferred energy seems low compared to the initial energy of the first mode but it is enough to enhance the damping of our smart structure.

These simple energy calculations validate our circuit and concept: scavenge energy on high frequency modes to enhance the damping of low frequency modes. A deeper study on the variation of the performances of our *SSDH* circuit according to the amount of energy on each modes must be realized in the future.

5.7 Conclusion

In this chapter, our new vibration modal control technique named *Synchronized Switching Damping and Harvesting* (*SSDH*) is proposed. The electri-

cal circuit and the control law were introduced to explain how the vibration energy can be transferred between different modes of a same structure to achieve damping effect on a target mode.

Firstly, the architecture of Modal *SSDH* control was presented, in particular, the switch control law was detailed.

Secondly, simulations were carried out with Simscape to optimize the electrical parameters. Then, the damping performance of the Modal *SSDH* control was compared with that Modal *SSDI*. The results concern the first mode and second mode of the smart structure for bi-sinusoidal and white noise excitations.

The simulations show that, on one hand, compared with non-control system, the displacement of the source mode was damped by pumping the modal energy; on the other hand, compared with Modal *SSDI,* Modal *SSDH* increases the damping effect of the target mode. The voltage inversion was greater, enlarged by the harvested energy of the source mode.

Thirdly, tests of robustness of Modal *SSDH* method are carried out. It shows that the Modal *SSDH* control develops good robustness.

Lastly, the energy transfer analyses of *SSDH* technique is started.

This principal chapter was built for Modal *SSDH* control by using the best promising techniques presented in the previous chapters (chapter 3 and 4). Other techniques namely other combinations were presented in the same chapters. So, the following chapter will present the variations of Modal *SSDH* by using these other techniques.

6 Other SSDH operating modes

6.1 Introduction

In the previous chapter, simulation work about the best promising Modal *SSDH* control technology has been carried out to predict the performance. In this chapter, two other functions are presented: Modal *SSDH* (II), Modal *SSDH* (III).

The objective of this chapter is to present with less details the other new function control modes of the *SSDH* circuit, and to understand each control techniques though simulation implements.

As the previous simulation works, in this chapter, the new function modes will be implemented under Matlab/Simulink™/Simscape™ environment to find the optimal parameters of the electrical components and predict the control performance.

Thereby, the capacity to harvest the modal energy and the performance of vibration control of the new function modes are predicted.

6.2 General description of the other operation modes

Due to different control law of the switches in the circuit, various functions will be presented in this section which are different from that in chapter 5. This chapter will present two other different electrical behavior of Modal *SSDH* techniques. To avoid confusion, we named the previous function mode Modal *SSDH* (I), and these two new function modes: Modal *SSDH* (II) and Modal *SSDH* (III).

- Modal *SSDH* (II)

  The second proposed behavior, Modal *SSDH* (II), can be seen as a combination of Modal *DSSH* series circuit for the harvesting part with *SSDVC* (I) for the damping part. The electrical circuit architecture is the same as Modal *SSDH* (I), shown in figure 6.1. Its operating mode will be detailed in the following sections.

- Modal *SSDH* (III)

  The third proposed behavior can be seen as a combination of Modal *DSSH* series circuit for the harvesting part with *SSDVC* (II) for the damping part. The electrical circuit architecture is shown in figure 6.1 there

is an added switch S_1 in the damping part). The difference between this circuit and the previous circuit is the vibration control part. Detailed principles will be presented in the following sections.

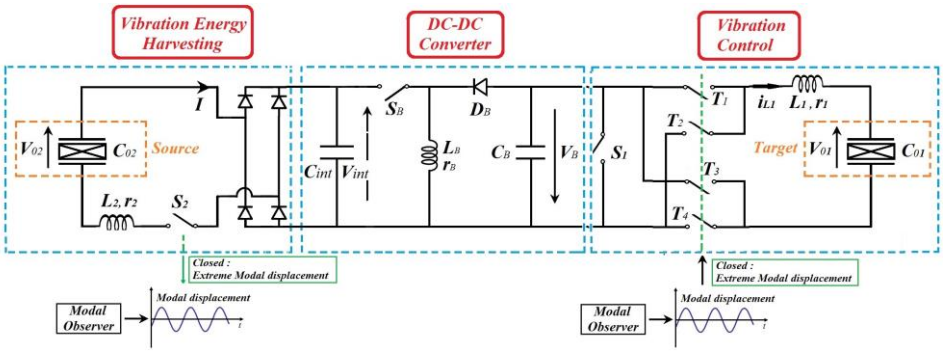

Figure 6.1 Electrical circuit of the Modal *SSDH* (III)

6.3 Second behavior: Modal *SSDH* (II)

6.3.1 Operating mode of Modal *SSDH* (II)

The switches S_2, and (T_1, T_2, T_3, T_4) present the same control principle as Modal *SSDH* (I). The main change is the command of the switch S_B now based on the transfer of charges stored into the capacitor C_{int}.

Simulations using the same conditions as Modal *SSDH (I)* (presented in chapter 5) have been carried out.

The waveforms of the voltages of the two piezoelectric elements (C_{01} and C_{02}), the modal displacements (q_1 and q_2) and the voltages of the intermediate capacitors C_{int} and C_B are shown in figure 6.2.

The sequence control law of the switches is shown in the table 6.1 and is described below.

Table 6.1 Sequence control law of the switches of Modal *SSDH* (II)

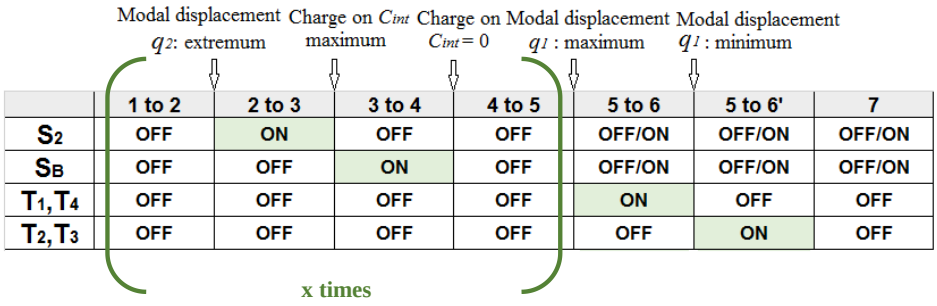

	1 to 2	2 to 3	3 to 4	4 to 5	5 to 6	5 to 6'	7
S_2	OFF	ON	OFF	OFF	OFF/ON	OFF/ON	OFF/ON
S_B	OFF	OFF	ON	OFF	OFF/ON	OFF/ON	OFF/ON
T_1, T_4	OFF	OFF	OFF	OFF	ON	OFF	OFF
T_2, T_3	OFF	OFF	OFF	OFF	OFF	ON	OFF

The principle of the Modal *SSDH (II)* operation can be described as follows:

During phase 1 to 2: Most of the time, the piezoelectric element is in open circuit and the intermediate converter is not operating (S_1, S_2 and S_B are open, D_B is blocked).

During phase 2 to 3: The switch S_2 is closed when the modal displacement q_2 reaches an extreme. An energy transfer occurs from the piezoelectric element C_{02} to the intermediate capacitor C_{int} through the inductor L_2 and the diode bridge rectifier.

During phase 3 to 4: When the first energy transfer from C_{02} to C_{int} is finished, the switch S_B is closed. Thus, the energy is transferred from the capacitor C_{int} to the inductor L_B.

During phase 4 to 5: Then, when the energy is maximal on the L_B (maximum current and no charge on C_{int}), S_B is open and diode D_B conducts, transferring the energy from L_B to the smoothing capacitor C_B.

The steps 2 to 5 occur x times as the frequency of the second mode is higher than the one of the first mode.

During phase 5 to 6 (6'): The four switches (T_1, T_2, T_3, T_4) are switched on when the modal displacement of the first mode q_1 reaches either a maximum (or a minimum). Then the energy is transferred from the capacitor C_B to the piezoelectric element C_{01} through these switches.

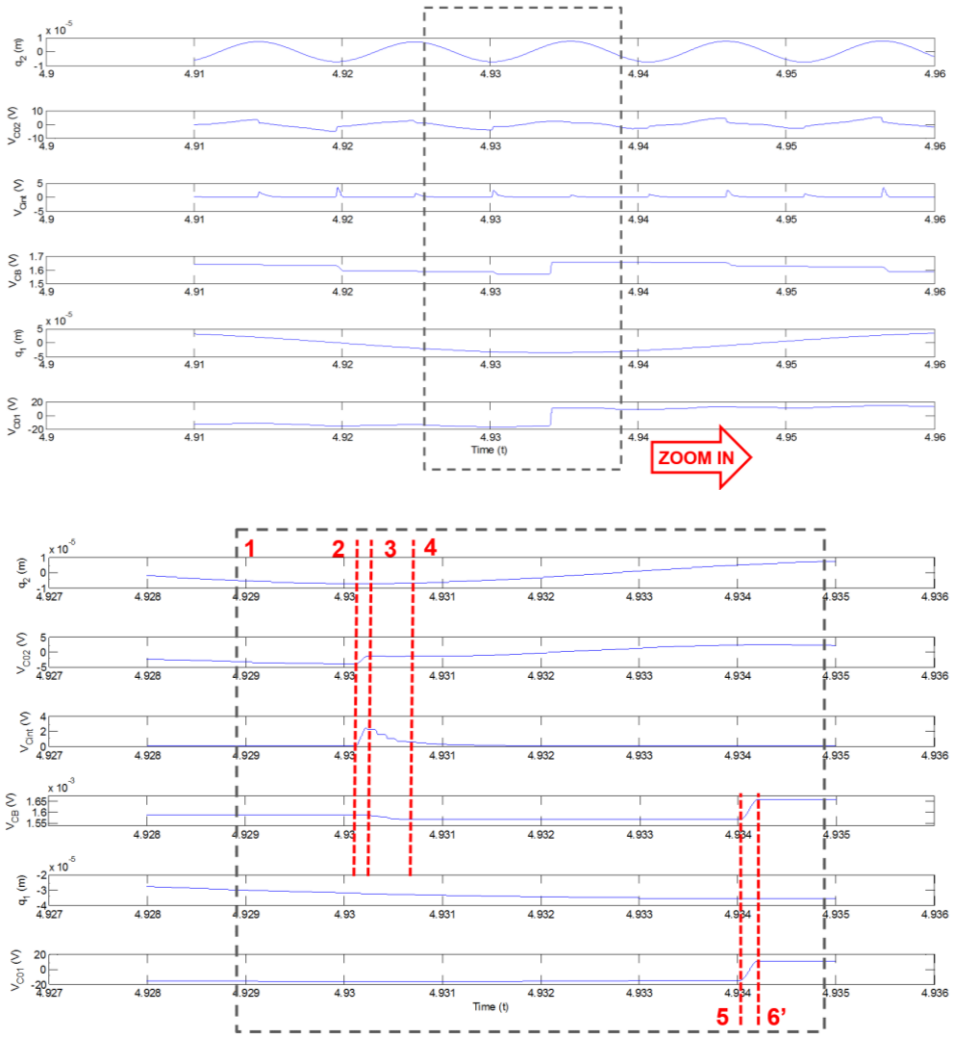

Figure 6.2 The zoom-in waveforms of Modal *SSDH* (II)

Note that the voltage on capacitor C_{int} is immediately increased by the switching action of S_2, and then rapidly drops down during switching of S_B. Even if there is a slightly decrease or increase, the voltage on the intermediate capacitors C_B is viewed as a *DC* voltage.

6.3.2 The optimization for Modal *SSDH* (II)

In chapter 5, a detailed optimization analysis about the optimal parameters of Modal *SSDH* (I) control technology has been discussed. In order to get the best performance of Modal *SSDH* (II), the optimization of the power flow between the energy-harvesting and vibration-control are discussed. The method of analysis here is similar to Modal *SSDH* (I), the optimal val-

ue of the parameters were found through simulation and theoretical formulas. The studied case is also a bi-sinusoidal excitation.

Optimization of Modal *DSSH* series parameters

The theoretical analysis was discussed in section 4.3.3.

According to the energy harvesting circuit Modal *DSSH* presented in section 4.3.3, the voltage of the intermediate capacitor is given by equation (4.55) after the energy transfer process of the piezoelectric element C_{0A} to intermediate capacitor C_{int}.

The expression of the harvested energy on the capacitor C_{int} for a single switch operation (occurring on an extreme of modal displacement q_2) is given by:

$$\left(E_{C_{\text{int}}}\right)_{out} = \frac{1}{2} C_{\text{int}} \left(V_{C_{\text{int}}}\right)^2_{end} = \frac{1}{2} C_{\text{int}} \left(\frac{C_{02}}{C_{\text{int}} + C_{02}} (1+\gamma) V_0 \right)^2 \tag{6.1}$$

We choose the intermediate capacitance value C_{int} as:

$$C_{\text{int}} = x \cdot C_{02} \tag{6.2}$$

The maximization of the harvested energy leads to the condition:

$$\left(C_{\text{int}}\right)_{opt} = C_{02} \tag{6.3}$$

According the equation (6.4) and (6.5), the relationship between the resistance r_B and the overall converter efficiency γ_C can be found, using the following expression

$$\gamma_C = e^{-\xi_{\text{int}} \pi} \tag{6.4}$$

$$\xi_{\text{int}} = \frac{1}{2} r_B \sqrt{\frac{C_{\text{int}}}{L_B}} \tag{6.5}$$

Leading to:

$$\gamma_C = e^{-\frac{1}{2} r_B \sqrt{\frac{C_{\text{int}}}{L_B}} \pi} \tag{6.6}$$

In the case of the energy harvesting circuit, the inversion factor is roughly equal to 0.75. In order to obtain an efficient circuit, the overall converter efficiency γ_C is chosen at least equal to 0.8. Figure 6.3 shows the corresponding overall converter efficiency versus resistance r_B. Note that, in the simulation work, the inductor is fixed at 0.05H. The resistance r_B should be smaller than 69 ohms to obtain a γ_C greater than 80%.

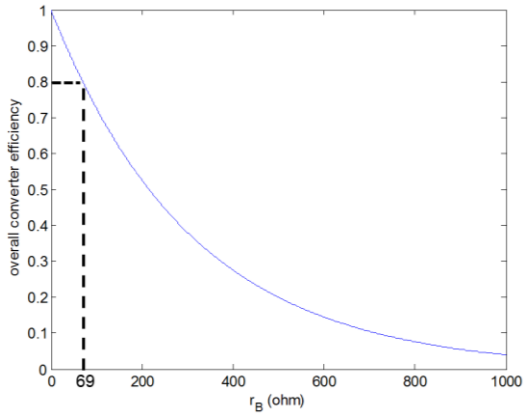

Figure 6.3 Overall converter efficiency versus resistance

Chosen parameters of the complete *SSDH* circuit

As presented in chapter 5, the intermediate capacitance C_B must be sufficiently larger than the capacitor C_{01} of the piezoelectric element, so that the tension on the capacitor C_B can be viewed as a perfect *DC* voltage and the level of output ripple is small enough to be negligible. The same value of C_B is chosen as Modal *SSDH* (I) in order to obtain constant voltage of C_B. So, 10000-μF capacitor (C_B) is used here. The initial voltage on the capacitor C_B is defined as 2V (see chapter 5).

Numerical data corresponding to the simulation setup are summarized in Table 6.2.

Table 6.2 Simulation parameters of Modal *SSDH* (II)

Parameter	Symbol	Value
Inductance(*H*)	L_1	0.5
Resistance(*Ohm*)	r_1	667
Inductance(*H*)	L_2	0.1
Resistance(*Ohm*)	r_2	298
Clamped capacitance of the PZT_2 (*F*)	C_{02}	35.8e-9
Clamped capacitance of the PZT_1 (*F*)	C_{01}	35.8e-9
Inductance (*H*)	L_B	0.05
Resistance(*Ohm*)	r_B	60
Clamped capacitance of the intermediate capacitor(*F*)	C_B	10000e-6
Clamped capacitance of the intermediate capacitor(*F*)	C_{int}	35.8e-9

6.3.3 Modal *SSDH* (II) simulation results

In this section, simulations are compared to Modal *SSDH (I)* and Modal *SSDI* to evaluate the effectiveness of proposed techniques. According to the discussion of the simulation in the chapter 5, the same simulation conditions are used for Modal *SSDH* (II).

Two excitations types are considered:

- Bi-Sinusoidal corresponding to the first and second resonance frequencies of the smart structure;
- White noise.

The presented results of simulations show:

- Modal displacement q_1 and q_2 of the first and second mode,
- The voltage on the transducers (V_{02} for the harvesting part on mode 2 and V_{01} for the control of the mode 1).

6.3.3.1 Bi-sinusoidal excitation

The figure 6.4 presents the modal displacement q_2 in the case of non-control and Modal *SSDH (II)* control. The attenuation of q_2 is 1.7 dB due to energy pumping of this mode.

The figure 6.5 presents the modal displacement q_1 in the case (i) non-controlled, (ii) controlled by Modal *SSDI* and (iii) Modal *SSDH (II)*. It shows that the use of harvested energy with Modal *SSDH* (II) increases the attenuation by 12.63 dB compared with Modal *SSDI* technique. The attenuation with the Modal *SSDH* (II) reaches 26dB.

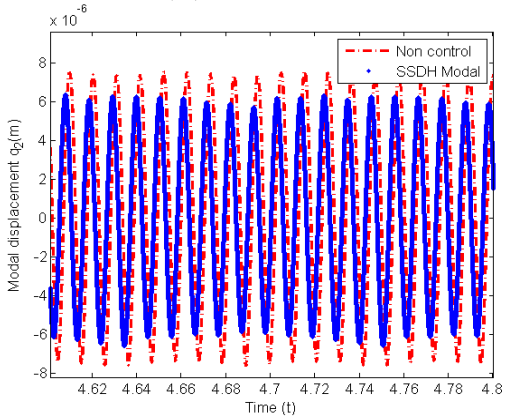

Figure 6.4 Modal displacement of the second mode

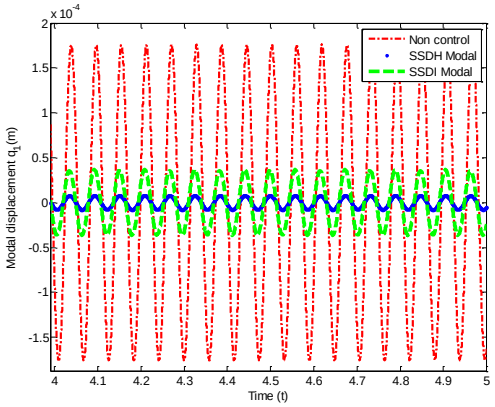

Figure 6.5 Modal displacement of the first mode

As shown in figure 6.6, thanks to the harvested energy from the piezoelectric element C_{02}, the voltage on the piezoelectric element C_{01} with Modal *SSDH* (II) is larger than that of the Modal *SSDI*. As Modal *SSDH* (I), it can be measured that the inversion coefficient is around 0.96. This explains the very good resulting attenuation.

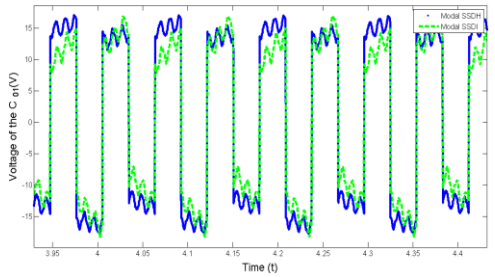

Figure 6.6 Waveforms the voltage of piezoelectric element C_{01}

Figure 6.7 illustrates that the intermediate voltages Vc_{int} is perfectly discharged at each transfer period, and the voltage Vc_B is not perfectly constant even if it globally oscillate around a constant value with slowly falls. To maintain this voltage, it should be interesting to increase the amplitude vibration of mode 2. These kind of analyses will be done in future works.

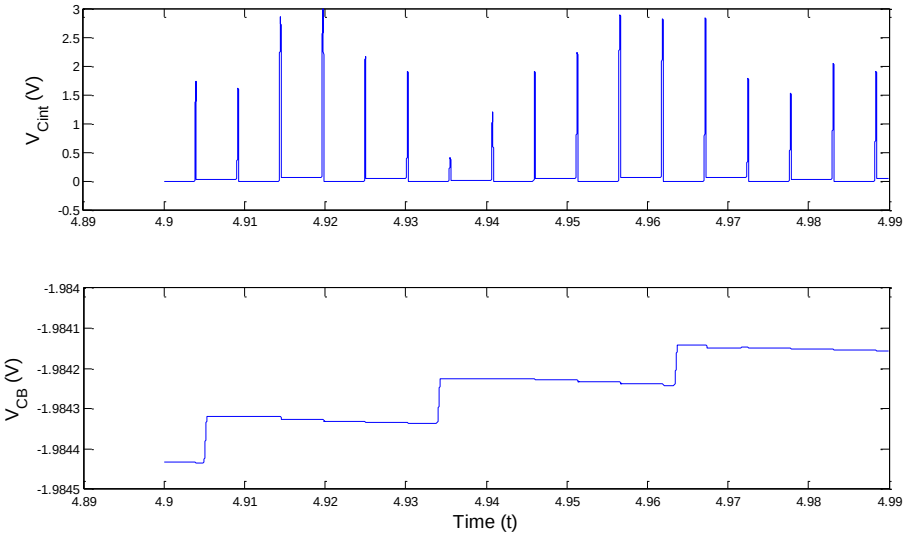

Figure 6.7 Voltage waveforms of C_B and C_{int}

6.3.3.2 White noise excitation

White noise excitation is used. As for previous simulation it is a spatially distributed excitation. The same parameter as presented in table 6.2 are used for this simulation.

Figure 6.8 shows the voltage V_{C01} for the two control methods: Modal *SSDI* and Modal *SSDH* (II). It can be seen that the switching time are globally correct driven by the modal observer.

Figure 6.9 shows the modal displacement q_1 of the two control methods: Modal *SSDI* and Modal *SSDH* (II).

Figure 6.10 shows the power spectral density of the signal measured on a PVDF sensor. On the first mode, the measured attenuation induced bu Modal *SSDH* (II) is approximately 13dB compared to non-controlled, and 4dB compared to Modal *SSDI* control.

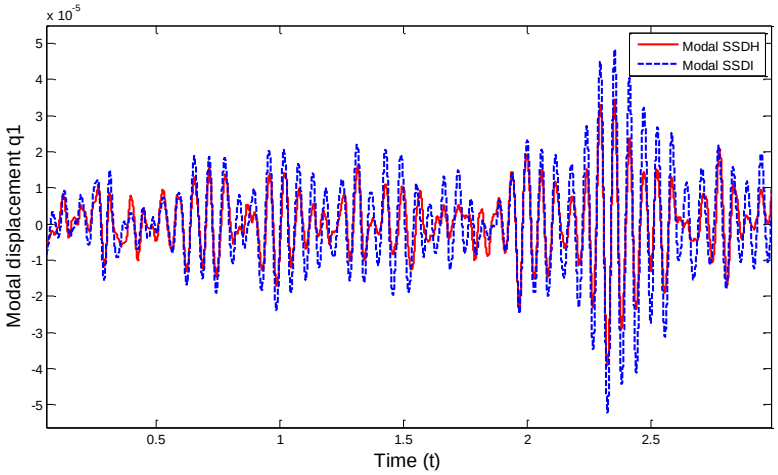

Figure 6. 8 The modal displacement of the mode 1

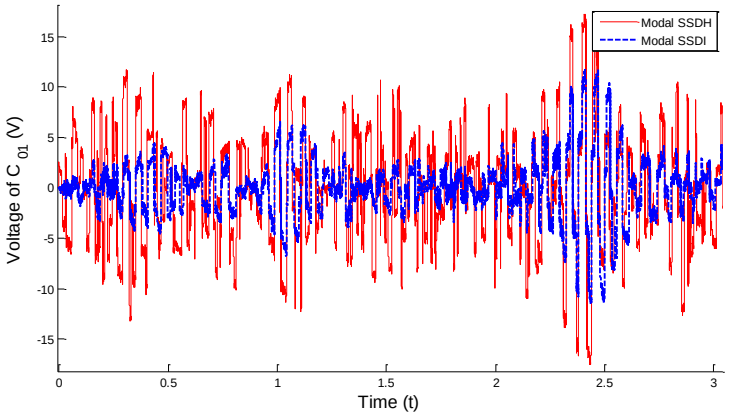

Figure 6.9 Voltage waveforms of Modal *SSDI* and Modal *SSDH* (II) control on transducers dedicated to control

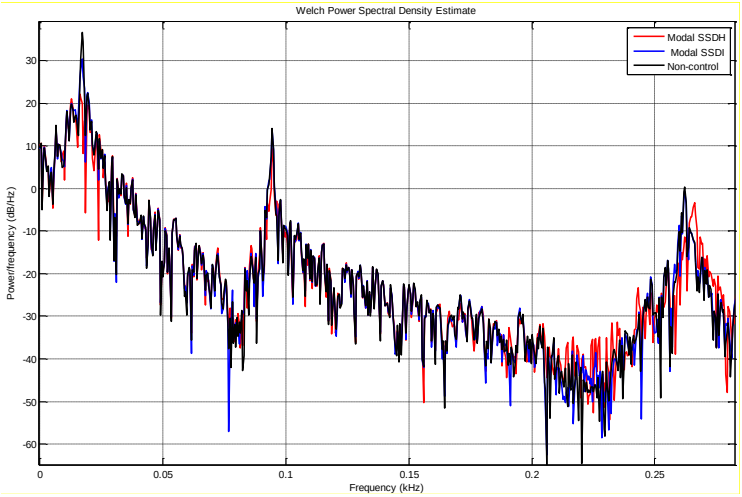

Figure 6.10 Power spectral density for the measured PVDF sensor voltage.

6.4 Third behavior: Modal *SSDH* (III)

6.4.1 Operating mode of Modal *SSDH* (III)

The architecture of the third operating condition Modal *SSDH* (III) was show in figure 6.1. Generally speaking, the different of this new proposed technique is that the control laws of switches S_B and S_1 are both depended on available charges on the two intermediate energy storage capacitors (C_{int}

and C_B). The switches S_2 develop the same control principle as Modal *SSDH* (I) and Modal *SSDH* (II). The energy transfer process is controlled by five switches (T_1, T_2, T_3, T_4 and S_1), which was detailed in the section 3.3.2. The global sequence control law of the switches as shown in the table 6.3.

Table 6.3 Sequence control law of the switches of Modal *SSDH* (III)

	Modal displacement q_2: extremum	Charge on C_{int} maximum	Charge on $C_{int}=0$	Modal displacement q_1 : maximum	Modal displacement q_1 : minimum	Voltage on $C_B=0$	Voltage on $C_B=0$	*Current* $i_{L1}=0$	
STEP	**1 to 2**	**2 to 3**	**3 to 4**	**4 to 5**	**5 to 6**	**5 to 6'**	**6 to 7**	**6' to 7**	**8**
S_2	OFF	ON	OFF	OFF	OFF/ON	OFF/ON	OFF/ON	OFF/ON	OFF/ON
S_B	OFF	OFF	ON	OFF	OFF/ON	OFF/ON	OFF/ON	OFF/ON	OFF/ON
S_1	OFF	OFF	OFF	OFF	OFF	OFF	ON	OFF	OFF
T_1,T_4	OFF	OFF	OFF	OFF	ON	OFF	ON	ON	OFF
T_2,T_3	OFF	OFF	OFF	OFF	OFF	ON	OFF	ON	OFF

x times

The different phases can be detailed as follows:

During phase 1 to 2: All switches are opened. The piezoelectric element is in the open state.

During phase 2 to 3: The switch S_2 is closed when the modal displacement q_2 reaches an extreme. The piezoelectric element C_{02} is used to charge the intermediate capacitor C_{int} through the inductor L_2 and the diode bridge rectifier.

During phase 3 to 4: When the first energy transfer from C_{02} to C_{int} is finished, the switch S_B is closed. Thus, the energy is transferred from the capacitor C_{int} to the inductor L_B.

During phase 4 to 5: Then, when the energy is maximal on the L_B (maximum current and no charge on C_{int}), S_B is open and diode D_B conducts, transferring the energy from L_B to the smoothing capacitor C_B.

The steps 2 to 5 are repeated x times as the frequency of the second mode is higher than the one of the first mode.

During phase 5 to 6 (6'): T_1 and T_4 (or T_2 and T_3) are closed when the modal displacement q_1 reaches a maximum (or a minimum). Then, the energy stored on the capacitor C_B is completely transferred to the piezoelectric element C_{01} during t_1.

During phase 6 (6') to 7: When the voltage across the capacitor C_B reduces to zero (end of the transfer process), S_1 is closed, while T_1, T_4 are still closed. S_1, T_1 and T_4 are closed during t_2 (oscillating LC circuit). V_{C01} is inverted. Closing S_1 on a zero-voltage value reduces the losses and the breaking failures.

During phase 8: All switches are open.

The typical waveforms are depicted in Figure 6.11. The detailed waveforms of the voltages and modal displacements are shown in figure 6.12.

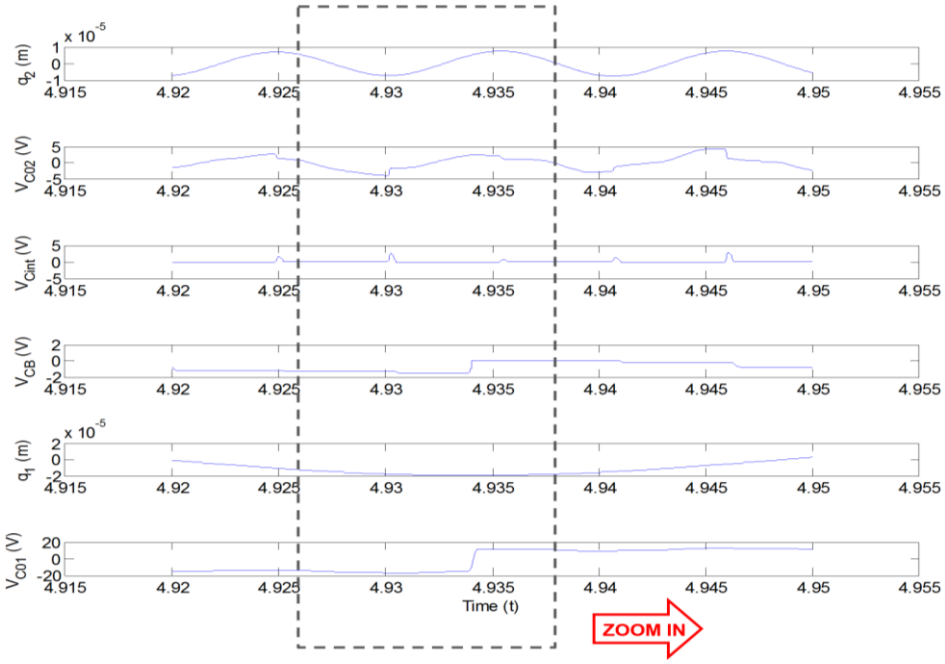

Figure 6.11 Simulation waveforms of Modal SSDH (III)

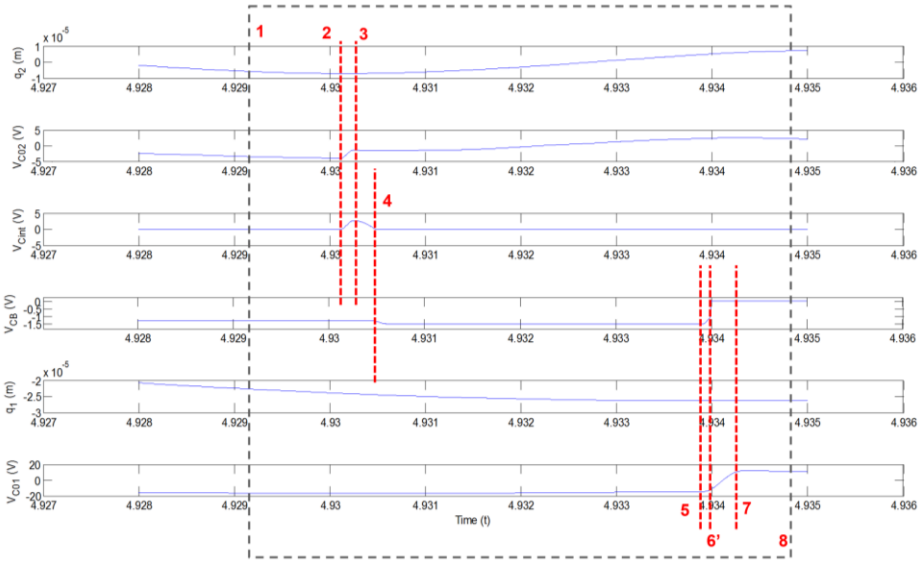

Figure 6.12 The zoom-in waveforms of Modal SSDH (III)

6.4.2 The optimization for Modal SSDH (III)

The optimization parameter analysis is the same as Modal SSDH (I) and Modal SSDH (II) in the previous section, which were realized through simulation and theory method.

For the energy harvesting circuit, the theoretical analysis is the same as Modal SSDH (II) which was presented in the section 6.3.2.

For the vibration damping circuit, the optimization analysis of SSDVC (II) is based on the maximum of the energy transfer between the intermediate capacitor C_B and piezoelectric element C_{0A}. The detailed discussion is presented in section 3.3.2.

Numerical data corresponding to the simulation setup of Modal SSDH (III) are summarized in Table 6.4.

Table 6.4 Simulation parameters of Modal SSDH (III)

Parameter	Symbol	Value
Inductance(*H*)	L_1	0.5
Resistance(*Ohm*)	r_1	667
Inductance(*H*)	L_2	0.1
Resistance(*Ohm*)	r_2	298
Clamped capacitance of the piezoelectric element (*F*)	C_{02}	35.8e-9
Clamped capacitance of the piezoelectric element (*F*)	C_{01}	35.8e-9
Inductance (*H*)	L_B	0.05
Resistance(*Ohm*)	r_B	60
Clamped capacitance of the intermediate capacitor(*F*)	C_B	143.2e-9
Clamped capacitance of the intermediate capacitor(*F*)	C_{int}	35.8e-9

Therefore, the switch on-time for the mode 2 is half period. Switching time t_1 and t_2 for SSDVC (II) were detailed in section 3.3.2.

6.4.3 Modal *SSDH* (III) simulation results

Simulations are considered to predict the performance of Modal SSDH (III).The environment and type of excitations are the same as previous cases.

6.4.3.1 Bi-sinusoidal excitation

First excitation case studied here is a bi-sinusoidal combination with the first and second resonant frequencies.

Figure 6.13 shows that the attenuation of the second mode is 3.1 dB due to the extraction of modal energy. Figure 6.14 shows clearly that

the damping effect on mode 1 is increased by 2.8 dB for the SSDH Modal (III) control in comparison with SSDI Modal technique. Indeed, the amplitude of voltage on the piezoelectric patch with Modal *SSDH* (III) technique is generally larger than that of the modal *SSDI*. The attenuation with the Modal SSDH (III) reaches -16.31dB. One can remember that in chapter 3, attenuations about -23dB were expected for SSDVC (II) method. This interesting attenuation value was conditioned to the value of the voltage created across the capacitance C_{int} (around 5V). Here, as the harvesting and damping part are connected, value of the voltage across the capacitance C_{int} is lower (figure 6.17). A more complex optimization process can be proposed to achieve better performances for this circuit;

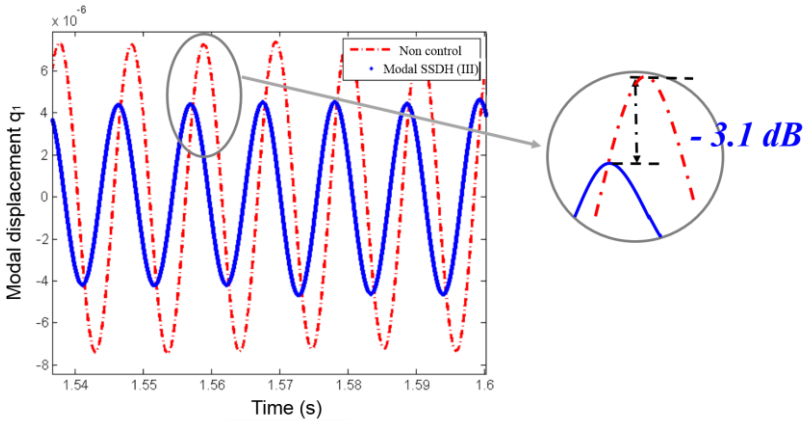

Figure 6.13 Modal displacement of the second mode

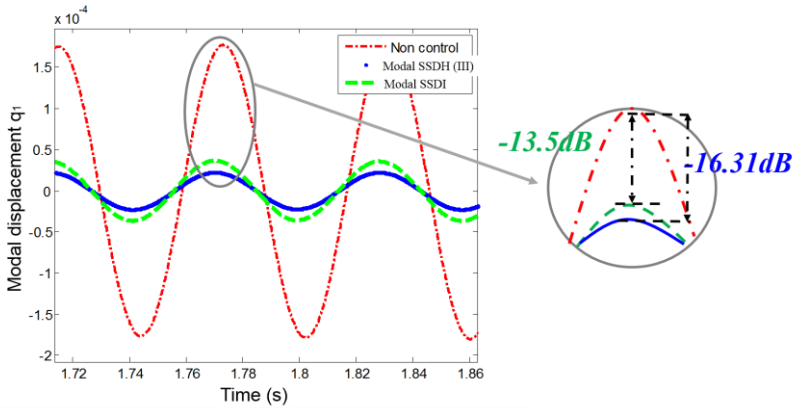

Figure 6. 14 Modal displacement of the first mode

As shown in Figure 6.15, due to the control law, it can be seen that the voltage on the piezoelectric element C_{01} is inverted at each extreme modal displacement. Figure 6.16 and 6.17 illustrate the fact that the intermediate voltages are perfectly discharged. However, the inversion coeffi-

cient is not constant. This is due to the voltages variations on the capacitance C_B, as shown in figure 6.17. So the transferred energy from C_B to C_{01} is modified for every energy transfer cycle.

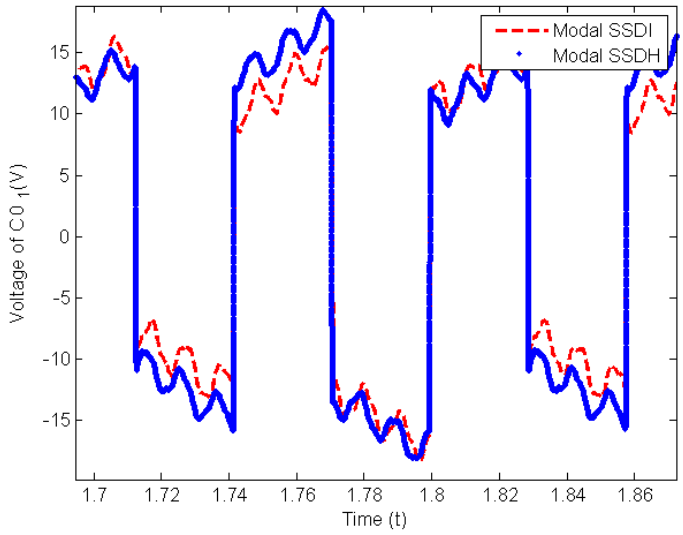

Figure 6.15 Voltage waveforms of C_{01} via Modal *SSDI* and Modal *SSDH* control

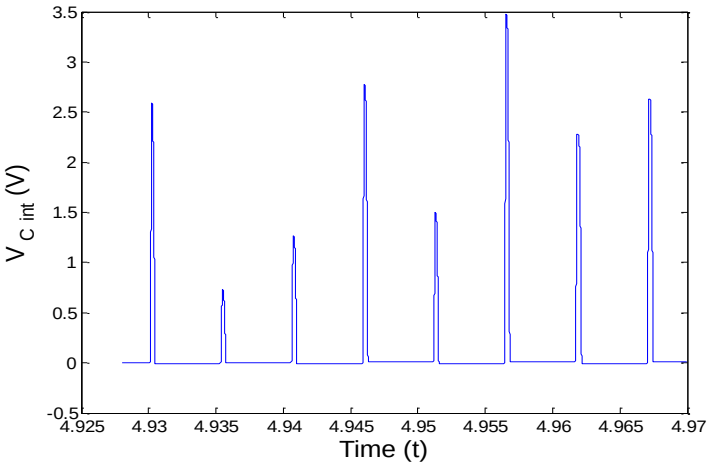

Figure 6.16 Voltage waveforms of C_{int}

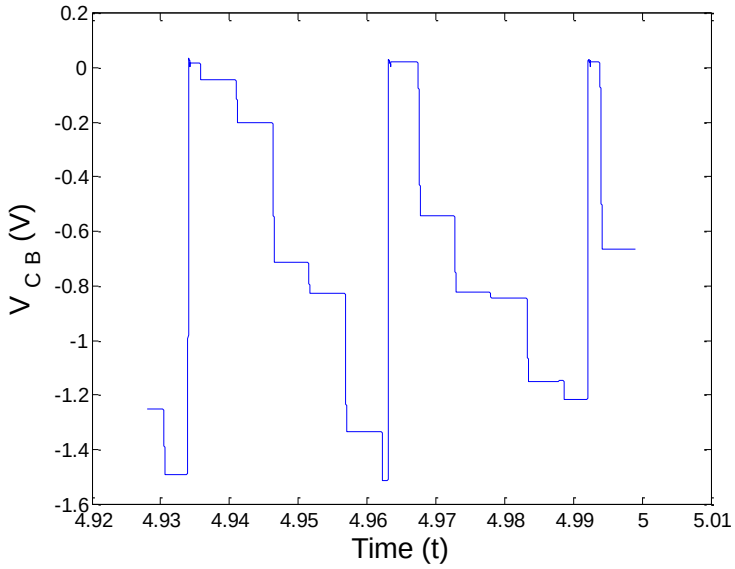

Figure 6.17 Voltage waveforms of C_B

6.4.3.2 White noise excitation

The second type excitation for the simulation is a White Noise. The parameters as presented in table 6.4 are used for this simulation.

Figure 6.18 shows the modal displacement of the non-controlled structure and of the two controlled structures: SSDI Modal and SSDH Modal (III). Figure 6.19(a) illustrates the voltage on the capacitor C_B of SSDH Modal (III) technique which falls to zero at each energy transfer period.

On the first mode, the measured attenuation is approximately 2dB compared to Modal SSDI control, which is a small gain in comparison with the complexity of the setup.

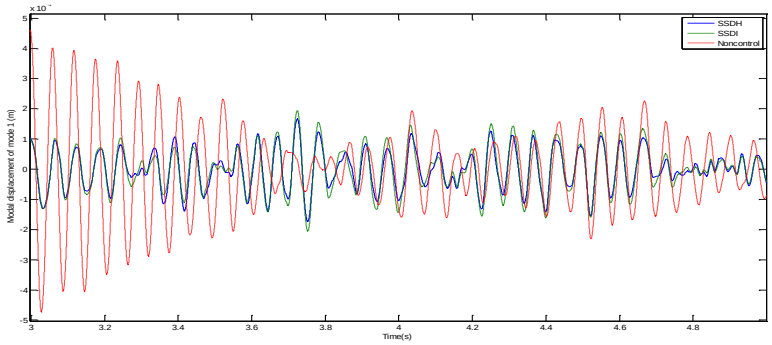

Figure 6.18 Modal displacement of the mode 1

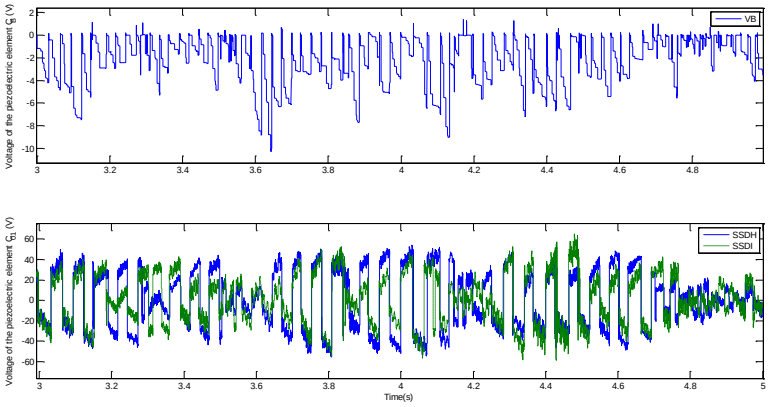

Figure 6.19 Voltage waveforms of Modal SSDI and Modal SSDH technique

a. The voltage on the capacitor C_B; b.Second first (b): The voltage on piezoelectric element C_{01}.

6.5 Comparison of the Modal SSDH techniques

By comparing the damping effect in case of bi sinusoidal excitation, it can be concluded that more damping effect is obtained by the Modal *SSDH* (I) and Modal *SSDH* (II) than with Modal *SSDH* (III). For the first mode, the attenuation is around 26dB with Modal *SSDH* (I) and (II) versus 13.5dB for the usual Modal SSDI technique. For the second mode, 1.7 dB is achieved by Modal *SSDH* (II) and 3.1 dB is achieved by Modal *SSDH* (III). Performances with white noise are drastically reduced. The use of the modal basis allows to find the correct time of switch, but the voltage fluctuations are to complex and clearly not sinusoidal. The inversion are no more optimized. Table 6.5 shows the results of attenuation by different Modal SSDH techniques.

Table 6.5 Attenuations of different Modal SSDH techniques

Technique	**SSDI**		**SSDH (I)**		**SSDH (II)**		**SSDH (III)**	
Excitation	Bi-sinusoidal	White noise	Bi-sinusoidal	White noise	Bi-sinusoidal	White noise	Bi-sinusoidal	White noise
Mode 1	13,5dB	8dB	26dB	14dB	26dB	13dB	17dB	2dB
Mode 2			0.84dB	1.2dB	1,7dB	0.8dB	3dB	0.3dB

It can be deduced that: a great value of capacitor holding an almost constant voltage, can provided an extra voltage to the damping circuit in the switching period which is efficient. A better damping effect is achieved by Modal *SSDH* (I) and Modal *SSDH* (II) techniques thanks to this higher constant voltage which increases the inversion voltage amplitude. The disadvantage of this control law is to use a large value of C_B, so charging time is long if the initial condition are null or if the second mode is poorly excited.

6.6 Conclusion

In this chapter, principles and the simulations of Modal SSDH (II) and Modal SSDH (III) are presented. For each new operating modes, the optimal value of the parameters were found through simulations and theroritical analyses. Then, the damping effect evaluated through simulations on an experimental modal model on various excitations.

The simulation results show that the Modal SSDH (II) presents better damping performances than Modal SSDH (III). Obviously, better performances are obtained under bi sinusoidal excitation than with white noise. With bi sinusoidal excitation, compared to non-control system, the amplitude of the first mode is reduced by 26 dB by Modal SSDH (II) technique. For Modal SSDH (III), the attenuation of the first mode is 16.17 dB.

Practically, the use of great value of capacitors seems more efficient by holding a constant voltage. This extra voltage increases significantly the inversion coefficient of the damping part. The other approaches, by full charge transfer seems less efficient, but do not necessitate a long charging time to reach the steady state.

7 Conclusion

This dissertation proposed a new control method based on the idea of using harvested energy to enhance the control of the vibration response. Many researches focus on vibration control of flexible structures. For practical reasons, these approaches are often modal. The main idea of this work is to harvest the energy of uncontrolled modes to improve the control of specific modes on a same structure.
In order to estimate the efficiency of the concept, an application on a simple smart structure is proposed. The piezoelectric materials present direct and inverse effects of electromechanical couplings which are used for the energy harvesting and the vibration control.

7.1 Sum up of the main contributions

- Damping circuit design by modal energy transferring

  Based on the idea of *SSDV* technique which enhances the damping effect of the usual SSD circuit by an extra voltage, two modal vibration control circuits *SSDVC* (I) and *SSDVC* (II) are proposed to develop a self-powered architecture to supply this extra energy. In this first step, the external voltage source necessary in the SSDV technique is replaced by a capacitor. Depending on the capacitor, two operating modes have been studied: full charge transfer named discharge capacitor mode; or constant voltage mode.

- Modal energy harvesting

  In order to obtain the desired extra voltage used in *SSDVC* control, four different energy harvesting topologies were studied. The originality of these topologies was to harvest modal energy based on modal approach. Those topologies include nonlinear parallel/series SSHI circuit to extract mechanical energy via piezoelectric elements. In order to maximize the extracted energy, a combination between SSHI circuit and a buck-boost converter was considered. Then, four different control laws of the switches were designed. The harvested energy depends on the choice of the control law and these control laws have different behaviors depending on the fre-

quency. So, according to our system, higher energy output and simplicity operation mode were considered to choose the more adapted control circuit.

- Modal energy transfer circuit design

  The new proposed architecture called *Modal Synchronized Switch Damping and Harvesting* (Modal SSDH) linking modal energy harvested with modal vibration control is the main originality of this work. The efficiency of the method depends on the choice of parameter of SSHI circuit, buck-boost converter, SSDVC circuit and of the smart structure. Detailed control law and architecture of *SSDH* were proposed. The application of this method was carried out on a cantilever smart beam. The modal energy is extracted from the second mode and used via SSDVC vibration modal control to enhance the damping effect on the first mode.

- Performance prediction of the proposed Modal *SSDH* method

  In order to predict the performance of proposed Modal *SSDH* method, optimization steps were carried out by. Simulations were implemented with *Simulink/Simscape*.

  Simulations showed that two benefits could be obtained with the proposed Modal *SSDH* technique: on one hand, the modal displacement of energy harvested mode was lightly damped by pumping the modal energy; on the other hand, the inversion factor on the transducer linked to the control is almost equal to one. The damping of the target mode was increased by using the extracted energy from the source mode. Consequently, the vibration of the smart structure was reduced compared with usual SSDI. Parametric stability analyses of the proposed technique using the variation of frequency error introduced in the structure model and different level power excitation of signal have been carry out. We can conclude that the Modal SSDH is robust if the operating conditions do not change drastically.

- Variants of Modal SSDH control method

  The corresponding chapters of the previous contributions presented several possible combinations of circuits, especially different control law of the switches. Each different combination leaded to variant of Modal SSDH control and to various performances. The optimization parameters of these combinations were found by mixing simulation parametric studies and theoretical formulae. Globally, the simulation results showed that using a constant voltage mode with a great value of the intermediate storage capacitor C_B is able to achieve a higher damping effect on a target mode. Nevertheless, each operating conditions has to be analyzed and the parameters optimized.

7.2 Suggestions for Further Work

Firstly, the promising results of our self-powered modal control method should be implemented in experiments to confirm the efficiency.

Secondly, our method could be extended to several harvested modes and / or controlled modes. The method could be improved in this case by optimizing the chosen of modes which could be the modes which have the more appropriate modal energy. In practice, complex systems included various structures. Consequently it could be adapted on a same system but on different structures to optimize the energy transfer.

Thirdly, in the case of multi-modal excitation or broadband excitation, the results can be improved by defining the inversion moment to maximize the voltage inversion: create a SSDH max. Previous studies has shown that it is possible to optimize these inversions by a more complex analyses of the voltage fluctuations.

Finally, our SSDH technique can be simplified in term of architecture or chosen components (diode instead of some switch T1 to T4). Some variations of our topology are under development

Bibliographie

[1] «IEEE Standard on Piezoelectricity». ANSI/IEEE Std 176-1987,1988.

[2] ***Preumont, A.,*** «Vibration control of active structures, an introduction third Edition».

[3] **Jani, J. M; Leary, M; Subic, A; Gibson, M. A,** « A Review of Shape Memory Alloy Research, Applications and Opportunities ». Materials and Design 56 (2014) 1078–1113.

[4] **Borroni-Bird CE,** « Smarter vehicles». Smart Structures and Materials 1997: Smart Electronics and MEMS 2 (June 19, 1997).

[5] **Wilkes, K. E.; Liaw, P. K.; Wilkes, K. E,** « The fatigue behavior of shape-memory alloys ». JOM (2000) 52 (10): 45.

[6] **Huang, W,** « On the selection of shape memory alloys for actuators ». Materials and Design, (2002) 23: 11–19.

[7] **Cederström J, Van Humbeeck J.** « Relationship Between Shape Memory Material Properties and Applications». Journal de Physique III (1995).IV 5: C2-335.

[8] **Joule, J.P,** « On the Effects of Magnetism upon the Dimensions of Iron and Steel Bars ». The London, Edinburgh and Dublin philosophical magazine and journal of science (Taylor & Francis). 30, Third Series: 76–87, 225–241. Retrieved 2009-07-19.

[9] **M. Vajquez,** « Magnetic Bistability of Amorphous Wires and Sensor Applications». IEEETRANSACTIONS ON MAGNETICS, VOL. 30, NO. 2, MARCH 1994.

[10] **Kexiang Wei, Guang Menga, Shuo Zhoua, Jinwu Liu,** «Vi bration control of variable speed/acceleration rotating beams using smart materi als ». Journal of Sound and Vibration 298 (2006) 1150–1158.

[11] **B. Nayak, S.K. Dwivedy, K.S.R.K. Murthy.** «Dynamic stability of a

rotating sandwich beam with magnetorheological elastomer core». European Journal of Mechanics A/Solids 47 (2014): 143-155

[12] **Y.S.Kim, K.W.Wang, H.S.Lee.** «Feedback control of ER-fluid-based structures for vibration suppression». Smart Materials Structure 1 (1992): 139-145.

[13] **Mohammad Hoseinzadeh, Jalil Rezaeepazhand.** «Vibration suppression of composite plates using smart electrorheological dampers». International Journal of Mechanical Sciences 84(2014): 31–40.

[14] **Manbachi, A., Cobbold R.S.C,** «Development and Application of Piezoelectric Materials for Ultrasound Generation and Detection». Ultrasound (2011).19 (4): 187–196.

[15] **S. O. R. Moheimani, A. J. Fleming,** « piezoelectric transducers for vibration control and damping », 2006

[16] **S. CARABELLI, A. TONOLI,** « System properties of flexible structures with self-sensing piezoelectric transducers », Journal of Sound and vibration (2000) 235(1), 1-23.

[17] **T. BAILEY; J. E. UBBARD,** « Distributed piezoelectric-polymer active vibration control of a cantilever beam», Journal of Guidance, Control, and Dynamics, Vol. 8, No. 5 (1985): 605-611.

[18] **A. Baz, S. Poh** « Performance of an active control system with piezoelectric actuators», Journal of Sound and VibrationVolume 26, Issue 2, 22 October 1988, Pages 327-343.

[19] **Hideyuki Ikeda, Takeshi Morita,** « High-precision positioning using a self-sensing piezoelectric actuator control with a differential detection method», Sensors and Actuators. A 170 (2011) 147– 155.

[20] **Inman, D. J,** « Vibration and Control John Wiley and Sons», Chichester, UK. 2006,

[21] **Nashif, A.D., Jones, D. I. G., and Henderson, J. P.,** « Vibration Damping», John Wiley and Sons, Inc, New York. 1985,

[22] **Ned Mohan, Tore M. Undeland, William P. Robbins,** « Power Electronics: Converters, Applications, and Design», Wiley, New York, 2002.

[23] **N.W. Hagood, A. von Flotow,** « Damping of structural vibrations with piezoelectric materials and passive electrical networks», Journal of Sound and Vibration Volume 146, Issue 2, 22 April 1991, Pages 243–268

[24] **Lesieutre, G. A.,** « Vibration damping and control using shunted piezoelectric materials», The Shock and Vibration Digest, 30(3), 187-195, (1998).

[25] **Wu, S. Y.,** « Piezoelectric shunts with a parallel R-L circuit for structural damping and vibration control», Proceedings SPIE, SSM Conference: Passive Damping and Isolation, (1996). 2720, 259-269,

[26] **Hollkamp, J. J.,** « Multimodal passive vibration suppression with piezoelectric materials and resonant shunts», Journal of Intelligent Material Systems and Structures, (1994).5(1), 49-57,

[27] **Wu, S. Y.,** « Method for multiple mode shunting damping of structure vibration using a single PZT transducer», Proceedings SPIE, SSM Conference: Passive Damping and Isolation, (1998).3327, 159-168,

[28] **S. Behrens, S.O.R. Moheimani, A.J. Fleming.** «Multiple mode current flowing passive piezoelectric shunt controller», Journal of Sound and Vibration 266 (2003): 929–942.

[29] **A J Fleming, S Behrens and S ORMoheimani,** « Reducing the inductance requirements of piezoelectric shunt damping systems», Smart Mater. Struct. 12 (2003) 57–64

[30] **B.F. Spencer, Jr., T.T. Soong,** « NEW APPLICATIONS AND DEVELOPMENT OF ACTIVE, SEMI-ACTIVE AND HYBRID CONTROL TECHNIQUES FOR SEISMIC AND NON-SEISMIC VIBRATION IN THE USA», Proceedings of International Post-SMiRT Conference Seminar on Seismic Isolation, Passive Energy Dissipation and Active Control of Vibration of Structures Cheju, Korea, August 23-25, 1999.

[31] **Rabih Alkhatib, M. F. Golnaraghi,** « Active Structural Vibration Control: A Review», The Shock and Vibration Digest 2003; 35; 367.

[32] **Fuller, C. R., Elliott, S. J., and Nelson, P. A.,** « Active Control of Vibration». Academic Press, New York. 1997,

[33] **W. W. Clark,** « semi-active vibration control with piezoelectric materials as variable stiffness actuators», SPIE conference on passive damping and isolation,

1999, Vol. 3672: 123-130.

[34] **K. A. Cunefare, S. De Rosa, N. Sadegh and G. Larson,** « state-switched absorber for semi-active structural control», Journal of Intelligent Material Systems and Structures, 2000, Vol. 11: 300-310

[35] **C. Richard, D. Guyomar, D. Audigier and G. Ching,** « semi-passive damping using continuous switching of a piezoelectric device», SPIE, 1999, Vol. 3672.

[36] **C. Richard, D. Guyomar, D. Audigier and H. Bassaler,** « enhanced semi passive damping using continuous switching of a piezoelectric device on an inductor», SPIE, 2000, Vol. 3989

[37] **C. L. Davis and G. A. Lesieutre,** « an actively tuned solid-state vibration absorber using capacitive shunting of piezoelectric stiffness», Journal of Sound and Vibration, 2000, 232 (3): 601-617

[38] **Clark, W. W.,** «Vibration Control with State-Switched Piezoelectric Materials», J. Intell.Mater. Syst. Struct. 11, 263-271 (2000).

[39] **Onoda, J., Endot, T., Tamaoki, H., and Watanabe, N.,** « Vibration suppression by variable stiffness members», AIAA Journal, vol.29, No. 6, 1991: 977-983.

[40] **Kenji, M. and Kyohei, K.,** « Semi-active vibration suppression of large space structures with a variable axial stiffness member», AIAA/ASME/ASCE/AHS/ASC Structures, Structural Dynamics, and Materials Conference, 34th and AIAA/ASME Adaptive Structures Forum (La Jolla, CA) A93-33876 13-39, 3305{3311 (1993).

[41] **E. Lefeuvre, A. Badel, L. Petit, C. Richard and D. Guyomar,** « semi-passive piezoelectric structural damping by synchronized switching on voltage sources», Journal of Intelligent Material Systems and Structures, 2006, Vol. 17: 653-660

[42] **Badel, A., Sebald, G., Guyomar, D., Lallart, M., Lefeuvre, E., Richard, C., and Qiu, J.,** « Piezoelectric vibration control by synchronized switching on adaptive voltage sources: towards wideband semi-active damping», *The Journal of the Acoustical Society of America*, 119, 2006, 2815- 2825.

[43] **C. Richard, D. Guyomar, and E. Lefeuvre.** «Self-powered electronic breaker with automatic switching by detecting maxima or minima of potential difference between its power electrodes». Brevet PCT/FR2005/003000, Publication number :WO/2007/063194, 2007.2.

[44] **Lallart, M., Lefeuvre, E., Richard, C. and Guyomar, D.**, «Self-Powered Circuit for Broadband, Multimodal Piezoelectric Vibration Control». Sensors and Actuators A: Physical, 143(2), 2008, 277- 382.

[45] **Lallart, M. and Guyomar, D.,** « Self-Powered and Low-Power Piezoelectric Vibration Control Using Nonlinear Approaches, ». Vibration Control, Mickael Lallart (Ed.), ISBN: 978-953-307-117-6, InTech, 2010, 265-292.

[46] ***Guyomar, D. and Badel, A.,*** «*Nonlinear semi-passive multimodal vibration damping: An efficient probabilistic approach*». Journal of sound and vibration*, 294(1), 2006, 249-268.*

[47] **Corr, L. R. and Clark, W. W.** «A novel semi-active multi-modal vibration control law for a piezoceramic actuator," Journal of Vibration and Acoustics, 125(2), 2003, 214-222.

[48] **Harari, S., Richard, C. and Gaudiller, L.,** « *Multimodal control of smart structures based on semipassive techniques and modal observer*». Motion and Vibration Control*, 1, 2009, 113-122.*

[49] ***Harari, S., Gaudiller, L. and Richard, C.,*** «*New semi-active multimodal vibration control using piezoceramic components*». Journal of Intelligent Material Systems and Structures*, 20(13), 2009, 1603-1613.*

[50] **Gaudiller, L., Harari, S. and Richard, C.,** «*Low energy multimodal semi-active control minimizing the number of transducers*». *Proceedings SPIE, SSM Conference: Active and Passive Smart Structures and Integrated Systems, 7288, (2009). 1603-1613.*

[51] ***Harari, S., Richard, C. and Gaudiller, L.,*** *"Hybrid active/semi-active modal control of smartstructures,"* Proceedings SPIE, SSM Conference: Active and Passive Smart Structures and Integrated systems*, 7288, (2009).*

[52] **Neubauer, M., Han, X. and Schwarzendahl, S. M.,** *"Enhanced switching law for synchronized switch damping on inductor with bimodal excitation,"* Journal of Sound and Vibration*, 330(12),2707-2720 (2011).*

[53] ***Chérif, A., Richard, C., Guyomar, D., Belkhiat, S. and Meddad, M.,*** *"Simulation of multimodal vibration damping of a plate structure using a modal SSDI-Max technique,"* Journal of Intelligent Material Systems and Structures*, 23(6), 675-689, (2012).*

[54] **Hande A.** « Indoor solar energy harvesting for sensor network router nodes». Microprocess and Microsystem, 2007, 31(2):420-432.

[55] **FANG Ke, LI Xin-xin, YANG Zhi-gang, CHENG Guang-ming, KAN Jun-wu,** « Research state on piezoelectric energy harvesting advice», TRANSDUCER AND MICROSYSTEM TECHNOLOGIES,2006, 25(10):7-15.

[56] **Roundy S., Wright P. K. and Rabaey J.** « A study of low level vibrations as a power source forwireless sensor nodes». Computer Communications, 2003, 26(11): 1131-1144.

[57] **Stanton S. R. and Sodano H. A.** « A review of power harvesting using piezoelectric materials (2003–2006) ». Smart Material and Structure, 2007, 16(3):1-21.

[58] **Roundy Shadrach Joseph,** «Energy Scavenging for Wireless Sensor Nodes with a Focus on Vibration to Electricity Conversion». thesis, 2003.

[59] **Sodano H A, Inman D J and Park G** « A review of power harvesting from vibration using piezoelectric materials Shock Vib».2004 Dig. 36 197–205

[60] **Poulin G, Sarraute E and Costa F** « Generation of electric energy for portable devices: comparative study of an electromagnetic and a piezoelectric system Sensors Actuators». 2004A 116 461–71

[61] **Lefeuvre E., Sebald G., Guyomar D., et al. «** Materials, structures and power interfaces for efficient piezoelectric energy harvesting**»** Journal of Electroceram, 2007, 22(1-3): 171-179

[62] ***Lefeuvre E., Audigier D., Richard C.*** *«* Buck-boost converter for sensorless power optimization of piezoelectric energy harvester*».* IEEE Transaction on Power Electronics, 2007, 22(5): 2018-2025.

[63] **G.K. Ottman, H.F. Hofmann, A.C. Bhatt, G.A. Lesieutre,** « Adaptive Piezoelectric Energy Harvesting Circuit for Wireless Remote Power Supply». IEEE Trans. Power Electron. 17, 2002, 669-676.

[64] **Ottman G. K., Hoffmann H.F. and Lesieutre G. A.,** «Optimized piezoelectric energy harvesting circuit using step-down converter in discontinuous conduction mode». IEEE Transactions on Power Electronics, 2003, 696-703.

[65] **Guyomar D., Badel A., Lefeuvre E.,** « Toward energy harvesting using active materials and conversion improvement by nonlinear processing IEEE Trans». Ultrason. Ferroelectr. Freq. Control, 2005, 52:584–94.

[66] **Lefeuvre E., Badel A., Richard C.,** « A comparison between several vibration-powered piezoelectric generators for standalone systems». Sensors and Actuators A, 2006, 126(2): 405-416.

[67] **Badel A., Guyomar D., Lefeuvre E., et al.** « Efficiency enhancement of a piezoelectric energy harvesting device in pulsed operation by synchronous charge inversion». Journal of Intelligent Material Systems and Structures, 2005, 16: 889 - 901.

[68] **Lefeuvre E., Badel A., Benayad A.,** « A comparison between several approaches of piezoelectric energy harvesting». Physique Coll, 2005, 128: 177 - 186.

[69] **Badel A., Guyomar D., Lefeuvre E., Richard C.,** « Piezoelectric energy harvesting using a synchronized switch technique». Journal of intelligent material system and structure, vol. 17,2006, 831–839.

[70] **Kim H. W., Batra A., Priya S.,** « Energy harvesting using a piezoelectric cymbal transducer indynamic environment». Japan Journal of Applied Physics, 2004, 43 (6): 178 - 183.

[71] **Han J., Von Jouanne A., Le T.,** « Novel power conditioning circuits for piezoelectric micro power generators». Proc. 19 th Ann. IEEE App lied Power Electronics Conf. And Exposition Conf, 2004, 1541 - 1546.

[72] **Lesieutre G. A., Ottman G. K., Hofmann H. F.** « Damping as a result of piezoelectric energy harvesting ». Journal of Sound and Vibration, 2004, 269 (3): 991 - 1001.

[73] **Shenck N. S. and Paradiso J. A.** « Energy scavenging with shoe-mounted piezoelectrics» IEEE Micro, 2001, 21:30–42.

[74] **Ammar Y., Buhrig A., Marzencki M., et al.**. «Wireless sensor network node with asynchronous architecture and vibration harvesting micro pow-

er generator» Proc. 2005 Joint Conf. on SmartObjects and Ambient ibeuntelligence: Innovative Context2Aware Services: Usages and Technologies(Grenoble) , 2005, 287 - 292.

[75] **Lefeuvre E., Badel A., Richard C., et al.** « Piezoelectric energy harvesting device optimization by synchronous electric charge extraction». Journal of Intelligent Material Systems and Structures, 2005, 16(10): 865-876.

[76] **lallart M., Garbuio L., Petit L.,** « Double synchronized switch harvesting (DSSH): A new energy harvesting scheme for efficient energy extraction», IEEE Transactions on ultrasonic, Ferroelectrics, and frequency Control, vol. 55, No. 10 2008, 2119–2130.

[77] ***Hui Shen, Jinhao Qiu , Hongli Ji, Kongjun Zhu and Marco Balsi,*** *Enhanced synchronized switch harvesting: a new energy harvesting scheme for efficient energy extraction. 2010 Smart Mater. Struct. 19 115017*

[78] **Li, K., Gauthier, J.-Y., and Guyomar, D.,** « Structural vibration control by synchronized switch damping energy transfer», Journal of Sound and Vibration, 330, 49-60, (2010).

[79] **Wu, D., Guyomar, D. and Richard, C.,** « A new global approach using a network of piezoelectric elements and energy redistribution for enhanced vibration damping of smart structure», Proceedings SPIE, SSM Conference: Active and Passive Smart Structures and Integrated Systems, 8868, (2011).

[80] ***Harari, S.,*** «Contrôle modal semi-actif et actif à faible consommation énergétique par composants piézoélectriques». *Ph.D. Dissertation, INSA-Lyon, (2009).*

[81] **Vincent Lhuillier,Simon Chesné , Charles Pezerat Luc Gaudiller ,** « *Contrôle actif de la transparence acoustique d'une double paroi*». *Résultats expérimentaux, 10ème congrès français d'acoustique, Lyon, 12-16 avril 2010.*

[82] ***M. H. Richardson and D. L. Formanti.*** « *Parameter estimation from frequency response measurements using rational fraction polynomials* ». *pages 167–181, 1982.*

[83] **M. H. Richardson and D. L. Formanti.** « *Global curve fitting frequency response measurements using the rational fraction polynmial method*».

pages 390–397, 1985.

*[84]***Mickaël LALLART,** *«Amélioration de la conversion electroactive de matériaux piézoélectriques et pyroélectriques pour le contrôle vibratoire et la récupération d'énergie». Ph.D. Dissertation, INSA de Lyon, (2008).*

[85] ***Badel, A.,*** «Récupération d'énergie et contrôle vibratoire par éléments piézoélectriques suivant une approche non linéaire». *Ph.D. Dissertation, Université de Savoie/INSA de Lyon, (2005).*

[86] **Luenberger, D.** «*An introduction to observers*». IEEE Transactions on Automatic Control*, 16(6), 596–602, (1971).*

LIST OF FIGURES

LIST OF TABLES

Annexe A

The model of the modal SSDH Modal is perfomed in Simulink Simscape environment. The architecture are shown in Figure A.1. In this figure, we can see that the system consists in:

- The model of the mechanical structure (electro-mechanical part: piezo-electric elements PZT and PVDF with the structure) constructed using experimental data and identification methods;
- Energy harvesting system (on the second mode): SSHI series presented in section 4.2.1;
- Buck-boost presented in section 4.2.2;
- Vibration control system: SSDI for the first resonance frequency of the smart structure;
- The modal observer which is used to obtain the modal coordinates.

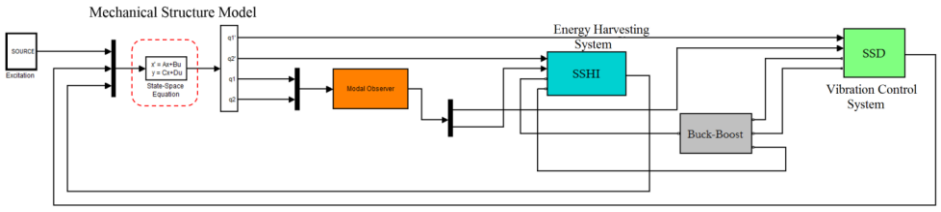

Figure A. 1 Simulink model of SSDH Modal technique

The details of the Simulink model are presented in the following: it can be divided to six parts:

A.1 Excitation

The simulations of proposed works carry out with different excitations:

- A sinusoidal excitation composed by the first resonance frequency and the second resonance frequency of the smart structure;
- White noise.

The amplitude of the excitation is chosen according to an experiment in which it drives the beam with a displacement magnitude of 2 mm without control. The excitation is a spatial distributed transverse force. Its distribution corresponds to the modal shapes.

A.2 The mechanical structure model

The smart structure is described with state-space equation. The outputs correspond to the two modal coordinates and two modal velocities shown in the figure A.2.

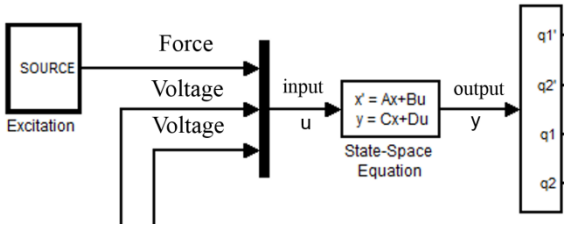

Figure A. 2 The diagram of the mechanical structure model

A.3 The modal observer

A.3.1 Observer

An observer is an internal closed loop of the control loop. Thanks to this technique, the output estimation $\hat{y}$ computed from the model of the structure converges to the real output y: the measurement.

The observer uses a model of the physical system described in state-space. So, the estimated model state $\hat{x}$ converges to the actual model state x. The observer can be adjusted to eliminate quickly the estimation error, but the adjustment should not increase noise.

The state equation of the observer [86] is:

$$\dot{\hat{x}} = A\hat{x} + Bu + L\left(y - \hat{y}\right) \tag{A.1}$$

with $y = Cx$, $\hat{y} = C\hat{x}$ and matrix of feedback gain L.

The matrix of observer gain L is optimized by a compromise between input and output noise as a Kalman filter.

In the presented case, the input values of the modal observer are constituted by: the values of the voltage of the PVDF and the control value. The outputs of the observer correspond to the estimation of modal coordinates.

A.3.2 Energy harvesting system

Figure A.3 illustrates the diagram of the energy harvesting circuit. The previous modal observer delivers the two first modal displacements and velocities. The switch control block (Figure A.3) is used to detect the extremum of the second modal displacement (The implementation method to detect the extremum of input signal unit is described in figure A.4).

When the "switch S_2" is closed by the "switch control block" on each extreme modal displacement q_2 for a short time Δt, the piezoelectric element, the inductance and the a resistance constitute an RLC oscillator circuit. It results in a quick inversion of the piezoelectric voltage on the "piezoelement C_{02}". The "voltage of C_{02}" feeds back to the mechanical structure model (see figure A.2). Thus, the energy transfers from the "piezoelectric element C_{02}" to the "intermediate capacitor C_{int}" through the "inductance L_2" and the "diode bridge" rectifier.

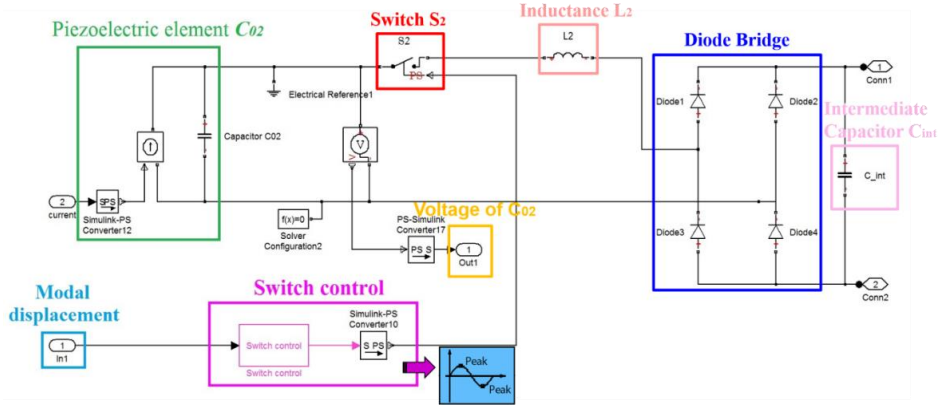

Figure A. 3 The diagram of the energy harvesting system: Modal SSHI

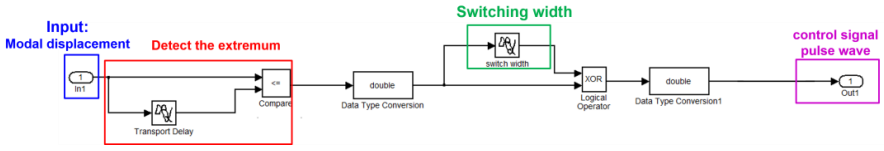

Figure A. 4 The diagram of switch control block

Principles of the switch control:

As shown in figure A.4, the "input: modal displacement q_2" is divided into two branches in the block "detect the extremum". The signal of the second branch is picked up and delayed the input signal for a very short time t, and then compared with the original signal of the first branch. The

value of the first branch signal (original signal) is larger or smaller than the value of the second branch signal (delayed signal), see figure A.5. If the time t is short enough, the watershed point for this comparison is almost equal to the maximum/minimum point of the input signal, as shown in figure A.5. The output "control signal pulse wave" is a pulse wave and the "switching width" is the switching time of S_2 which is given by the equation ($\Delta t = \pi\sqrt{L_2 C_{02}}$).

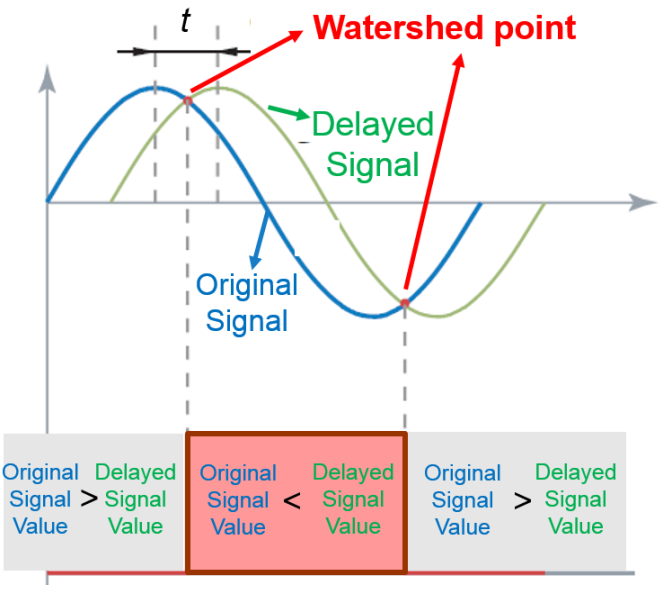

Figure A. 5 The logic of detect the extremum

A.3.3 Buck-boost converter

The "buck-boost converter" was presented in section 4.2.2. The diagram of the buck-boost converter in Simscape is shown in figure A.6. The "buck-boost converter" is connected with the "energy harvesting system" and the "vibration control system".

The output voltage of the "energy harvesting system" is the input voltage of "buck-boost converter". The "switch S_B control" block generates the pulse wave control signal including the switching frequency f_B and a duty cycle D. When the "switch S_B" is closed, the energy of the C_{int} (see figure A.3) is transfered to the "inductor L_B". When the "switch S_B" is open, the energy stored in the "inductor L_B" is transferred to the storage "intermediate capacitor C_B".

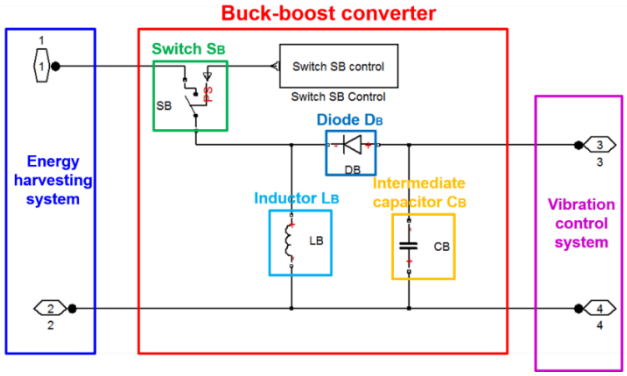

Figure A. 6 The diagram of the buck-boost converter

A.3.4 Vibration control system

Figure A.7 shows the Simulink diagram of the "vibration control system" block, which is connected with the "buck-boost converter" circuit.

There are two switch control blocks here, the "switch S_1 control" which controls the "switch S_1". The other block named "switches control" is to control (as presented in section 3.2.2) the "switches T1, T2, T3 and T4" (The detailed diagrams are shown in the figure A.8 and figure A.9).

When closing the switches by the "switches control" block on each extreme "modal displacement q_1", a RLC oscillator circuit is connected, constituted by the "piezoelectric element C_{01}", the "inductance L_1" and the associated resistance. The "voltage of C_{01}" feeds back to the mechanical structure model (see figure A.2). During the switch control period, the stocked energy of the "intermediate capacitor C_B" (see figure A.6) is transfered to the "piezoelectric element C_{01}".

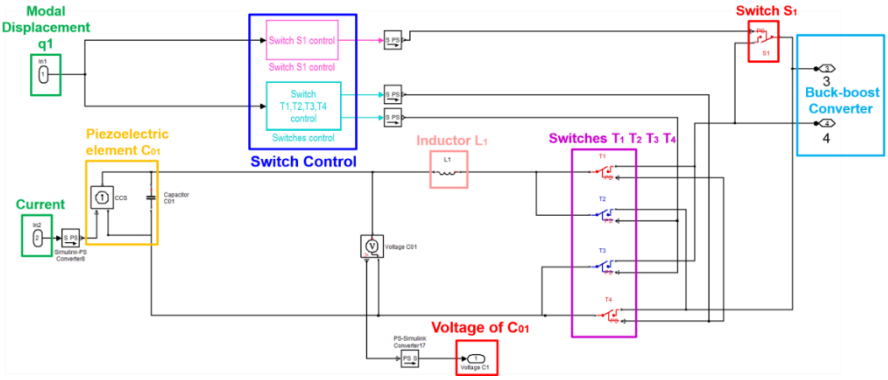

Figure A. 7 The diagram of the vibration control system

Principles of the switch control S_1:

The same type of control strategy presented in the part "Energy harvesting system" is used for the first modal displacement. For the "switch S_1 control" block, the "switching time t_1" block is used to delay the switch S_1 after the time t_1 which was presented in section 3.2.2. The "switching time t_2" block is used to control the width of the pulse wave "output control signal" which is equal to the switching time t_2.

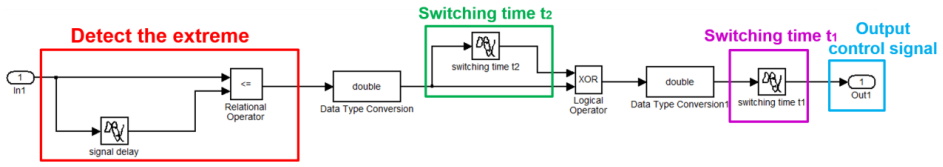

Figure A. 8 The diagram of the switch S_1 control block

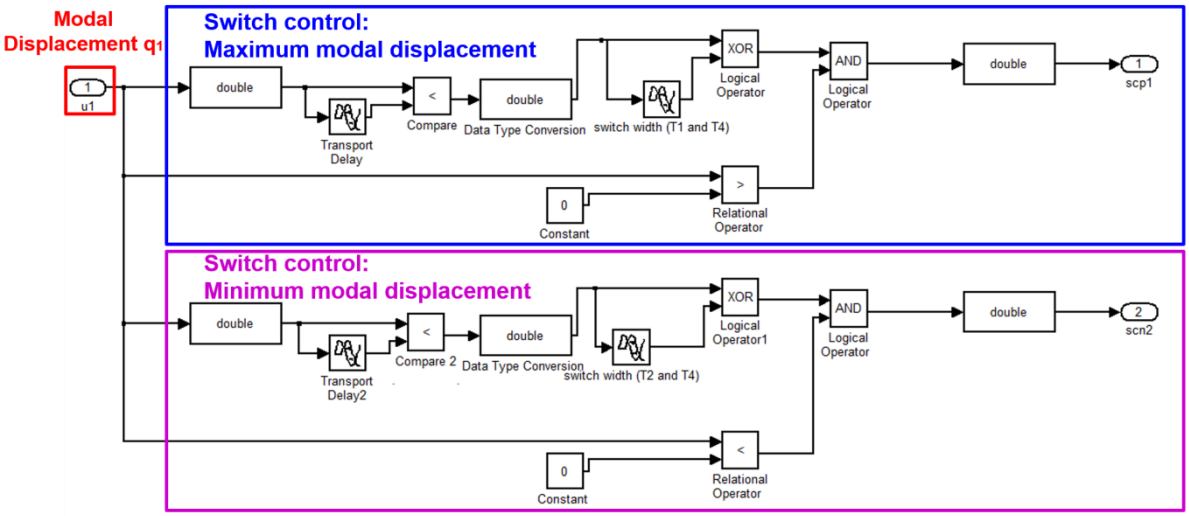

Figure A. 9 The diagram of switches control block of T_1, T_2, T_3, T_4

Principles of the switches control (T_1, T_2, T_3, T_4):

The same type of control strategy is also used as previously for the first modal displacement for the "switches control" block.

The maximum and minimum modal displacements are detected by the "switches control", as shown in the figure A.9. The first branch part controls the maximum and the second branch part is for the minimum. The switching width (T_1, T_4) or (T_2, T_3) of this pulse control is controlled by the switching time t_1 and t_2 which are presented in section 3.2.2.

Annex B

To implement our *SSDH* topology, basic combinations must be firstly tried:

- the harvesting part namely the Modal *SSHI* circuit associated with the Buck-boost converter
- the damping part, i.e. the *SSDVC* circuit operating under a constant voltage mode

We present here our first result regarding the harvesting part.

Our smart structure described in the chapter 2 is used to realize these tests. A DSPACE interface is employed to control in real-time our structure: record voltage from the piezoelectric sensor and send order to the switches. The switch is in fact realized thank to on home-made circuit insuring precision and rapidity. An electromagnet is used to generate the excitation.

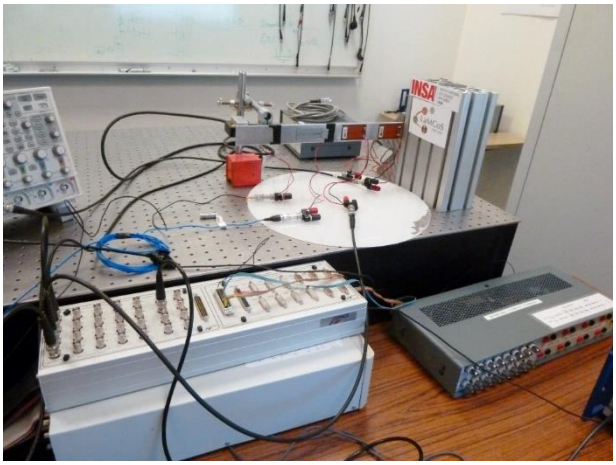

Figure B. 1 Experiments

B1. Modal Harvesting energy series-*SSHI*

The figure B.1 shows the topology of the series-*SSHI* circuit and the value of the components used in these experiments. One can underline that an adaptive circuit must be used to record the electrical signal (impedance adaptation).

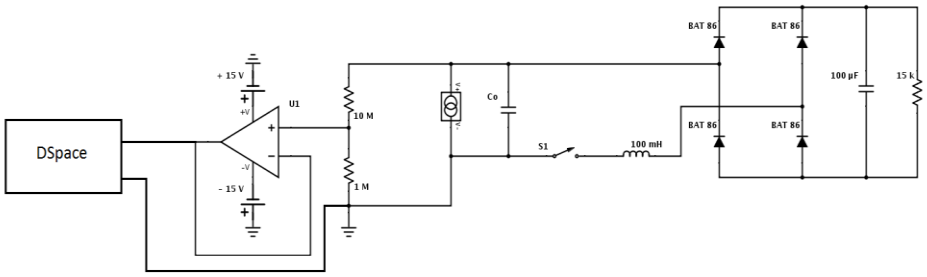

Figure B. 2 Real circuit of the series *SSHI* technique

Before presenting the results it is important to mention that the value of the resistive charge was not choose in a random way. The circuit was tested with different values of the resistive charge to see which value has the optimal power dissipation. This was done to obtain the maximum extraction of energy possible. The results of the different resistance values are shown in the next table:

Table B. 1 Output power and voltage of different value of resistance

R (kΩ)	P (mW)	V
10	0,121	1,1
15	0,1288	1,39
20	0,1286	1,6
22	0,1282	1,68
47	0,0974	2,14
56	0,0904	2,25
100	0,063	2,51

The waveforms of this technique with an optimal load of 15kΩ under sinusoidal excitation are shown in the next figure:

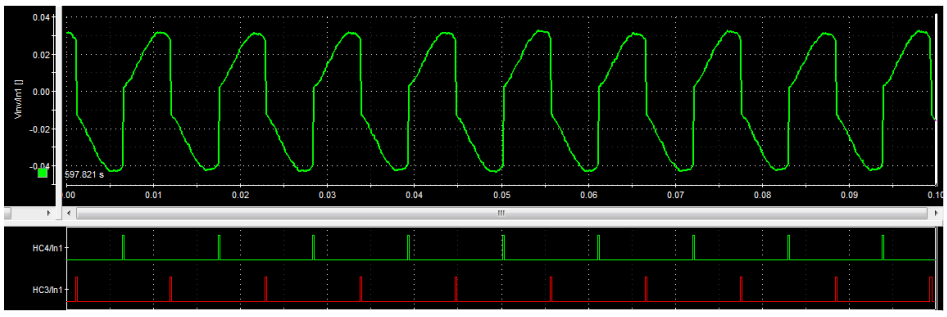

Figure B. 3 Voltage of the PZT patch used for the SSHI series modal technique

We can see that the waveforms are correct with an interesting inversion coefficient of 0.73. The rectified voltage of the resistive charge R is 1.2 V; this value is considered a good value of recuperated energy for the purposes of this project.

B2. Modal *SSHI* associated with a buck-boost converter

The parameters of the Buck-Boost are chosen to have a perfect match between the optimal resistance for the harvesting circuit (output resistance) and the input resistance of the converter. The circuit schematic is shown in the next figure:

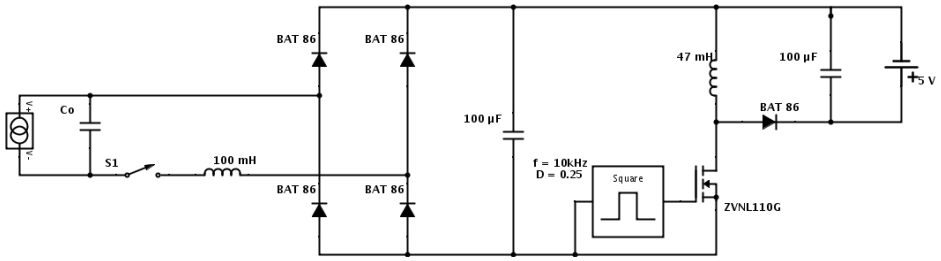

Figure B. 4 Schematic of the SSHI series + Buck-Boost circuit

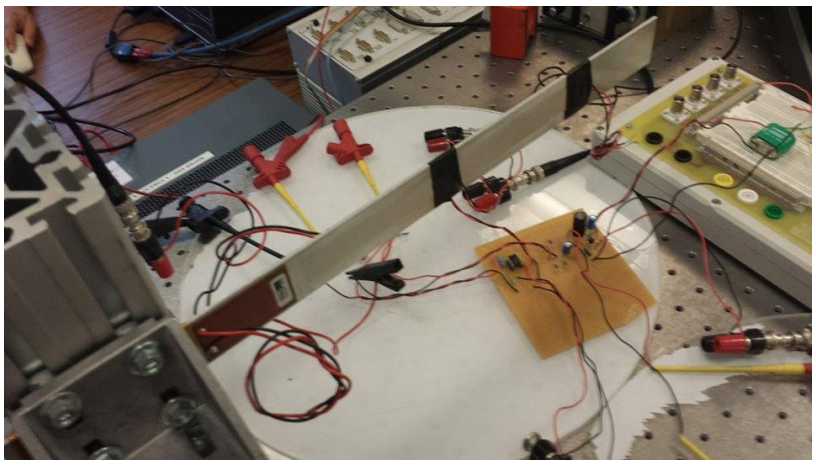

Figure B. 5 Photography of the tests set-up

The figure B.6 shows the typical waveforms measured from that circuit.

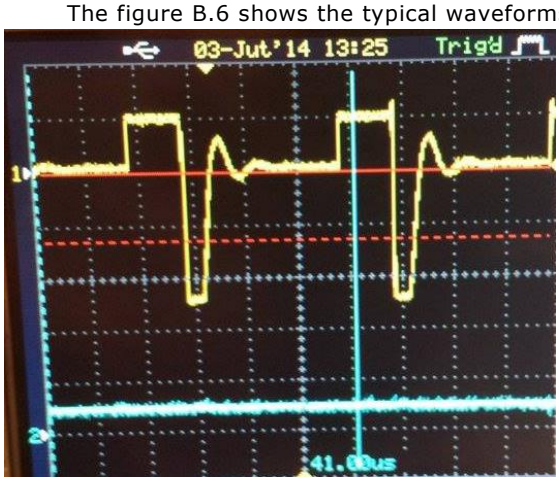

Figure B. 6 Waveforms of the Buck-Boost's inductor voltage (yellow) and SSHI series recuperated energy (blue)

The waveform of the signal are in agreement with the theory. The harvested voltage is a constant. One can note that in the buck-boost converter dynamic effect appear such as Miller effect. These effect must be taken into account in the future modelling to improve its accuracy. The next step is to test the damping part and to associate the two circuits to create our *SSDH*.